

14. PLIOCENE-PLEISTOCENE BIOGENIC AND TERRIGENOUS FLUXES AT EQUATORIAL ATLANTIC SITES 662, 663, AND 664¹

W. F. Ruddiman² and T. R. Janecek^{2,3}

ABSTRACT

High-resolution analyses of sediments at equatorial Atlantic Sites 662, 663, and 664 define the accumulation rates of biogenically produced CaCO_3 and opal and of eolian dust from North Africa over the last 3.7 m.y. The mean flux of opal increased abruptly by 60%–70% near 2.5 Ma (2.65 to 2.3 Ma), reflecting pulses of increased opal productivity along the equator due mainly to increased upwelling. The mean winter-plume dust influx from Sahelian and Saharan Africa also increased at this time by between 35% and 75%, following smaller increases earlier in the late Pliocene.

The increased opal flux implies a stronger zonal component of the southern trade winds in Southern Hemisphere winter. Consistent with this wind configuration, the stronger dust flux suggests a weaker southwesterly monsoonal flow into Africa in Northern Hemisphere summer, thus increasing Sahelian aridity and winter-plume dust fluxes. Dust fluxes to the equator may possibly have also been enhanced by stronger Northern Hemisphere winter trade winds and a more southerly position of the Intertropical Convergence Zone over Africa.

These late Pliocene biogenic and terrigenous flux changes coincided with the appearance of Northern Hemisphere ice sheets, implying an ultimate causal link. The immediate control on changes in tropical circulation may, however, have been changes in the Atlantic sector of the Southern Ocean.

A steady background trend of increasing winter-plume dust flux occurred from the late Pliocene until the middle Pleistocene. This may reflect a progressive, tectonically induced aridification of northern and eastern Africa because of the gradual uplift of the Tibetan Plateau.

INTRODUCTION

Leg 108 cored three sites along the equator in the Atlantic Ocean (Fig. 1 and Table 1). Two sites in the eastern equatorial Atlantic (662 and 663) are combined to provide a nearly complete record of most of the last 3.7 m.y. of equatorial sedimentation. Site 664 in the central equatorial Atlantic provides a comparable record of the latest Neogene.

Because divergence occurs today along the equator, one objective was to study the Pliocene-Pleistocene history of equatorial divergence based on CaCO_3 and opal, two biogenic components produced by plankton in surface waters and partially preserved in sediments. The second objective was to monitor terrigenous sediment influxes from Africa as an index of continental aridity and atmospheric circulation.

STRATIGRAPHY AND CHRONOLOGY

All three Leg 108 equatorial sites are bedeviled by late Pliocene to middle Pleistocene slumps (Fig. 2). In addition, the remanent magnetism of the sediments was too weak for the shipboard magnetometers to provide useful stratigraphies, except for the upper Pleistocene section at Site 664. Despite these problems, we also obtained long undisturbed late Pliocene and Pleistocene sequences at Sites 662, 663, and 664.

Age-Depth Trends

Age-depth curves from Holes 662A, 663A, 664B, and 664D are shown in Figure 2, along with slumps and turbidites. Many slumps have totally disturbed the sediments, creating folded, flowed, and contorted layers that are of no use to this study. Other slumps have deformed the sediments to a lesser degree,

causing slight tilting of layers or sharpening of contrasts across originally bioturbated contacts.

The age-depth trends in Figure 2 for Holes 663A, 664B, and 664D are based on datums reported during Leg 108 (Ruddiman, Sarnthein, et al., 1988). For Hole 662A, we also list in Table 2 one revised discoaster datum determined by Chepstow-Lusty et al. (this vol.) and a revised foraminiferal datum from Karlin et al. (this vol.). Nannofossil datums are most numerous in the Pliocene and lowermost Pleistocene sections between and below the slumps. In all four holes, deposition rates in sections with pelagic deposition range between 30 and 50 m/m.y.

Shipboard chronostratigraphic control was poor in the short sections lying between the early and middle Pleistocene slumps (Fig. 2). The interval encompassing Cores 108-664D-11H and -12H has two datums; the interval encompassing Cores 108-662A-8H and -9H has none.

Stratigraphic control was generally somewhat better above the slumps. The *Pseudoemiliania lacunosa* extinction at 0.47 Ma (Thierstein et al., 1977) is observed at all sites, as is the oxidized layer at the sediment-water interface marking the Holocene. At Site 664, the Brunhes/Matuyama boundary and Jaramillo event were also determined, but no magnetic reversals were detected at Sites 662 and 663.

Additional Isotopic Stratigraphy

To supplement age control in the upper Pleistocene section of Hole 663A, we analyzed the planktonic foraminifer *Globigerinoides ruber* for $\delta^{18}\text{O}$ values across two intervals, one (4.5–8 mbsf) located about half-way between the top of Core 108-662A-1H and the *P. lacunosa* datum, and the other (22–32 mbsf) just above the uppermost slump (Fig. 2). All *G. ruber* analyses are based on the >330-m size fraction and were made with a Carousel-48 automatic carbonate preparation system attached to a Finnegan MAT-251 mass spectrometer. Calibration to the PDB standard is via the NBS-16, NBS-17, and NBS-20 standards.

¹ Ruddiman, W., Sarnthein, M., et al., 1989. Proc. ODP, Sci. Results, 108: College Station, TX (Ocean Drilling Program).

² Lamont-Doherty Geological Observatory, Palisades, NY 10964.

³ Present address: Ocean Drilling Program, 1000 Discovery Drive, College Station, TX 77840.

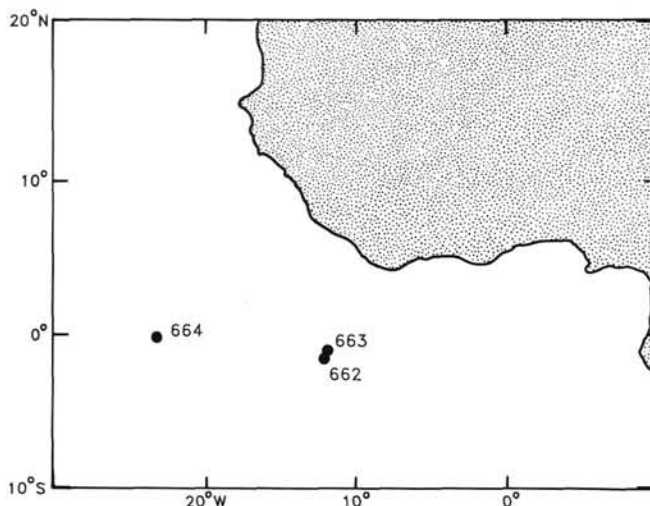


Figure 1. Locations of Leg 108 Sites 662, 663, and 664.

The $\delta^{18}\text{O}$ sequences are shown in Figure 3 and listed in Table 3. Both are correlative with the SPECMAP isotopic stratigraphy of Imbrie et al. (1984). The upper sequence begins in the lower part of isotopic stage 6, extends through stage 7, and ends at the stage 7/8 boundary. We selected the prominent heavy $\delta^{18}\text{O}$ event (7.4) in the lower-middle portion of interglacial stage 7 for time control.

The lower sequence begins in the upper part of isotopic stage 16, extends through stages 17–22, and ends in stage 23. All isotopic stages appear to correlate with the SPECMAP isotopic "stack" (Imbrie et al., 1984). The stage 18.4 event is stronger in our record than in the SPECMAP stack, but it is similar to the amplitude observed in several other high-resolution $\delta^{18}\text{O}$ records (Prell, 1982; Shackleton and Hall, 1983; Shackleton et al., 1984). From this sequence, we selected glacial event 16.2, interglacial event 19.1, and glacial event 22.4 for time datums. Depths and ages of these three isotopic events are listed in Table 2.

COMPOSITE DEPTH MODELS

We constructed two preliminary composite depth sections, one for eastern equatorial Atlantic Holes 662A and 663A, and the other for central equatorial Atlantic Holes 664B and 664D (Fig. 4). These sections rely on cores with undisturbed pelagic sedimentation and avoid slumps. There are intervals of time not represented in these composite sections: 0.8–1.4 Ma at combined Sites 662 and 663, and roughly 1.2–2.0 Ma and 2.4–2.5 Ma at Site 664.

There has been as yet no attempt to obtain continuous signals across core breaks by splicing into offset holes. Small discontinuities thus occur at each core break, probably averaging 25 cm or less (roughly 5,000–8,000 yr).

ANALYTICAL METHODS

The percentage of CaCO_3 was determined on 0.5-g sediment samples using the vacuum-gasometric method of Jones and Kaiteris (1983), with a precision of about 1%. The CaCO_3 values ranged from 55% to 90%. Duplicate analyses were run on all outlier values to verify the initial results.

Opal content was determined on 0.5-g sediment samples using the silica extraction technique of Mortlock and Froelich (in press), with a precision of 6% relative to the absolute value measured. The amount of silica measured is multiplied by 2.4 to convert to opal (incorporating water of hydration). Measured opal contents ranged from 0% to

Table 1. Site locations and depths.

Hole	Latitude	Longitude	Depth (mbfs)
662A	1°23.4' S	11°44.4' W	3824
663A	1°11.9' S	11°52.7' W	3708
664B	0°06.4' N	23°13.7' W	3817
664D	0°06.4' N	23°16.5' W	3812

12%, indicating precision errors of no more than 0.7%. Duplicate analyses were run on all outlier values to verify the initial results.

The percentage of nonbiogenic sediment was calculated as a residual by subtracting the percentage of CaCO_3 and the percentage of opal from the bulk sediment. Most nonbiogenic sediment is eolian dust from Africa. Some may be authigenic clays and minerals formed on the mid-Atlantic Ridge, as well as other ocean-derived sediments such as manganese micronodules. But shipboard smear-slide and X-ray diffraction (XRD) analyses (Ruddiman, Sarnthein, et al., 1988) indicate that such mineral types are rare. Thus, we call the nonbiogenic fraction the "terrigenous" sediment. It ranges from 4% to 43% of the total.

All percentage values of these three major sediment components are listed in Tables 4 (Hole 662A), 5 (Hole 663A), 6 (Hole 664B), and 7 (Hole 664D) at the end of this chapter.

RESULTS

We first present the downcore trends of the carbonate, opal, and terrigenous fractions. These form the basis for calculating changes in absolute fluxes across selected time intervals.

Percentage Trends

The percentage values of carbonate, opal, and terrigenous sediment during the late Pliocene and Pleistocene are shown in Figure 5 for the eastern equatorial Atlantic (Holes 662A and 663A) and in Figure 6 for the central equatorial Atlantic (Holes 664B and 664D). All sections were analyzed at 10-cm intervals, equivalent to average time steps ranging between 2000 and 3300 yr.

There are several major trends and features in these percentage records. One is a slow drift toward lower CaCO_3 and higher opal and terrigenous percentages over the entire 3.5 Ma, but most noticeably after about 2.6 Ma.

In addition, there are several more abrupt changes, including an important one in the late Pliocene. In the earliest part of each record, the sediment is almost exclusively CaCO_3 ooze, except for scattered weak pulses of lower CaCO_3 and higher opal and terrigenous values. Near 3.6–3.4 Ma and 3.0–2.9 Ma, a somewhat greater range of variation began to occur, with larger opal and terrigenous maxima and lower CaCO_3 minima.

A more fundamental change occurred between 2.6 and 2.4 Ma. Maximum values of opal and terrigenous dust began oscillatory increases as early as 2.6 Ma and reached very large values by 2.4 Ma (Figs. 5 and 6). The CaCO_3 minima oscillated toward progressively lower values over the same interval. These high-amplitude oscillations have persisted since the late Pliocene.

A second (more subtle) change is the progressive shift to weaker CaCO_3 maxima and terrigenous minima during the late Pleistocene, particularly after 0.47 Ma. The CaCO_3 minima and the terrigenous maxima do not, however, differ markedly from values in earlier sections.

The interpretation of percent data is ambiguous because changes in only one component in a closed system may create artifactual responses in the other components. The history of the change of each component requires the calculation of mass fluxes per unit time.

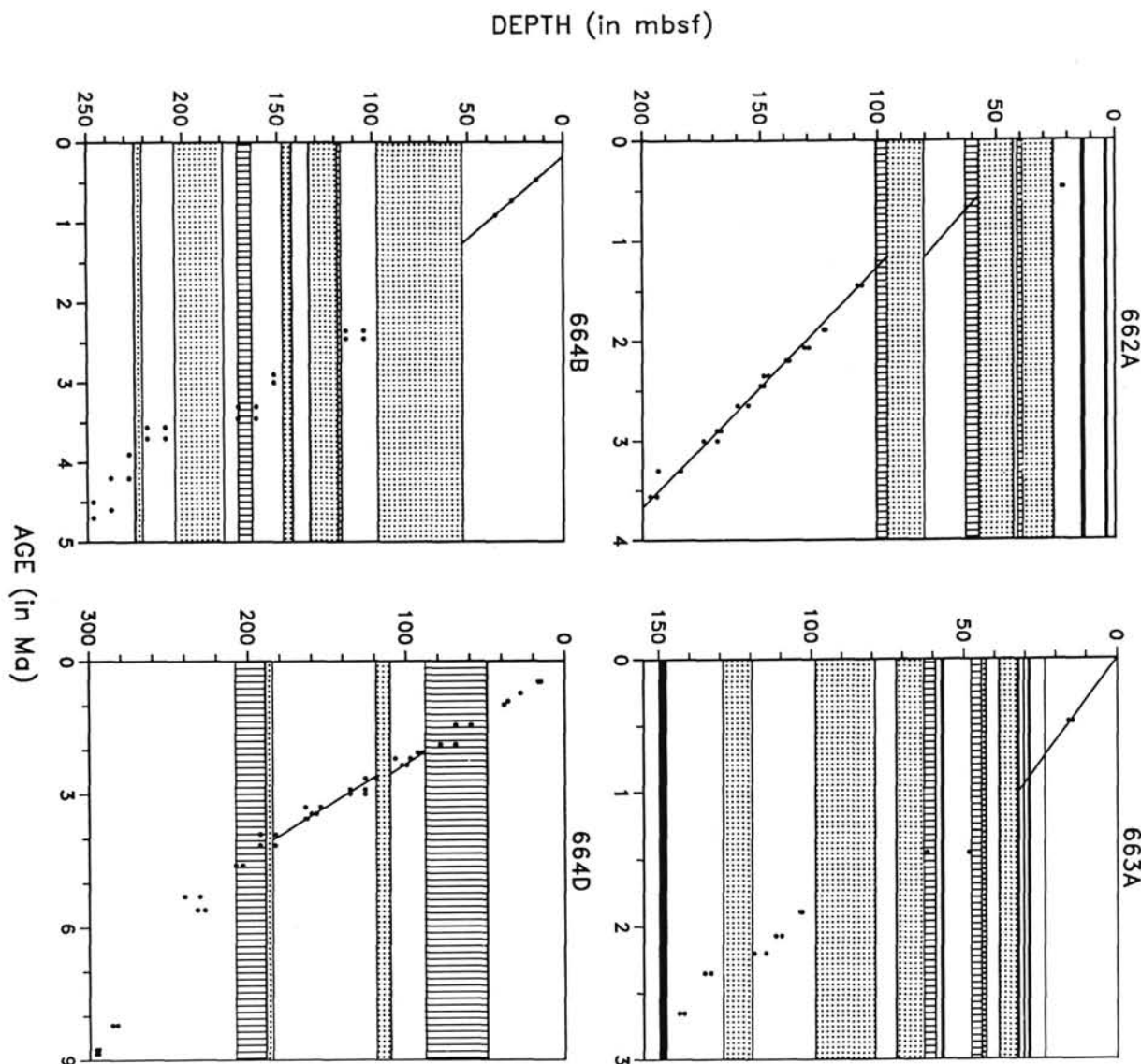


Figure 2. Age/depth plots for Holes 662A, 663A, 664B, and 664D. Datums are from Ruddiman, Sarnthein, et al. (1988), with revised datums at Hole 662A from Chepstow-Lusty et al. (this vol.). Turbidites are black; confirmed slumps are heavy dots; less disturbed sediments (slight tilting indicating slumping) shown by vertical ruling. Solid diagonal lines mark sections analyzed in this study.

Calculation of Long-Term Fluxes

Mass flux calculations require time control, and the chronologic datums chosen in turn define the maximum resolution at which flux changes can be meaningfully resolved. We list in Table 2 all datums used for our flux calculations. We retain all paleomagnetic and isotopic levels from the middle and late Pleistocene because their depths are closely fixed and their ages accurately known (Mankinen and Dalrymple, 1979; Imbrie et al., 1984).

For the two upper Pliocene sections, we omit several datums from shipboard and shore-based work in order to minimize errors in flux calculations. These errors become larger as the intervals over which fluxes are calculated become smaller, because the uncertainties involved (in fixing the

depths of the datums and in knowledge of their true ages) become larger fractions of the duration of the interval through which the fluxes are being calculated. By integrating over intervals considerably longer than these uncertainties, we minimize errors in the flux calculations.

Flux determinations require calculations of the form:

$$\begin{aligned} \text{(component mass flux)} &= \text{(fraction of component)} \\ &\times \text{(sedimentation rate)} \times \text{(dry-bulk density)} \\ [\text{g/cm}^2/\text{k.y.}] &= [\text{g/g}] \times [\text{cm/k.y.}] \times [\text{g/cm}^3] \end{aligned}$$

Sample-by-sample calculations of flux values are made, and all flux values lying between constraining time datums are averaged to calculate mean fluxes across that interval.

Table 2. Datum levels constraining flux calculations shown in Figures 7 and 8.

Hole	Depth (mbsf)	Age (m.y.)	Datum
662A	107.65	1.450	LO <i>Calcidiscus macintyreai</i>
662A	149.25	2.450	LO <i>Discoaster surculus</i>
662A	167.70	2.900	LO <i>Dentogloboquadrina alispira</i>
662A	195.30	3.560	LO <i>Reticulofenestra pseudoumbilicula</i>
663A	7.21	0.228	SPECMAP $\delta^{18}\text{O}$ Event 7.4
663A	15.15	0.470	LO <i>Pseudoeumiliania lacunosa</i>
663A	22.49	0.631	SPECMAP $\delta^{18}\text{O}$ Event 16.23
663A	26.99	0.734	SPECMAP $\delta^{18}\text{O}$ Event 19.1
663A	31.01	0.814	SPECMAP $\delta^{18}\text{O}$ Event 22.4
664B	14.00	0.470	LO <i>Pseudoeumiliania lacunosa</i>
664B	27.00	0.734	Brunhes/Matuyama Boundary
664B	35.50	0.900	Top Jaramillo Subchron
664D	89.60	2.070	FO <i>Discoaster triradiatus acme</i>
664D	102.40	2.350	LO <i>Discoaster pentaradiatus</i>
664D	135.30	3.000	LO <i>Sphaerodinellopsis seminulina</i>
664D	163.80	3.560	LO <i>Reticulofenestra pseudoumbilicula</i>
664D	182.80	3.900	LO <i>Globigerina nepenthes</i>

Note: Midpoints of range of uncertainty in depth placement of biostratigraphic datums were used. LO = last occurrence and FO = first occurrence.

Dry-bulk density (Dbd) is calculated as:

$$\text{Dbd} = \rho_{\text{sed}} (1 - \phi),$$

where ρ_{sed} is sediment grain density (taken as 2.65 g/cm³) and ϕ is the sediment porosity.

The sediment porosity is derived from:

$$\phi = \frac{(A \times W_d)/\rho_{\text{sw}}}{(A \times W_d) + (1 - W_d)(1 - A)} / \rho_{\text{sed}},$$

where A (1.03646) is a constant that converts pure water mass to seawater mass, W_d is dry water content (in g/g), and ρ_{sw} is the density of pore fluids, assumed to be seawater at 35 per mil salinity (1.02336 g/cm³).

Water content values for most samples were determined directly from samples taken on shipboard. Samples were stored in plastic vials refrigerated at 5°C, and then weighed, dried, and weighed again in the lab. Values for most samples are listed in Tables 4 through 7.

At Hole 662A, water-content values were lacking for a few samples in Core 108-662A-13H, and for a majority of samples in Cores 108-662A-21H and -22H. In these three cores, we averaged the available water-content measurements on a section-by-section basis in order to calculate average dry bulk densities per section and thus longer-term flux changes.

No laboratory water contents or bulk density values were made on samples from Cores 108-664D-15H through -19H. For the purposes of flux calculations, we assigned dry-bulk densities to each of these samples based on shipboard GRAPE measurements. We first calculated average bulk densities for each core using the 5 to 6 GRAPE values per core reported in Ruddiman, Sarnthein, et al. (1988). We next multiplied these averages by 1.06 to convert the GRAPE bulk densities to laboratory values. This conversion was based on a comparison of laboratory and GRAPE bulk densities over the interval 130–200 m of Hole 662A, through which mean bulk densities were nearly constant with little high-frequency variability. We then used these adjusted averages as dry-bulk densities for each sample in each core for the flux calculations.

Long-term flux trends for the eastern and central equatorial Atlantic are shown in Figures 7 and 8. The fluxes are

plotted as histograms of average values between constraining datum levels.

Gradual Flux Trends over the Last 3.5 m.y.

The long-term flux patterns (Figs. 7 and 8) confirm some, but not all, of the trends predicted by the percentage curves (Figs. 5 and 6). The flux of CaCO₃ was nearly constant through the Pliocene but decreased in the middle to late Pleistocene.

The mass fluxes of opal and terrigenous sediment increased from the late Pliocene into the early and middle Pleistocene, in basic agreement with the percentage data. Both fluxes, however, then decreased during the late Pleistocene. These decreases (not evident in the percent trends) are caused mainly by lower sedimentation rates (Figs. 7 and 8).

Abrupt Late Pliocene Flux Changes

Major opal and terrigenous flux changes occurred ~2.5 Ma (Figs. 7 and 8). Although it is difficult to pinpoint the age of these changes exactly due to uncertainties in depth placement and age of the chronostratigraphic datum levels, it is likely that the flux change is linked to the prominent late Pliocene changes in percentage values for opal and terrigenous dust previously noted. These percent changes occur well below datum levels dated to 2.35 Ma and just below a datum dated to 2.45 Ma, but above a datum dated to 2.65 Ma (Figs. 5 and 6). Linear interpolation suggests that this percentage change (and probably the flux change) began between 2.6 and 2.4 Ma, with a midpoint age of about 2.5 Ma. At Hole 664D, the major flux changes appear to occur within a short interval lost to slumping, but constrained between 2.35 and 2.65 Ma (Fig. 8). For the rest of this paper, we refer to these flux changes as occurring “near 2.5 Ma.”

Given the chronostratigraphic uncertainties, the flux of the dominant CaCO₃ component stayed roughly constant at both sites near 2.5 Ma (Figs. 7 and 8). As a result, sedimentation rates and total sediment fluxes remained nearly constant at both sites. In contrast, the mean accumulation rates of the smaller opal and terrigenous dust fractions increased markedly at this time. The average accumulation of opal increased by ~60%–70% at both sites, with the exact value depending on the intervals chosen as baselines for the calculations. The average accumulation of terrigenous dust increased by about 35% at Site 662 and 75% at Site 664.

Much of the actual late Pliocene flux increases probably occurred within the short pulses evident in the percent data (Figs. 5 and 6). If sedimentation rates over these short intervals stayed roughly linear as in well-dated late Pleistocene piston cores at these sites (Mix and Ruddiman, 1986; McIntyre et al., 1989), then the opal and terrigenous flux increases during these pulses may have been several times larger than the mean flux changes. Curry and Lohman (1986) suggested that terrigenous influxes to the Sierra Leone Rise at 3°–5°N increased by a factor of 2 or more during late Pleistocene glacial intervals.

For both the terrigenous and opal fractions, the flux change near 2.5 Ma may have had smaller precursors. The mean terrigenous flux appears to have increased slightly across datum boundaries at 2.9 Ma (Fig. 7) and 3.0 Ma (Fig. 8). At Site 664, the increase in mean opal percentages after about 3.0 Ma appears to indicate some increase in flux (Fig. 8). At this point, however, the time resolution is not sufficient to assess whether these are significant changes in accumulation rates.

Flux Changes during the Late Pleistocene

Additional flux changes are recorded during the late Pleistocene: large decreases in opal and terrigenous sediment occur, along with even larger decreases in CaCO₃ (Figs. 7 and

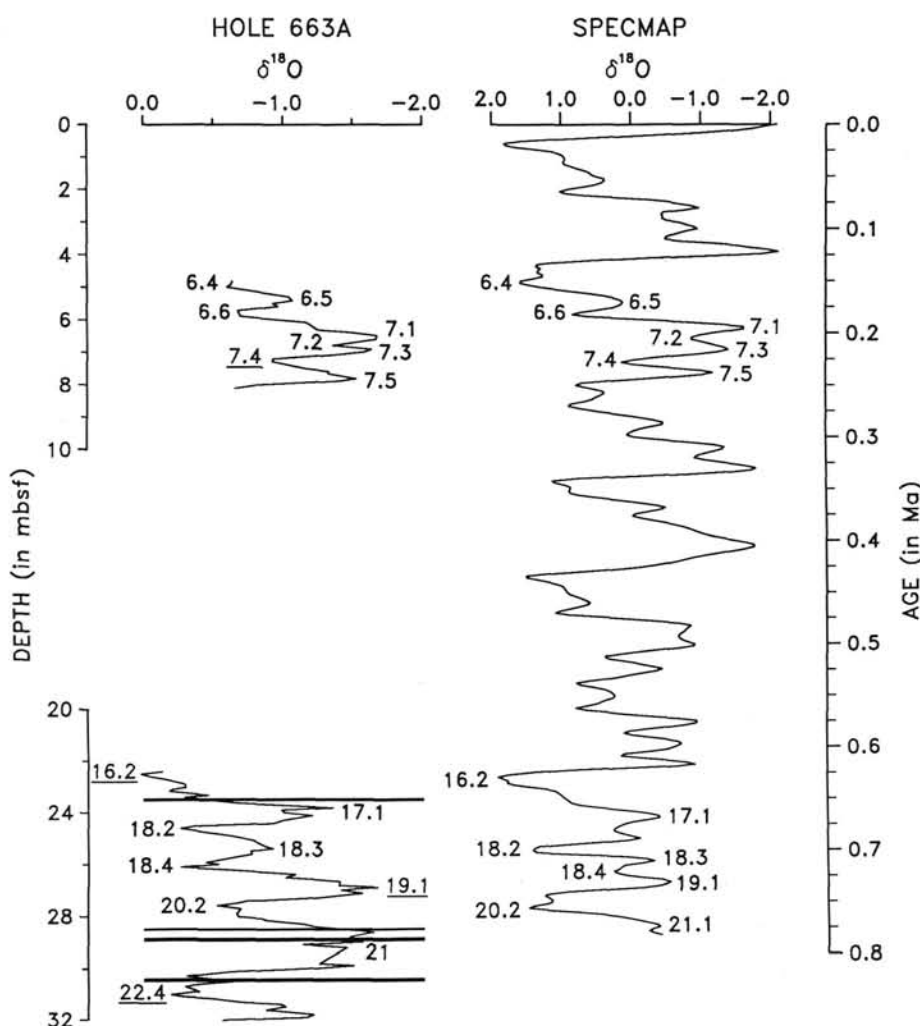


Figure 3. Oxygen isotopic ($\delta^{18}\text{O}$) record for middle Pleistocene and late Pleistocene sections from Hole 663A, using planktonic foraminifer *Globigerinoides ruber*. Major isotopic stages in Hole 663A are determined by correlation to the composite $\delta^{18}\text{O}$ record of SPECMAP from Imbrie et al. (1984), shown on the right with the age scale. Datums with asterisks in the Hole 663A record were used for time control in flux calculations. Thin solid horizontal lines are turbidites.

8). For the opal and terrigenous fractions, the flux changes appear to have begun prior to the *P. lacunosa* datum at (0.47 Ma) and to have continued to the present. For CaCO_3 , the flux change appears to have occurred mainly after 0.47 Ma.

Several problems make it difficult to determine whether the late Pleistocene flux changes shown in Figures 7 and 8 are indicative of real climatic change or are artifacts of complications specific to the locations of these sites. One complication results from combining records from different locations. Ideally, flux calculations should be specific to a single site and water depth.

The late Pleistocene flux changes at Site 664 are unequivocally determined, because the last million years or more of record is derived from a single hole (664B). In addition, splicing the late Pleistocene section from Hole 664B to the late Pliocene section from Hole 664D does not alter the fluxes: Holes 664B and 664D are located within 1000 m (lateral distance) and 5 m (water depth) of each other, and the mean sedimentation rates above the Jaramillo Subchron differ by only 1%.

This is not the case in the eastern equatorial Atlantic, where the numerous slumps forced us to combine the late

Pleistocene record from Site 663 with the late Pliocene and early Pleistocene record from Site 662. This introduces two potential complexities: (1) Site 663 was located in water 116 m shallower than Site 662, possibly causing weaker dissolution of upper Pleistocene sediments; (2) Site 663 had sedimentation rates about one-third lower than Site 662 during the latest Pleistocene, possibly causing lower fluxes.

We can reject the first of these possibilities. Because Site 663 is shallower than Site 662, it should have weaker depth-dependent dissolution and thus higher CaCO_3 fluxes during the late Pleistocene, opposite to the observed trend. This makes the observed decrease in CaCO_3 flux in the combined record all the more significant, whatever its cause.

We can also for the most part reject the second possibility. The sedimentation rate for the middle Pleistocene (0.81–0.47 Ma) section of Site 663 is 46 m/m.y., slightly larger than the 42 m/m.y. average for the late Pliocene portion of Site 662 (Figs. 2 and 7). Thus, the shift from Site 662 to 663 (and from Hole 664B to 664D) across the middle Pleistocene slumps introduces no decrease, and in fact a small increase, in sedimentation rates and fluxes in the uppermost Matuyama and lowermost Brunhes Chrons (Figs. 7 and 8). Switching sites

Table 3. Middle Pleistocene oxygen-isotopic data from the planktonic foraminifer *Globigerinoides ruber* (>250- μm size fraction) at Hole 663A, relative to PEE DEE Belemnite.

Core, section, interval (cm)	Depth (mbsf)	$\delta^{18}\text{O}$ (‰)
108-663A-2H-1, 11	4.81	-0.64
108-663A-2H-1, 21	4.91	-0.63
108-663A-2H-1, 29	4.99	-0.60
108-663A-2H-1, 59	5.29	-1.04
108-663A-2H-1, 71	5.41	-1.07
108-663A-2H-1, 79	5.49	-0.93
108-663A-2H-1, 89	5.59	-0.97
108-663A-2H-1, 101	5.71	-0.68
108-663A-2H-1, 119	5.89	-0.70
108-663A-2H-1, 131	6.01	-0.98
108-663A-2H-1, 139	6.09	-1.17
108-663A-2H-2, 11	6.31	-1.25
108-663A-2H-2, 19	6.39	-1.49
108-663A-2H-2, 29	6.49	-1.68
108-663A-2H-2, 41	6.61	-1.67
108-663A-2H-2, 59	6.79	-1.36
108-663A-2H-2, 71	6.91	-1.64
108-663A-2H-2, 79	6.99	-1.59
108-663A-2H-2, 89	7.09	-1.36
108-663A-2H-2, 101	7.21	-0.93
108-663A-2H-2, 119	7.29	-0.93
108-663A-2H-2, 131	7.51	-1.17
108-663A-2H-2, 139	7.59	-1.33
108-663A-2H-2, 146	7.66	-1.33
108-663A-2H-3, 11	7.81	-1.53
108-663A-2H-3, 19	7.89	-1.40
108-663A-2H-3, 29	7.99	-0.86
108-663A-2H-3, 41	8.11	-0.66
108-663A-3H-6, 71	22.41	-0.13
108-663A-3H-6, 79	22.49	0.02
108-663A-3H-6, 89	22.59	-0.04
108-663A-3H-6, 101	22.71	-0.16
108-663A-3H-6, 119	22.89	-0.29
108-663A-3H-6, 131	23.01	-0.30
108-663A-3H-6, 139	23.09	-0.20
108-663A-3H-6, 146	23.16	-0.18
108-663A-3H-7, 11	23.31	-0.46
108-663A-3H-7, 19	23.39	-0.29
108-663A-3H-7, 29	23.49	-0.95
108-663A-3H-7, 41	23.61	-0.65
108-663A-4H-1, 11	23.81	-1.35
108-663A-4H-1, 19	23.89	-0.98
108-663A-4H-1, 29	23.99	-1.00
108-663A-4H-1, 41	24.11	-1.20
108-663A-4H-1, 59	24.29	-0.99
108-663A-4H-1, 71	24.41	-0.92
108-663A-4H-1, 79	24.49	-0.38
108-663A-4H-1, 89	24.59	-0.26
108-663A-4H-1, 119	24.89	-0.62
108-663A-4H-1, 131	25.01	-0.73
108-663A-4H-1, 137	25.07	-0.78
108-663A-4H-2, 11	25.31	-0.87
108-663A-4H-2, 19	25.39	-0.92
108-663A-4H-2, 29	25.49	-0.76
108-663A-4H-2, 41	25.61	-0.77
108-663A-4H-2, 59	25.79	-0.57
108-663A-4H-2, 71	25.91	-0.44
108-663A-4H-2, 79	25.99	-0.53
108-663A-4H-2, 89	26.09	-0.26
108-663A-4H-2, 101	26.21	-0.59
108-663A-4H-2, 119	26.39	-1.08
108-663A-4H-2, 131	26.51	-1.01
108-663A-4H-2, 139	26.59	-1.24
108-663A-4H-2, 146	26.66	-1.40
108-663A-4H-3, 11	26.81	-1.39
108-663A-4H-3, 19	26.89	-1.67
108-663A-4H-3, 29	26.99	-1.41
108-663A-4H-3, 41	27.11	-1.56
108-663A-4H-3, 59	27.29	-1.22
108-663A-4H-3, 71	27.41	-0.73
108-663A-4H-3, 79	27.49	-0.67
108-663A-4H-3, 89	27.59	-0.52
108-663A-4H-3, 101	27.71	-0.69

Table 3 (continued).

Core, section, interval (cm)	Depth (mbsf)	$\delta^{18}\text{O}$ (‰)
108-663A-4H-3, 119	27.89	-0.66
108-663A-4H-3, 131	28.01	-0.67
108-663A-4H-3, 139	28.09	-0.84
108-663A-4H-3, 146	28.16	-0.87
108-663A-4H-4, 11	28.31	-1.14
108-663A-4H-4, 19	28.39	-1.20
108-663A-4H-4, 29	28.49	-1.42
108-663A-4H-4, 41	28.61	-1.64
108-663A-4H-4, 59	28.79	-1.47
108-663A-4H-4, 71	28.91	-1.54
108-663A-4H-4, 79	28.99	-1.56
108-663A-4H-4, 89	29.09	-1.13
108-663A-4H-4, 101	29.21	-1.45
108-663A-4H-5, 11	29.81	-1.25
108-663A-4H-5, 19	29.89	-1.50
108-663A-4H-5, 29	29.99	-1.23
108-663A-4H-5, 41	30.11	-0.63
108-663A-4H-5, 59	30.29	-0.30
108-663A-4H-5, 71	30.41	-0.14
108-663A-4H-5, 79	30.49	-0.65
108-663A-4H-5, 89	30.59	-0.40
108-663A-4H-5, 101	30.71	-0.29
108-663A-4H-5, 119	30.89	-0.39
108-663A-4H-5, 119	30.89	-0.39
108-663A-4H-5, 131	31.01	-0.19
108-663A-4H-5, 139	31.09	-0.28
108-663A-4H-5, 146	31.16	-0.48
108-663A-4H-6, 11	31.31	-0.70
108-663A-4H-6, 19	31.39	-0.97
108-663A-4H-6, 29	31.49	-1.01
108-663A-4H-6, 41	31.61	-0.87
108-663A-4H-6, 59	31.79	-1.21
108-663A-4H-6, 71	31.91	-1.16
108-663A-4H-6, 79	31.99	-0.56
108-663A-4H-6, 89	32.09	-0.75
108-663A-4H-6, 101	32.21	-1.05

does not appear to be the origin of the late Pleistocene flux decreases.

Despite these arguments, we remain uncertain that the calculated late Pleistocene flux changes are typical of the equatorial Atlantic divergence region. This uneasiness derives mainly from the fact that the late Pleistocene decrease in sedimentation rate (along with higher water contents) is the main factor driving the decreased fluxes of all three sediment components (Figs. 7 and 8). Simultaneous decreases in all three sediment fractions could coincidentally occur for climatic reasons, but they also could be a warning that there are complications from local factors. The major decrease in sedimentation rates occurs above the *P. lacunosa* datum (0.47 Ma), and the central question is whether these decreases are real or represent local anomalies.

All three equatorial sites lie in local basins receiving more sediment than the surrounding topographic highs. Except for obvious slumps and turbidites, most of this sediment is probably transported by very slow particle-by-particle redistribution of otherwise "pelagic"-looking sediment, a process active in many portions of the Mid-Atlantic Ridge system. If this local redistribution for some reason decreased at both sites during the late Pleistocene, the fluxes to these core sites would also diminish, but not because of a decreased input of CaCO_3 , opal, and terrigenous dust from surface waters.

Similar decreases in mean sedimentation rates occurred above the *P. lacunosa* datum at Site 663 (30%), Hole 664B (40%), and Hole 664D (26%). The comparably large decreases imply that such a trend may be broadly typical of the equatorial Atlantic. On the other hand, the mean (turbidite-free) sedimentation rate at Site 662 above the *P. lacunosa* datum

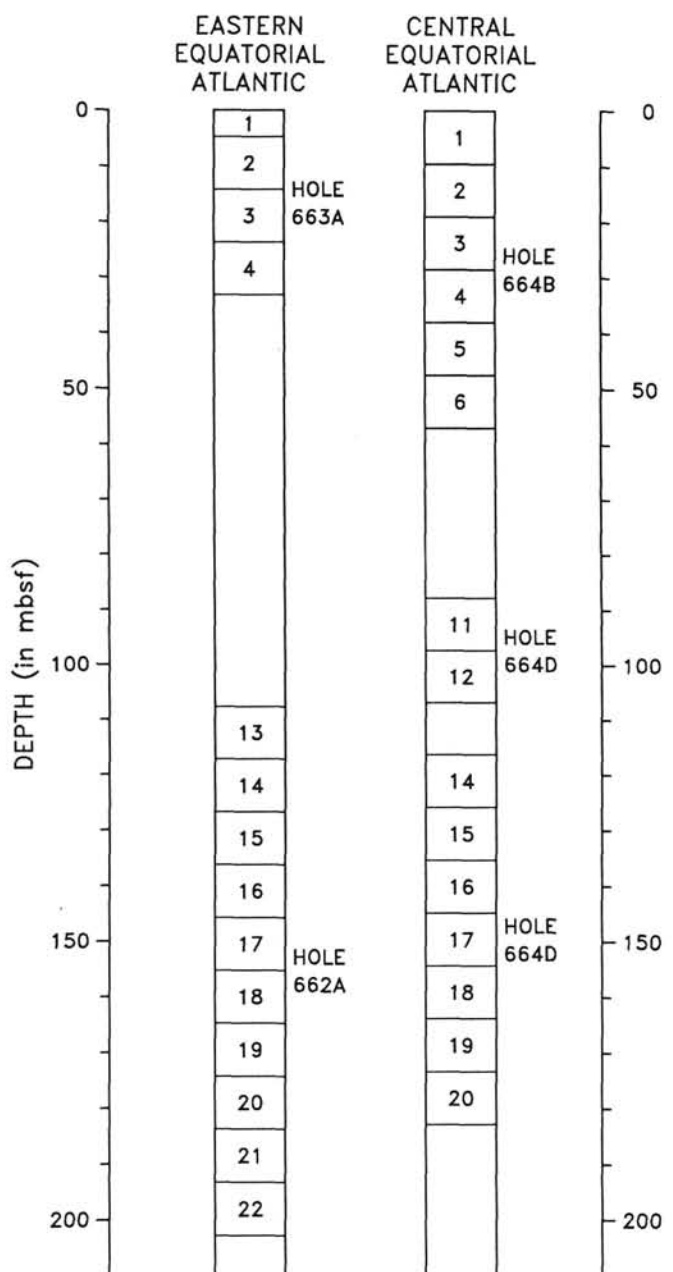


Figure 4. Composite depth sections for eastern equatorial Atlantic Sites 662/663 (combined) and for central equatorial Atlantic Site 664 (Holes 664B/664D). All depths shown in meters are in ODP sub-bottom depth units (from Ruddiman, Sarnthein, et al., 1988). Core numbers indicated in middle of depth sections. Sections disturbed by slumping are left blank.

(47 m/m.y.) remained much higher than that at the other sites and was also higher than the late Pliocene rate at Site 662 (Fig. 2).

All flux studies ultimately face this same problem. Are the observed flux changes characteristic of the region as a whole, or do they merely indicate the local response of a subset of cores in response to sediment redistribution on the sea floor? Determining the correct possibility would require a study of many sites and of high-resolution seismic records to eliminate local effects, and no other ODP sites exist near the equator in the Atlantic Ocean to address this question. At Leg 108 sites along the African margin, sedimentation rates in the last 1

m.y. either stayed constant or increased (Ruddiman, Sarnthein, et al., 1988), although previously reported DSDP sites farther to the north along the African margin had reduced rates in the late Pleistocene (e.g., Stein and Sarnthein, 1984).

We remain uncertain whether the decreases in sedimentation rate along the equator after 0.47 Ma should be regarded as a regionally typical trend or as local anomalies. This in turn leaves unclear whether the late Pleistocene flux decreases in CaCO_3 , opal, and terrigenous sediment (Figs. 7 and 8) are regionally representative.

DISCUSSION

We review here possible explanations for three trends evident in the percentage and flux data (Figs. 5–8): (1) the relatively abrupt late Pliocene increases in opal and terrigenous dust near 2.5 Ma; (2) the less abrupt late Pleistocene decreases in all components during the last 0.7–0.4 m.y.; and (3) the slow background trends spanning all or most of the last 3.7 m.y.

Late Pliocene Increase in Opal Flux

Opal preservation in sea-bed sediments is a function mainly of opal productivity in surface waters (Broecker and Peng, 1982; Pokras and Molfino, 1986). Silica derived from oceanic production dominates the opal signals derived here, with opal from sponge spicules and from freshwater diatoms and other continental sources orders of magnitude less abundant (Pokras and Mix, 1985; Stabell, 1986).

Our flux data argue for an increase in mean opal productivity of ~60%–70% in the equatorial Atlantic near 2.5 Ma (Figs. 7 and 8). It is likely that the increases were much larger during episodic high-opal pulses that began at that time and have continued subsequently. In contrast, mean CaCO_3 productivity appears to have remained constant near 2.5 Ma, to within the error of our estimates (Figs. 7 and 8).

These trends suggest two changes along the equator near 2.5 Ma. First, overall productivity (CaCO_3 plus opal) appears to have increased slightly (Figs. 7 and 8). Second, the data imply a shift toward silica productivity, suggesting some combination of higher silica content of upwelled waters and greater advection of silica-rich water at or below the surface. Studies of modern sediment traps (Dymond and Lyle, 1985) and of late Pleistocene CaCO_3 and opal fluxes (Lyle et al., 1988) show that CaCO_3 and opal components may have weakly related or even opposed productivity trends on a seasonal and long-term basis because of shifts from one kind of productivity to another. Without exception, however, silica deposition today is concentrated in regions of high overall productivity. We thus infer that a major net productivity increase occurred at the equator near 2.5 Ma.

Stronger equatorial productivity implies stronger upwelling along the equator, which in turn suggests that the trade winds became stronger and/or more zonal on a periodic basis after 2.5 Ma. A similar change has been proposed to explain late Pleistocene changes in sea-surface temperature and marine diatom deposition in the equatorial Atlantic (Gardner and Hays, 1976; Mix et al., 1986; Pokras, 1987; McIntyre et al., 1989).

It is also possible that there was an increase in the silica and nutrient content of the waters being upwelled. This implies shoaling of silica-rich South Atlantic Central Waters and/or upper Antarctic Intermediate Water or increased northward penetration of waters from circumantarctic sources. Increased advection from the south has also been proposed for the late Pleistocene (Gardner and Hays, 1976;

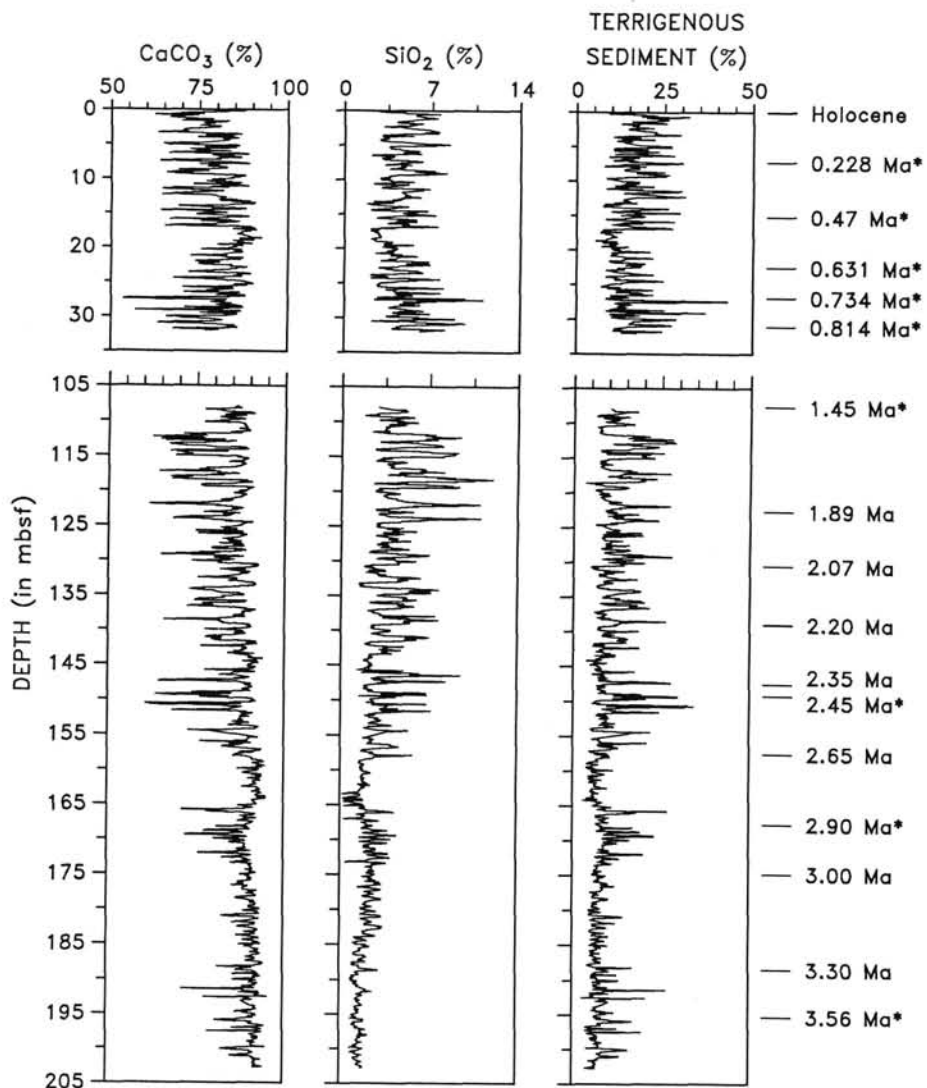


Figure 5. Weight-percent of CaCO_3 , opal, and terrigenous sediment vs. sub-bottom depth in Pliocene-Pleistocene sections at Holes 662A and 663A. Ages and levels of chronostratigraphic datums used in flux calculations indicated by asterisks on right.

Labracherie, 1980; Mix et al., 1986; Pokras, 1987; McIntyre et al., 1989).

The fact that the late Pliocene change in opal flux along the equator (Figs. 5–8) is relatively abrupt and dates to near 2.5 Ma points to two (probably interrelated) explanations. The change may be associated with the initial development of Northern Hemisphere ice sheets, which attained sufficient size to send ice rafted sediment to the Atlantic just prior to 2.4 Ma (Backman, 1979; Shackleton et al., 1984; Curry and Miller, this vol.). Conceivably, the appearance of ice sheets might have altered Northern Hemisphere winter circulation and caused upwelling of opal along the equator.

Upwelling could be enhanced along the equator in Northern Hemisphere winter either by increased trade-wind strength or by a more southerly position of the Intertropical Convergence Zone (ITCZ), but opinions on this are mixed. Gardner and Hays (1976) inferred that Northern Hemisphere winter trade winds intensified during glaciations, but Parkin and Padgham (1975) interpreted eolian grain-size data as evidence that they weakened. Nicholson and Flohn (1980) hypothesized a southward displacement of the ITCZ in glacial

winters, but Gardner and Hays (1976) inferred no significant change in its position. Mix et al. (1986) inferred that the mean annual position of the ITCZ over the Atlantic may have been farther south during the last deglaciation.

The general circulation model (GCM) experiments to date (without ocean upwelling) also do not point to systematic direct impacts of ice sheets on trade winds over the equatorial Atlantic (summarized in Ruddiman et al., this vol.). Additional GCM experiments with interactive oceans that include upwelling would be needed to test whether the appearance of Northern Hemisphere ice sheets could affect equatorial upwelling during Northern Hemisphere winter. In any case, neither GCM experiments nor data observations at this point provide strong evidence for winter circulation changes due to ice sheets as the cause of increased opal fluxes.

Alternatively, the increased opal flux may be associated with prominent changes in circumantarctic circulation near 2.5 Ma, including a shift to colder radiolarian faunas in the southwest Atlantic sector of the Antarctic (Cieselski and Grinstead, 1986; Mead et al., 1988). These changes in antarctic sea-surface temperature (SST) and presumably in antarctic

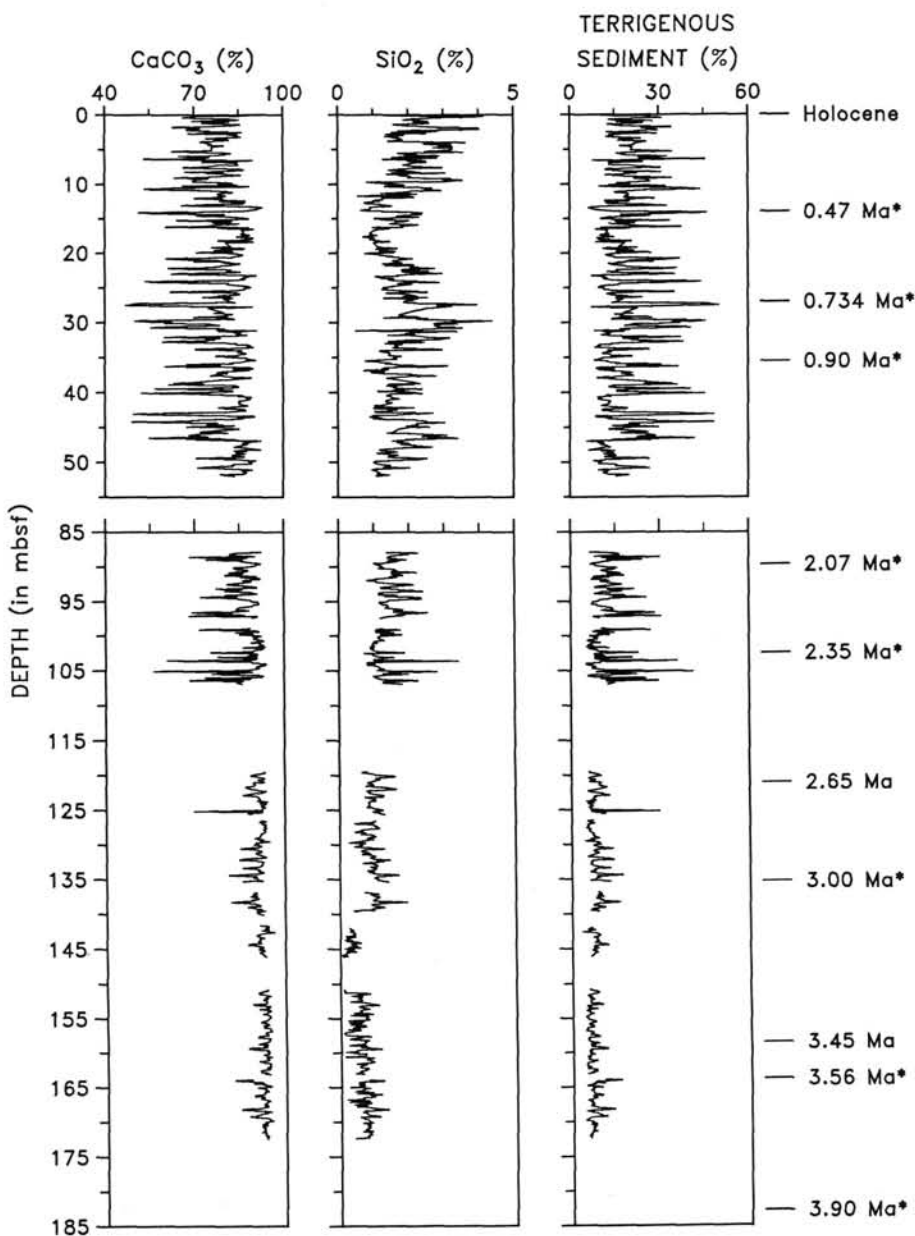


Figure 6. Weight-percent of CaCO_3 , opal, and terrigenous sediment vs. sub-bottom depth in Pliocene-Pleistocene sections at Holes 664B and 664D. Ages and levels of chronostratigraphic datums used in flux calculations indicated by asterisks on right.

sea ice could effect equatorial Atlantic upwelling and SST by altering southern trade winds and northward advection (Gardner and Hays, 1976; Mix et al., 1986; McIntyre et al., 1989). In addition, changes in circumantarctic circulation could have increased the silica content of Antarctic Intermediate Water and South Atlantic Central Water, which upwell near the equator. Ultimately, the Southern Ocean circulation changes may still have been driven by Northern Hemisphere ice sheets (Cieselski and Grinstead, 1986; Mead et al., 1988).

Southern Hemisphere control of atmospheric circulation over the equatorial Atlantic is also consistent with variations at annual and orbital time scales. Because the thermal equator in the Atlantic lies in the Northern Hemisphere throughout the year, modern ocean temperatures at the equator follow the Southern Hemisphere pattern (August cooler than February). During the last 200,000 yr, equatorial

Atlantic and subantarctic sea-surface responses had similar phasing and high coherences at the 23,000-yr orbital precession period, suggesting that the equatorial Atlantic response has been at least in part forced from the circumantarctic (McIntyre et al., 1989).

Previously published data on long-term opal trends in the tropical Atlantic are from coastal regions and have been explained by different mechanisms. Using semiquantitative smear-slide analyses, Stein and Sarnthein (1984) noted the appearance of opal after 3.2 Ma at Deep Sea Drilling Project (DSDP) sites from the northwest African margin, and Stein (1985a) put the major increase at Site 397 at 2.55 Ma. This was attributed either to (1) increased coastal upwelling due to stronger trade winds in northern summer, or (2) increased fluvial delivery of nutrients as a result of shifts in coastline position due to sea-level changes.

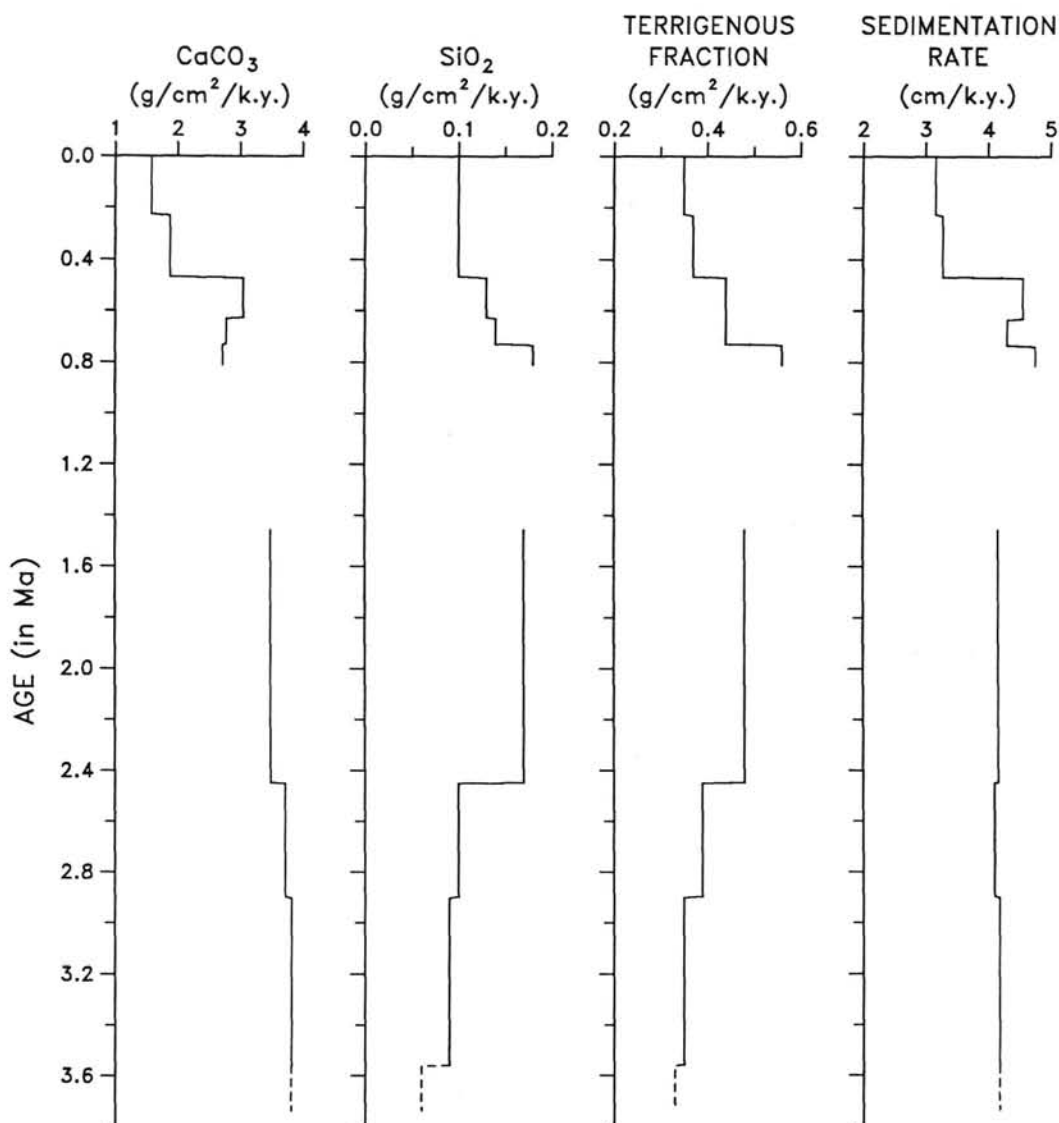


Figure 7. Mass fluxes of CaCO_3 , opal, and terrigenous sediment in the eastern equatorial Atlantic (Holes 662A and 663A). Bar graphs indicate average fluxes between datum levels used as absolute time constraints. Dashed lines show fluxes calculated by downward extrapolation of sedimentation rates in overlying layer. The dotted line shows alternative calculation of late Pleistocene fluxes using sedimentation rates from Hole 662A in place of Hole 663A.

Late Pliocene Increase in Terrigenous Dust Flux

Winds are the primary transporting agent of terrigenous sediments to Sites 662, 663, and 664. This conclusion is based on comparing the late Pleistocene total terrigenous fluxes (Figs. 7 and 8) against the late Pleistocene fluxes of the eolian component isolated by Janecek (1985) in nearby equatorial Atlantic piston cores (Fig. 9). The flux numbers for both data sets are in the same range (350–460 $\text{mg}/\text{cm}^2/\text{k.y.}$).

The dominant dust sources for these sites lie north of the equator, and the dust is carried southwestward in the winter dust plume. Southern Hemisphere sources have previously been proposed as more important along the equator, because the ITCZ was thought to form a barrier to dust from the north (Fütterer, 1978; Sarnthein et al., 1982; Stein, 1985a). Modern dust-induced "haze" patterns, however, show that measurable southern-source haze does not reach the equator, whereas northern dust reaches south of the equator in winter over the

easterly and central Atlantic (McDonald, 1938; Prospero, 1981). The northward increase of average eolian mass fluxes during the last 300,000 yr (Fig. 9) also clearly identifies North Africa as the main long-term dust source for Atlantic sediments along the equator.

Prospero (1981) summarized dust injection and transport in the modern winter-haze plume. Dust is injected into the lower and middle troposphere at altitudes of 1.5–7 km by winter storms in the Sahel. The mean flow toward the west-southwest at these altitudes carries dust far out over the equatorial Atlantic between latitudes 0° and 20°N , with measurable haze reaching the coast of South America just north of the equator. The ultimate barrier to southward dust transport is the moist ITCZ, the lower boundary of which lies at a mean position of 3° – 5°N in winter; however, the ITCZ slopes upward gradually to the south, allowing dust transport well south of the equator at altitudes of 1.5–3 km (see Prospero, 1981, fig. 11). We thus infer that dust delivery to Sites 662, 663, and 664 has mainly

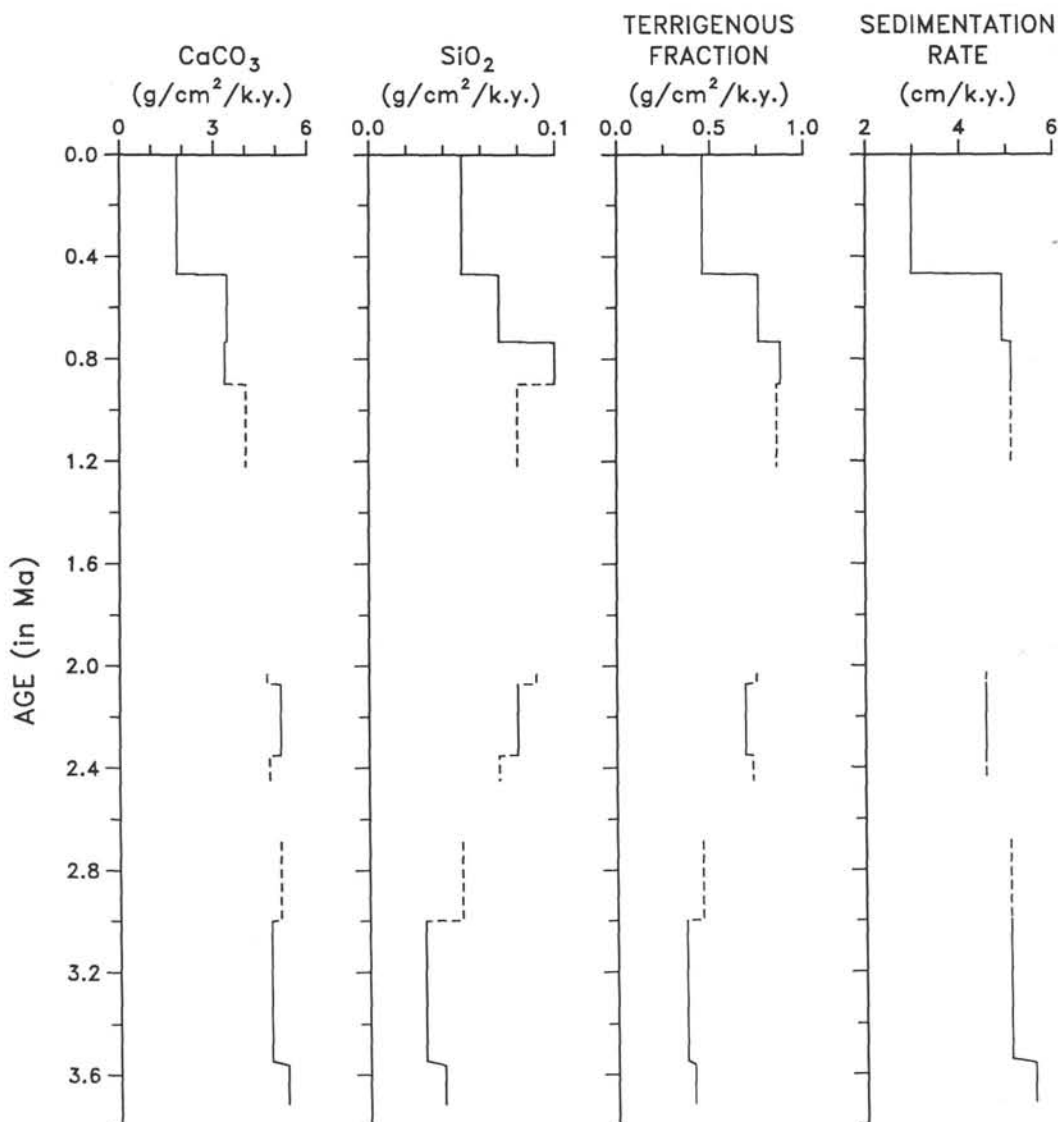


Figure 8. Mass fluxes of CaCO_3 , opal, and terrigenous sediment in the central equatorial Atlantic (Holes 664B and 664D). Bar graphs indicate average fluxes between datum levels used as absolute time constraints. Dashed lines are estimated fluxes for interval without constraining datum levels at both ends; for these intervals, sedimentation rates are extrapolated from adjacent interval.

occurred in the winter plume at altitudes above 1.5 km from sources in the Sahel and southern Sahara.

Thus, our records (Figs. 5–8) indicate relatively abrupt increases in the magnitude of oscillatory pulses of dust influx from North Africa to the equatorial Atlantic between 2.6 and 2.4 Ma. Two factors may be involved in these changes: (1) increased dust availability due to changes in moisture balance in the source areas and (2) increased winter-plume dust transport to the equator by altered atmospheric circulation.

Today, rain in the Sahelian and southern Saharan source regions for the winter dust plume falls entirely in Northern Hemisphere summer. This rainfall occurs in connection with a component of the southern winter trade-wind flow that crosses the equator and turns northeastward into Africa in a monsoonal circulation. To increase aridity in the Sahel and thus enhance winter-plume dust fluxes, this meridional flow of moisture into Africa would have to weaken. Such a change is consistent with the increased zonal component of southern trade-wind flow along the equator needed to explain the

increased opal flux after 2.5 Ma; the two changes suggest a redirection from meridional toward zonal flow. The oscillatory fluxes of both dust and opal suggest, however, that this configuration was not permanent; intervening wetter intervals occurred (apparently at frequencies lying within the orbital band) and probably replenished the soils that formed the basic dust supply during more arid intervals.

Evidence from East Africa also indicates increased aridity during this same late Pliocene interval. Pollen-bearing lake and fluvial sediments, dated by interbedded volcanicogenic deposits, indicate a shift toward cyclical high-elevation cooling and low-elevation aridity between 2.52 and 2.38 Ma, with aridity cycles continuing through the rest of the Pliocene and into the Pleistocene (Bonnefille, 1983, 1985). East African antelope and micromammal taxa also changed to types indicative of drier climates between 2.52 and 2.38 Ma (Vrba, 1985; Wesselman, 1985). The full geographical extent of Sahelian aridification near 2.5 Ma is not known; dated deposits from the western and central Sahel do not exist.

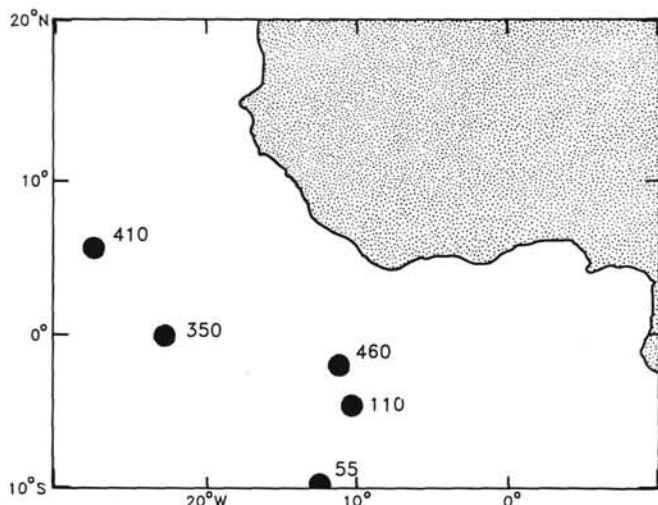


Figure 9. Late Pleistocene (0–0.25 Ma) mass fluxes ($\text{g}/\text{cm}^2/\text{k.y.}$) of eolian sediment in five equatorial Atlantic piston cores (from Janecek, 1985).

The timing of the increase in dust delivery near 2.5 Ma implies a causal link to the appearance of Northern Hemisphere ice sheets. As noted above, the direct effects of ice sheets on northern trade-wind strength or ITCZ position in the tropics are possible, but unproven.

A more credible case can be made that ice sheets had some influence on moisture balances in Africa. The greater southward extent of dunes in the southern Sahara during the last glacial maximum (Sarnthein, 1978) may indicate that ice sheets imposed a glacial tempo on African aridity; however, the very large increase in dune extent since 6000 yr ago argues that factors other than Northern Hemisphere ice sheets must be involved in these aridity cycles. Pokras and Mix (1985), studying phytolith abundances in marine cores, detected a southward shift of the grass belt along the West African coast 18,000 yr ago, as part of a longer-term glacial/interglacial tempo of aridity near the African coast over the last 150,000 yr.

A GCM experiment (Joussaume and Sadourny, 1987) predicted a doubling (relative to today) of the annual average dust deposited along the equator in the Atlantic during late Pleistocene glacial maxima due mainly to drier source areas and increased convective activity in the Sahel. Thus, changes in glacial boundary conditions during the late Pliocene may have enhanced aridification along at least the coastal regions of West Africa, and this aridification may have increased winter-plume dust fluxes from these areas to the equatorial Atlantic.

Other evidence argues, however, that the extent of glacial aridification of Africa is not large, and that an entirely different tempo of aridity dominates much of the interior of North Africa. Pokras and Mix (1985, 1987) found that winter-plume transport of diatoms from freshwater lakes in the Sahel during the late Pleistocene occurred mainly at the 23,000-yr period of orbital precession, rather than at the 100,000-yr period that dominates ice-volume change. This indicates that aridity cycles in central Africa occurred mainly at the precessional period, consistent with lake-level data and GCM results suggesting the dominance of precessional insolation forcing (Kutzbach, 1981; Kutzbach and Street-Perrott, 1985).

Evidence from sediments in the Niger delta indicates that the highest freshwater discharge during the last 20,000 yr occurred between 13,000 and 4500 yr ago (Pastouret et al., 1978), which is basically the tempo of aridity indicated by

precessional insolation forcing rather than that predicted by glacial/interglacial changes. This suggests that even the western parts of the Sahel lying within the Niger basin were influenced mainly by insolation forcing of monsoon strength.

It seems plausible that the northern summer cooling of the central Sahara caused by the combined effects of ice sheets, high-latitude SST, and CO_2 (Ruddiman et al., this vol.) would have been sufficient to reduce the strength of the monsoonal inflow into Africa and thus enhance aridification. Most GCM studies, however, find negligible changes in moisture flux to the interior between glacial and modern-day climates (summary in Ruddiman et al., this vol.).

Because cycles of aridity in most of central Africa thus had little resemblance to rhythms of ice-sheet variation during the late Pleistocene, ice sheets apparently had little influence on the moisture balance in these regions within the orbital band. This suggests that direct ice-sheet effects do not explain the more fundamental change in aridity in North African source areas of winter-plume dust near 2.5 Ma.

As suggested earlier, circulation changes in the Southern Ocean may have been the intermediary between the "first cause" (initial appearance of Northern Hemisphere ice sheets) and the ultimate result (changes in atmospheric circulation near the equator). To some extent, the geographic pattern of changes in dust fluxes supports this idea. The large dust-flux increase near 2.5 Ma is recorded at all sites under the winter dust plume (Sites 662 and 664 from this paper; Sierra Leone Rise Site 366 reported by Stein, 1985b), but it does not appear in any of the sites under the summer dust plume farther north (Site 659 in Tiedemann et al., this vol.; Site 397 in Stein, 1985a; and Site 141 in Stein, 1986). This suggests that the strongest aridity changes near 2.5 Ma were registered in source regions tapped by the winter but not the summer dust plume. The most likely such regions lie in the southernmost Sahel, which by geographic proximity suggest a connection to the circulation changes in the equatorial Atlantic.

We do not, however, suggest that changes over the equatorial Atlantic caused those over Africa. The synchronous changes in both regions are interpreted as different parts of a common response to changes imposed via the Southern Ocean.

Late Pleistocene Decrease in Carbonate

For all discussions of late Pleistocene flux changes, we assume that the reduced accumulation rates of carbonate, opal, and terrigenous sediment are due to climate-induced changes in the delivery of these components and not to local factors that affect sediment redistribution.

Average CaCO_3 fluxes decreased by more than half at both equatorial sites after 0.47 Ma (Figs. 7 and 8). Stein and Sarnthein (1984) detected similar decreases in CaCO_3 accumulation at several DSDP sites in the eastern subtropical Atlantic. The CaCO_3 percentages decrease at most Leg 108 sites (Ruddiman, Sarnthein, et al., 1988), but higher sedimentation rates at some sites may offset the lower CaCO_3 percentages. In any case, a late Pleistocene decrease in long-term average CaCO_3 fluxes appears to be characteristic of deeper tropical Atlantic sites.

The cause of this apparent flux decrease in the late Pleistocene is not clear. Leg 108 shipboard studies did not detect worsening preservation in the late Pleistocene, but observations are too widely spaced to be definitive. Curry and Lohman (1986) found that dissolution reduced CaCO_3 accumulation in Sierra Leone Rise cores below 3951 m, but it only affected cores above 3527 m during extreme intervals. Gardner (1975) found little dissolution in cores as deep as 3750 m. Thus, Sites 662, 663, and 664 lie in the depth range (3708–3824

m) at which late Pleistocene dissolution has been found to become significant.

Studies of late Pleistocene $\delta^{13}\text{C}$ trends in deep Atlantic cores have shown that the formation of deep water in the North Atlantic was suppressed during glaciations (Boyle and Keigwin, 1985). As a result, waters of southern (antarctic) origin moved farther northward in the western Atlantic, bringing higher nutrient and CO_2 concentrations and a greater capacity for dissolving CaCO_3 to the equatorial Atlantic region (Oppo and Fairbanks, 1987).

Deep basins in the eastern equatorial Atlantic were affected by southern-source waters passing eastward through deep fracture zones (Curry and Lohman, 1986). These changes predict strong CaCO_3 dissolution at the equator in the late Pleistocene, driven largely at the 100,000-yr and 41,000-yr tempo of Northern Hemisphere ice sheets (Boyle and Keigwin, 1985; Mix and Fairbanks, 1985). Longer-term $\delta^{13}\text{C}$ records, however, indicate that the greatest suppression of northern-source waters may have occurred between 0.85 and 0.4 Ma (Ruddiman et al., in press; Raymo et al., in press), prior to the large decrease in CaCO_3 flux observed here.

Curry and Lohman (1986) also found that CaCO_3 productivity in surface waters near the Sierra Leone Rise decreased by a factor of 2 or more during late Pleistocene glacial stages. Thus, both productivity suppression and dissolution may have been factors in decreased CaCO_3 fluxes in the late Pleistocene (see also Pfleiderer, 1986).

Late Pleistocene Decrease in Opal

Mean opal fluxes at both equatorial sites decreased by around half over the last 0.8 m.y., reaching the lowest levels in the last 2.5 m.y. (Figs. 7 and 8). These flux decreases preceded those of the carbonate fraction by several hundred thousand years. If these flux decreases are not artifacts of local sediment redistribution, they imply a return part of the way toward the climatic regime that prevailed prior to 2.5 Ma, with weaker equatorial upwelling. This in turn implies a weaker zonal component of the southern trade-wind flow along the equator during Northern Hemisphere summer.

Despite the mean decrease in opal flux, however, strong percentage variations continued, suggesting that the change in opal flux was not registered by a complete cessation of the periodic opal pulses that began at 2.5 Ma (Figs. 5 and 6). Because of the dominant influence of the CaCO_3 fluxes on the oscillating percentage trends, it is impossible to infer anything about the tempo of decreasing opal fluxes at higher frequencies.

Two factors may have altered opal fluxes between 0.8 and 0.4 Ma. Forcing by Northern Hemisphere ice sheets is a possibility, because this is the interval during which they changed from smaller variations at 41,000 yr to larger 100,000-yr variations (Pisias and Moore, 1981; Prell, 1982; Ruddiman et al., 1986). Forcing from the Southern Hemisphere is also possible; significant changes in radiolarian and foraminifer faunas in subantarctic sediments have been reported for this interval, but these changes have been variously interpreted as a shift toward periodically warmer intervals (Keay and Kennett, 1972) or as a long-term cooling (Hays, 1967). In view of this disagreement, it is premature at this time to try to link the apparent late Pleistocene change in equatorial opal fluxes to changes in the high latitudes of the Southern Hemisphere.

Stein (1985a) noted a decreased opal flux at Site 397 on the northwest African margin after 0.5 Ma (see also results from Site 658 in Tiedemann et al., this vol.). Stein noted that this change could be attributed either to reduced fluvial delivery of nutrients due to aridification of northwest Africa or to a lower silica content of upwelled waters. As noted earlier, opal fluxes

along the continental margin are probably controlled by factors different from those along the equator.

Late Pleistocene Decrease in Terrigenous Dust

Terrigenous dust fluxes decreased by as much as half in the last 0.7 m.y. at both equatorial locations (Figs. 7 and 8). If the decreases are real, they require either reduced dust availability in tropical North Africa or reduced transport to the equatorial Atlantic.

In general, evidence from North Africa favors increasing aridity over the last 0.7 m.y. Dupont et al. (this vol.) found a trend toward pollen taxa indicative of increasingly arid glacio- and interglacials during the last 0.5 m.y. Tiedemann et al. (this vol.) found slowly increasing influxes of siliciclastic sediment during the same interval, suggesting slowly increasing aridity over Sahelian Africa (see also Stein, 1985b). Thus, the basic late Pleistocene trend in Africa appears to be toward greater aridity. This should enhance dust fluxes unless the climate becomes one of continually hyperarid conditions; the late Pleistocene alternations observed between wetter and drier climates (Street-Perrott and Harrison, 1984) argue against continual hyperaridity. Thus, evidence for long-term aridification of Africa opposes the decreased winter-plume dust fluxes after 0.47 Ma.

There is scattered evidence suggesting that aridification is not the only long-term trend in Africa during the late Pleistocene. Oscillatory increases in the accumulation of terrestrial organic carbon, clay, and feldspar at Site 658 have been interpreted as indications of periodically increased influxes of river sediments (Stein et al., this vol.; Tiedemann et al., this vol.). These alternated with evidence of increased aridity, suggesting that the amplitude of cycles of aridity and humidity increased in the late Pleistocene. Jansen et al. (1984) found intervals of lower accumulation rates of terrigenous sediment on the Zaire Fan during the last 350,000 yr and noted that one possible interpretation is a shift to more humid climates in the Zaire basin in south equatorial Africa. At present, there are too few land-based records to characterize aridity trends in Africa over the last 500,000 yr.

Another possibility is that changes in atmospheric circulation diminished the influence of the winter dust plume at the equator by redirecting the dust flux somewhat farther north. Siliciclastic fluxes increased during the late Pleistocene in the low-resolution record at Site 660, which is located within the winter dust plume (Tiedemann et al., this vol.). This could indicate a partial redirection of the winter dust plume away from the equator.

As with the late Pleistocene opal fluxes discussed above, the ultimate explanations for the decreased terrigenous dust fluxes may lie in changes of Northern Hemisphere ice volume, with more immediate control by changes in circumantarctic circulation.

Gradual Flux Trends over the Last 3.5 M.Y.

There are three factors that could contribute to the very gradual trends over the last 3.5 m.y.: (1) plate tectonics, (2) seafloor subsidence, and (3) tectonic uplift.

Over long time intervals, the northward drift of the Atlantic seafloor due to plate tectonics can impact fluxes to equatorial Atlantic sediments (Stein, 1985b). The rate of motion has been estimated at about 0.25° of latitude (25 km) per m.y. (Slater et al., 1977). Over the last 3.5 m.y., however, this effect should be small, because less than 1° of plate motion has occurred beneath the relatively gentle lateral gradients in surface-ocean productivity (EQUALANT, 1973), biosiliceous deposition (Pokras and Molino, 1986), and atmospheric dust load (Prospero, 1981).

Seafloor subsidence (Slater et al., 1977) could lead to gradual increases in dissolution and reduced fluxes of CaCO_3 at these sites. The age of the crust under all three equatorial sites is about 10 Ma. Subsidence curves predict a total of roughly 1000 m of total seafloor deepening, with about 200 m in the last 3.5 m.y. The major decrease in CaCO_3 flux occurs in the youngest part of the record when subsidence was slowest, but subsidence might still be a factor if the most recent increases in depth led to initial contact with the top of the lysocline.

Tectonic uplift can also effect long-term trends, as summarized in the paleoenvironmental synthesis (Ruddiman et al., this vol.). There is ample evidence for a large-scale uplift of the Tibetan Plateau during the late Cenozoic, with as much as a doubling of mean elevation during the last 5 m.y. (Mercier et al., 1987). The GCM experiments show that Tibetan uplift not only increases the strength of the monsoon circulation in India and Asia (Manabe and Terpstra, 1974), but it also causes substantial increases in aridity over northern and eastern Africa (Kutzbach et al., in press).

Thus, the gradual uplift of Tibet predicts a slow increase in aridity in northern and eastern Africa, and probably in the central Sahara region as well (Ruddiman et al., this vol.). This increase in aridity may contribute to the slow background increase in percentages of terrigenous dust visible at both equatorial sites (Figs. 5 and 6). It is also consistent with the slowly increasing accumulation rate of terrigenous dust at both sites from 3.6 to 0.8 Ma (Figs. 7 and 8), but not with the rather abrupt decrease since that time. The steady long-term increase in dust fluxes is also visible at Leg 108 sites in the summer dust plume farther north (Tiedemann et al., this vol.).

The lack of a really persuasive background increase in dust flux at Site 664 (and perhaps Site 662) prior to about 2.5 Ma may also have a tectonic explanation. The uplift experiments predict an increase in moisture in tropical western Africa and the southwestern Sahel (see the paleoenvironmental synthesis in Ruddiman et al., this vol.). Increased moisture in this part of the winter-plume source area may have offset the drying underway elsewhere in North Africa.

SUMMARY

The mean flux of opal at equatorial Atlantic Sites 662 and 664 increased abruptly by 60%–70% near 2.5 Ma, with stronger increases during shorter-term pulses of opal deposition. This increase suggests the initiation of a periodically stronger zonal component of southern trade-wind flow along the equator during Southern Hemisphere winter. This change in circulation may be ultimately linked to the appearance of Northern Hemisphere ice sheets, but it is probably driven via the intermediary of major circulation changes in the Southern Ocean.

The mean flux of winter-plume dust from North Africa also increased abruptly (by 35%–75%) near 2.5 Ma, with shorter pulses of stronger influx also evident since that time. This increase suggests periodically increased aridity and dust availability in North African source areas for winter-plume dust, possibly accompanied by periodically increased transport by low-level easterly winds. Increased aridity in winter-plume source areas implies a weaker meridional monsoonal flow into Africa during the Northern Hemisphere summer, consistent with the stronger zonal flow of southern trade winds deduced from opal deposition.

The decreased deposition of CaCO_3 , opal, and terrigenous dust after 0.8 Ma may be an artifact of changes in local sediment redistribution or may reflect changes in deep-water flow, equatorial winds and surface-water productivity, and African aridity, respectively.

A slow background increase in the deposition of terrigenous dust during the late Pliocene and early-middle Pleis-

tocene may reflect gradual aridification of northern and eastern Africa due to the slow uplift of Tibet and the consequent alteration of low-level and upper easterly winds.

ACKNOWLEDGMENTS

We thank Wayne Riley, Linda Baker, and Pat Malone for laboratory work; Christina Hardy for data entry; Ann Esmay for data analysis and figure plotting; Flip Froelich, Connie Sancetta, and Peter Demenocal for in-house manuscript review; and Michael Sarnthein and an anonymous reviewer for other reviews. This research was funded partly from USSAC proposal TAMRF PO #77351 and partly from Grant OCE-8608238 from the Marine Geology and Geophysics Program of the National Science Foundation. This is Lamont-Doherty Geological Observatory Contribution No. 4403.

REFERENCES

- Backman, J., 1979. Pliocene biostratigraphy of DSDP Sites 111 and 116 from the North Atlantic Ocean and the age of Northern Hemisphere Glaciation. *Stockholm Contrib. Geol.*, 32:115–137.
- Bonnefille, R., 1983. Evidence for a cooler and drier climate in the Ethiopian Highlands towards 2.5 m.y. ago. *Nature*, 303:487–491.
- _____, 1985. Evolution of the continental vegetation: the paleobotanical record from East Africa. *S. Afr. J. Sci.*, 81:267–270.
- Boyle, E. A., and Keigwin, L. D., 1985. Comparison of Atlantic and Pacific paleochemical records for the last 215,000 years: changes in deep ocean circulation and chemical inventories. *Earth Planet. Sci. Lett.*, 76:135–150.
- Broecker, W. S., and Peng, T.-H., 1982. *Tracers in the Sea*. Palisades, NY (Eldigio Press).
- Ciesielski, P. F., and Grinstead, G. P., 1986. Pliocene variations in the position of the antarctic convergence in the southwest Atlantic. *Paleoceanography*, 1:197–232.
- Curry, W. B., and Lohman, G. P., 1986. Late Quaternary carbonate sedimentation at the Sierra Leone Rise (eastern equatorial Atlantic Ocean). *Mar. Geol.*, 70:223–250.
- Dymond, J., and Lyle, M., 1985. Flux comparisons between sediments and sediment traps in the eastern tropical Pacific: implications for atmospheric CO₂ variations during the Pleistocene. *Limnol. Oceanogr.*, 30:699–712.
- EQUALANT, 1973. In *Oceanographic Atlas, EQUALANT I and EQUALANT II* (Vol. II: Physical Oceanography): Paris (UNESCO).
- Fütterer, D., 1978. Late Neogene silt at the Sierra Leone Rise (Leg 41 Site 366): terrigenous and biogenous components. In Lancelot, Y., Seibold, E., et al., *Init. Repts. DSDP*, 41: Washington (U.S. Govt. Printing Office), 1049–1059.
- Gardner, J. V., 1975. Late Pleistocene carbonate dissolution cycles in the eastern equatorial Atlantic. In Sliter, W. V., Bé, A.W.H., and Berger, W. H. (Eds.), *Dissolution of Deep-Sea Carbonates*. Spec. Publ., Cushman Found. Foraminiferal Res., 13:129–141.
- Gardner, J. V., and Hays, J. D., 1976. Responses of sea-surface temperature and circulation to global climatic change during the past 200,000 years in the eastern equatorial Atlantic ocean. In Cline, R. M., and Hays, J. D. (Eds.), *Investigation of Late Quaternary Paleoceanography and Paleoclimatology*. Mem. Geol. Soc. Am., 145:221–247.
- Hays, J. D., 1967. Quaternary sediments of the Antarctic Ocean. *Prog. Oceanogr.*, 4:117–131.
- Imbrie, J., Hays, J. D., Martinson, D. G., McIntyre, A., Mix, A., Morley, J. J., Pisias, N. G., Prell, W. L., and Shackleton, N. J., 1984. The orbital theory of Pleistocene climate: support from a revised chronology of the marine $\delta^{18}\text{O}$ record. In Berger, A. L., Imbrie, J., Hays, J., Kukla, G., and Saltzman, B. (Eds.), *Milankovitch and Climate* (Pt. 1). Dordrecht (D. Reidel), 269–305.
- Janecek, T. R., 1985. The Brunhes record of terrigenous (eolian) input into the equatorial Atlantic Ocean. *Geol. Soc. Am., Abstr. Annu. Meet.*, p. 618.
- Jansen, J. H. F., van Weering, T. C. E., Gieles, R., and van Iperen, J., 1984. Middle and late Quaternary oceanography and climatology of the Zaire-Congo Fan and the adjacent eastern Angola Basin. *Neth. J. Sea Res.*, 17:201–249.
- Jones, G. A., and Kaiteris, P., 1983. A vacuum-gasometric technique for rapid and precise analysis of calcium carbonate in sediments and soils. *J. Sediment. Petrol.*, 53:655–660.

- Joussaume, S., and Sadourny, R., 1987. Desert dust and climate: investigation using an atmospheric general circulation model. In NATO Advanced Research Workshop Paleoclimatology and Paleometeorology, Abstr. of Proceedings.
- Kean, J., and Kennett, J. P., 1972. Pliocene-early Pleistocene paleoclimatic history recorded in antarctic-subantarctic deep-sea cores. *Deep-Sea Res.*, 19:529-548.
- Kutzbach, J. E., 1981. Monsoon climate of the early Holocene: climatic experiment using the earth's orbital parameters for 9000 years ago. *Science*, 214:59-61.
- Kutzbach, J. E., Guetter, P., Prell, W. L., and Ruddiman, W. F., in press. The sensitivity of climate to late Cenozoic uplift of the Tibetan and Colorado Plateaus: numerical experiments. *J. Geophys. Res.*
- Kutzbach, J. E., and Street-Perrott, F. A., 1985. Milankovitch forcing of fluctuations in the level of tropical lakes from 18 to 0 kyr BP. *Nature*, 317:130-134.
- Labracherie, M., 1980. Les radiolaires témoins de l'évolution hydrologique depuis le dernier maximum glaciaire au large de Cap Blanc (Afrique du Nord-Ouest). *Palaeogeogr., Palaeoclimatol., Palaeoecol.*, 32:163-184.
- Lyle, M., Murray, D. W., Finney, B. P., Dymond, J., Robbins, J. M., and Brooksforce, K., 1988. The record of late Pleistocene biogenic sedimentation in the eastern tropical Pacific Ocean. *Paleoceanography*, 3:39-60.
- Manabe, S., and Terpstra, T. B., 1974. The effects of mountains on the general circulation of the atmosphere as identified by numerical experiments. *J. Atmos. Sci.*, 31:3-42.
- Mankinen, E. A., and Dalrymple, G. B., 1979. Revised geomagnetic polarity time-scale for the interval 0-5 m.y. *B.P. J. Geophys. Res.*, 84:615-626.
- McDonald, W. F., 1938. *Atlas of Climatic Charts of the Oceans*. Washington (Dept. of Agriculture, Weather Bureau).
- McIntyre, A., Ruddiman, W. F., Karlin, K., and Mix, A. C., 1989. Surface water response of the equatorial Atlantic Ocean to orbital forcing. *Paleoceanography*, 4:19-55.
- Mead, G. A., Hodell, D. A., and Cieselski, P. F., 1988. Southern Ocean response to the onset of Northern Hemisphere glaciation at 2.4 Ma. *Geol. Soc. Am., Abstr. Annu. Meet.*, p. A252.
- Mercier, J.-L., Armijo, R., Tapponnier, P., Carey-Gailhardis, E., and Lin, H. T., 1987. Change from late Tertiary compression to Quaternary extension in southern Tibet during the India-Asia collision. *Tectonics*, 6:275-304.
- Mix, A. C., and Fairbanks, R. G., 1985. North Atlantic surface-ocean control of Pleistocene deep-ocean circulation. *Earth Planet. Sci. Lett.*, 73:231-243.
- Mix, A. C., and Ruddiman, W. F., 1986. Structure and timing of the last deglaciation: oxygen-isotope evidence. *Quat. Sci. Rev.*, 4:59-108.
- Mix, A. C., Ruddiman, W. F., and McIntyre, A., 1986. Late Quaternary paleoceanography of the tropical Atlantic, I: spatial variability of annual mean sea-surface temperatures, 0-20,000 yr B.P. *Paleoceanography*, 1:43-66.
- Mortlock, R. A., and Froelich, P. M., in press. A simple method for the rapid determination of biogenic opal in deep-sea sediments. *Deep-Sea Res.*
- Nicholson, S. E., and Flohn, H., 1980. African environmental and climatic changes and the general atmosphere circulation in late Pleistocene and Holocene. *Clim. Change*, 2:313-348.
- Oppo, D., and Fairbanks, R. G., 1987. Variability in the deep and intermediate water circulation of the Atlantic Ocean during the past 25,000 years: Northern Hemisphere modulation of the Southern Ocean. *Earth Planet. Sci. Lett.*, 86:1-15.
- Parkin, D. W., and Padgham, R. C., 1975. Further studies on trade winds during the glacial cycles. *Proc. Trans. R. Soc. London, Ser. A*, 346:245-260.
- Pastouret, L., Chamley, H., Delibrias, G., Duplessy, J. C., and Thiede, J., 1978. Late Quaternary climatic changes in western tropical Africa deduced from deep-sea sedimentation off the Niger delta. *Oceanol. Acta*, 1:217-232.
- Pflaumann, U., 1986. Sea-surface temperatures during the last 750,000 years in the eastern equatorial Atlantic: planktonic foraminiferal record of "Meteor" cores 13519, 13521, and 16415. *Meteor Forschungsergebnisse, Reihe C*, 40:137-161.
- Pisias, N. G., and Moore, T. C., 1981. The evolution of Pleistocene climate: a time series approach. *Earth Planet. Sci. Lett.*, 52:450-458.
- Pokras, E. M., 1987. Diatom record of late Quaternary climatic change in the eastern equatorial Atlantic and tropical Africa. *Paleoceanography*, 2:273-286.
- Pokras, E. M., and Mix, A. C., 1985. Eolian evidence for spatial variability of late Quaternary climates in tropical Africa. *Quat. Res.*, 24:137-149.
- _____, 1987. Earth's precession cycle and Quaternary climatic change in tropical Africa. *Nature*, 326:486-487.
- Pokras, E. M., and Molfino, B., 1986. Oceanographic control of diatom abundances and species distributions in surface sediments of the tropical and southeast Atlantic. *Mar. Micropaleontol.*, 10:165-188.
- Prell, W. L., 1982. Oxygen and carbon isotope stratigraphy for the Quaternary of Hole 502B: evidence for two modes of isotopic variability. In Prell, W. L., Gardner, J. V., et al., *Init. Repts. DSDP*, 68: Washington (U.S. Govt. Printing Office), 455-464.
- Prospero, J. M., 1981. Arid regions as sources of mineral aerosols in the marine environment. In Pewe, T. L. (Ed.), *Desert Dust: Origins, Characteristics, and Effects on Man*. Geol. Soc. Am., Spec. Pap., 186:71-86.
- Raymo, M. E., Ruddiman, W. F., Backman, J., Clement, B. M., and Martinson, D. G., in press. Late Pliocene variation in Northern Hemisphere ice sheets and North Atlantic deep circulation. *Paleoceanography*.
- Ruddiman, W. F., Raymo, M. E., and McIntyre, A., 1986. Matuyama 41,000-yr cycles: North Atlantic Ocean and Northern Hemisphere ice sheets. *Earth Planet. Sci. Lett.*, 80:117-129.
- Ruddiman, W. F., Raymo, M. E., Martinson, D. G., Clement, B. M., and Backman, J., in press. Pleistocene evolution of Northern Hemisphere climate. *Paleoceanography*.
- Ruddiman, W. F., Sarnthein, M., et al., 1988. *Init. Repts. ODP*, 108: College Station, TX (Ocean Drilling Program).
- Sarnthein, M. S., 1978. Sand deserts during glacial maximum and climatic optimum. *Nature*, 272:43-46.
- Sarnthein, M., Thiede, J., Pflaumann, U., Erlenkeuser, H., Fütterer, D., Koopman, B., Lange, H., and Seibold, E., 1982. Atmospheric and oceanic circulation patterns off northwest Africa during the past 25 million years. In von Rad, U., Hinz, K., Sarnthein, M., and Seibold, E. (Eds.), *Geology of the Northwest African Continental Margin*: Berlin-Heidelberg-New York (Springer-Verlag), 545-604.
- Sclater, J. G., Hellinger, S., and Tapscott, C., 1977. The paleobathymetry of the Atlantic Ocean from the Jurassic to the Recent. *J. Geol.*, 85:509-522.
- Shackleton, N. J., and Hall, M. A., 1983. Stable isotope record of Hole 504 sediments: high resolution record of the Pleistocene. In Cann, J., Langseth, M., et al., *Init. Repts. DSDP*, 69: Washington (U.S. Govt. Printing Office), 431-441.
- Shackleton, N. J., Backman, J., Zimmerman, H., Kent, D. V., Hall, M. A., Roberts, D. G., Schnitker, D., Baldau, J. G., Desprairies, A., Homrighausen, R., Huddlestun, P., Keene, J. B., Kaltenback, A. J., Krumsiek, K.A.O., Morton, A. C., Murray, J. W., and Westberg-Smith, J., 1984. Oxygen isotope calibration of the onset of ice rafting: history of glaciation in the North Atlantic region. *Nature*, 307:620-623.
- Stabell, B., 1986. Variations of diatom flux in the eastern equatorial Atlantic during the last 400,000 years ("Meteor" cores 13519 and 13521). *Mar. Geol.*, 72:305-323.
- Stein, R., 1985a. Late Neogene changes of paleoclimate and paleoproductivity off northwest Africa (DSDP Site 397). *Palaeogeogr., Palaeoclimatol., Palaeoecol.*, 49:47-59.
- _____, 1985b. The post-Eocene sediment record of DSDP Site 366: implications for African climate and plate tectonic drift. *Mem. Geol. Soc. Am.*, 163:305-315.
- _____, 1986. Late Neogene evolution of paleoclimate and paleoceanic circulation in the Northern and Southern Hemispheres—a comparison. *Geol. Rundsch.*, 75:125-138.
- Stein, R., and Sarnthein, M., 1984. Late Neogene events of atmospheric and oceanic circulation offshore northwest Africa: high-resolution record from deep-sea sediments. *Palaeoecol. Afr.*, 16:9-36.
- Street-Perrott, F. A., and Harrison, S. P., 1984. Temporal variations in lake levels since 30,000 yr B.P.—an index of the global

- hydrological cycle. In Hansen, J. E., and Takahashi, T. (Eds.), *Climate Processes and Sensitivity*: Washington (American Geophysical Union). Geophys. Monogr. Ser., 29:118–129.
- Thierstein, H. R., Geitzenauer, K. R., Molfino, B., and Shackleton, N. J., 1977. Global synchrony of late Pleistocene coccolith datum levels: validation by oxygen isotopes. *Geology*, 5:400–404.
- Vrba, E. S., 1985. African Bovidae: evolutionary events since the Miocene. *S. Afr. J. Sci.*, 81:263–266.
- Wesselman, H. B., 1985. Fossil micromammals and indicators of climatic change about 2.4 m.y. ago in the Omo Valley, Ethiopia. *S. Afr. J. Sci.*, 81:260–261.

Date of initial receipt: 2 March 1988

Date of acceptance: 12 February 1989

Ms 108B-165

Table 4 Percentages of carbonate, opal, and terrigenous fraction, and dry-bulk densities at Hole 662A.

Core, section, interval (cm)	Depth (mbsf)	CaCO ₃ (%)	SiO ₂ (%)	Terrigenous fraction (%)	Dry-bulk density (g/cm ³)
108-662A-13H-1, 29	107.98	86.6	3.0	10.4	0.87
108-662A-13H-1, 41	108.11	85.6	3.3	11.1	
108-662A-13H-1, 50	108.20	87.6			
108-662A-13H-1, 59	108.29	84.6	4.0	11.4	1.05
108-662A-13H-1, 71	108.41	77.1	5.1	17.9	0.95
108-662A-13H-1, 79	108.48	81.1	4.7	14.2	0.84
108-662A-13H-1, 89	108.58	81.7	5.2	13.1	1.08
108-662A-13H-1, 101	108.70	83.0	5.0	12.0	0.98
108-662A-13H-1, 110	108.79	85.3			
108-662A-13H-1, 117	108.86	89.7	3.0	7.3	1.01
108-662A-13H-1, 131	109.01	91.0	2.7	6.3	1.02
108-662A-13H-1, 139	109.08	83.6	2.9	13.5	0.84
108-662A-13H-1, 146	109.16	82.6	1.8	15.6	1.03
108-662A-13H-2, 11	109.31	88.7	3.2	8.1	0.94
108-662A-13H-2, 19	109.39	84.4	5.2	10.4	0.80
108-662A-13H-2, 29	109.48	81.3	5.7	13.0	0.94
108-662A-13H-2, 41	109.61	83.5	4.6	11.9	1.04
108-662A-13H-2, 50	109.70	87.0			
108-662A-13H-2, 59	109.79	88.4	3.0	8.6	1.11
108-662A-13H-2, 71	109.91	85.9	4.3	9.8	1.05
108-662A-13H-2, 79	109.98	81.2	4.8	13.9	0.86
108-662A-13H-2, 89	110.08	81.8	4.3	13.9	1.02
108-662A-13H-2, 101	110.20	77.1	6.0	17.0	1.02
108-662A-13H-2, 110	110.29	86.7			
108-662A-13H-2, 119	110.39	87.3	3.8	8.9	1.04
108-662A-13H-2, 131	110.51	88.3	3.7	8.0	1.13
108-662A-13H-2, 139	110.58	88.5	5.1	6.5	0.82
108-662A-13H-3, 146	110.66	88.1	4.2	7.7	1.02
108-662A-13H-3, 11	110.81	88.8	3.4	7.7	1.02
108-662A-13H-3, 19	110.89	88.5	3.8	7.7	0.82
108-662A-13H-3, 29	110.98	89.2	3.5	7.3	0.98
108-662A-13H-3, 41	111.11	88.5	3.5	8.0	1.25
108-662A-13H-3, 50	111.20	86.8			
108-662A-13H-3, 59	111.29	89.6	3.4	7.1	1.06
108-662A-13H-3, 71	111.41	88.8	3.8	7.5	1.14
108-662A-13H-3, 79	111.48	89.9	2.4	7.7	0.86
108-662A-13H-3, 89	111.58	88.7	3.2	8.1	0.94
108-662A-13H-3, 101	111.70	84.3	3.7	12.0	1.06
108-662A-13H-3, 110	111.79	87.6			
108-662A-13H-3, 119	111.89	71.2	7.4	21.4	0.94
108-662A-13H-3, 131	112.01	76.1	6.6	17.3	0.97
108-662A-13H-3, 139	112.08	74.4	7.1	18.4	0.79
108-662A-13H-3, 145	112.16	77.8	7.2	15.1	0.97
108-662A-13H-4, 11	112.31	62.5	9.5	28.1	0.90
108-662A-13H-4, 19	112.39	71.9	7.6	20.5	0.81
108-662A-13H-4, 29	112.48	77.2	6.6	16.2	1.03
108-662A-13H-4, 41	112.61	64.8	7.6	27.6	1.05
108-662A-13H-4, 50	112.70	82.9			
108-662A-13H-4, 59	112.79	66.1	5.1	28.8	1.17
108-662A-13H-4, 71	112.91	72.2	3.0	24.8	1.41
108-662A-13H-4, 79	112.98	85.9	3.1	11.0	0.89
108-662A-13H-4, 89	113.08	79.0	5.8	15.2	1.01
108-662A-13H-4, 101	113.20	77.3	6.4	16.3	1.01
108-662A-13H-4, 110	113.29	67.1			

Table 4 (continued).

Core, section, interval (cm)	Depth (mbsf)	CaCO ₃ (%)	SiO ₂ (%)	Terrigenous fraction (%)	Dry-bulk density (g/cm ³)
108-662A-13H-4, 119	113.39	68.1	7.9	24.0	1.01
108-662A-13H-4, 131	113.51	69.2	7.9	22.9	1.37
108-662A-13H-4, 139	113.58	69.7	8.1	22.2	0.79
108-662A-13H-4, 145	113.66	77.3	5.9	16.7	1.00
108-662A-13H-5, 11	113.81	80.4	4.0	15.6	1.56
108-662A-13H-5, 19	113.89	88.8	3.7	7.5	0.91
108-662A-13H-5, 29	113.98	86.9	2.7	10.4	1.12
108-662A-13H-5, 41	114.11	89.5	2.7	7.8	1.06
108-662A-13H-5, 50	114.20	80.3			
108-662A-13H-5, 59	114.29	67.5	6.9	25.6	1.02
108-662A-13H-5, 71	114.41	83.7	7.1	9.2	1.02
108-662A-13H-5, 79	114.48	69.1	9.3	21.6	0.79
108-662A-13H-5, 89	114.58	71.8	8.9	19.3	1.01
108-662A-13H-5, 101	114.70	71.8	9.0	19.2	0.99
108-662A-13H-5, 110	114.79	73.8			
108-662A-13H-5, 115	114.85	71.5	8.2	20.3	0.79
108-662A-13H-5, 120	114.90	72.2			
108-662A-13H-5, 131	115.01	69.1	8.1	22.9	1.07
108-662A-13H-5, 139	115.08	84.1	5.0	10.9	0.88
108-662A-13H-5, 145	115.16	87.4	3.2	9.3	1.10
108-662A-13H-6, 7	115.27	86.3	4.0	9.7	1.11
108-662A-13H-6, 19	115.39	89.4	3.0	7.6	0.87
108-662A-13H-6, 29	115.48	89.3	3.1	7.6	1.06
108-662A-13H-6, 41	115.61	88.1	2.8	9.1	1.12
108-662A-13H-6, 50	115.70	88.6			
108-662A-13H-6, 59	115.79	87.7	4.9	7.4	1.00
108-662A-13H-6, 71	115.91	83.9	5.2	10.9	1.06
108-662A-13H-6, 79	115.98	87.7	4.5	7.8	0.86
108-662A-13H-6, 89	116.08	88.0	3.6	8.4	1.01
108-662A-13H-6, 101	116.20	88.8	3.7	7.5	1.07
108-662A-13H-6, 110	116.29	88.1			
108-662A-13H-6, 115	116.35	87.8	4.1	8.1	1.08
108-662A-13H-6, 118	116.38	87.7			
108-662A-13H-6, 131	116.51	87.2	4.1	8.7	1.07
108-662A-13H-6, 139	116.58	86.4	3.8	9.8	0.93
108-662A-13H-6, 146	116.66	86.2	4.1	9.7	1.16
108-662A-13H-7, 11	116.81	77.5	6.4	16.1	1.08
108-662A-13H-7, 19	116.89	78.1	6.7	15.2	0.88
108-662A-13H-7, 29	116.98	75.6	6.6	17.8	1.07
108-662A-13H-7, 41	117.11	79.9	6.2	13.9	1.11
108-662A-13H-7, 50	117.20	66.3			
108-662A-13H-7, 54	117.24	64.4	8.2	27.4	1.06
108-662A-14H-1, 11	117.31	81.5	4.5	14.0	1.00
108-662A-14H-1, 18	117.39	80.7	6.4	12.9	0.87
108-662A-14H-1, 29	117.49	82.1	4.8	13.1	0.83
108-662A-14H-1, 41	117.61	86.8	3.7	9.5	0.93
108-662A-14H-1, 50	117.70	78.9	4.9	16.2	1.03
108-662A-14H-1, 59	117.79	82.6	5.0	12.4	0.93
108-662A-14H-1, 71	117.91	75.1	7.5	17.4	0.82
108-662A-14H-1, 79	117.99	67.5	9.0	23.5	0.79
108-662A-14H-1, 89	118.09	73.6	7.5	18.9	0.83
108-662A-14H-1, 101	118.21	69.5	10.5	20.1	0.78
108-662A-14H-1, 110	118.30	67.9	12.1	20.0	0.84
108-662A-14H-1, 119	118.39	71.1	10.5	18.4	0.80
108-662A-14H-1, 131	118.51	80.8	10.4	8.7	0.85
108-662A-14H-1, 139	118.59	89.3	7.2	3.5	0.94
108-662A-14H-1, 146	118.66	86.9	5.3	7.9	0.98
108-662A-14H-2, 11	118.81	90.7	3.4	6.0	0.97
108-662A-14H-2, 19	118.89	89.3	2.6	8.1	1.00
108-662A-14H-2, 29	118.99	86.1	5.1	8.7	0.93
108-662A-14H-2, 41	119.11	77.7	8.2	14.1	0.82
108-662A-14H-2, 50	119.20	76.3	8.9	14.9	0.91
108-662A-14H-2, 59	119.29	76.4	8.1	15.6	0.83
108-662A-14H-2, 71	119.41	77.2	9.3	13.5	0.82
108-662A-14H-2, 79	119.49	86.7	6.1	7.2	0.86
108-662A-14H-2, 89	119.59	91.0	3.0	6.1	0.97
108-662A-14H-2, 101	119.71	90.0	3.3	6.8	0.92
108-662A-14H-2, 110	119.80	89.3	3.0	7.7	1.04
108-662A-14H-2, 119	119.89	89.6	2.8	7.6	0.97
108-662A-14H-2, 131	120.01	89.0	2.7	8.3	0.94
108-662A-14H-2, 139	120.09	86.9	3.0	10.1	0.96
108-662A-14H-2, 146	120.16	89.0	3.9	7.1	0.95
108-662A-14H-3, 11	120.31	86.8	4.6	8.6	0.90
108-662A-14H-3, 19	120.39	85.4	4.3	10.4	0.90
108-662A-14H-3, 29	120.49	87.1	3.5	9.5	0.90

Table 4 (continued).

Core, section, interval (cm)	Depth (mbsf)	CaCO ₃ (%)	SiO ₂ (%)	Terrigenous fraction (%)	Dry-bulk density (g/cm ³)
108-662A-14H-3, 41	120.61	89.1	3.3	7.6	0.91
108-662A-14H-3, 50	120.70	88.0	3.5	8.5	1.02
108-662A-14H-3, 59	120.79	88.3	3.5	8.2	0.96
108-662A-14H-3, 71	120.91	87.7	3.6	8.7	0.92
108-662A-14H-3, 79	120.99	87.7	3.8	8.5	0.93
108-662A-14H-3, 89	121.09	86.1	4.4	9.5	0.96
108-662A-14H-3, 101	121.21	85.1	4.3	10.5	0.93
108-662A-14H-3, 110	121.30	81.8	4.6	13.6	1.00
108-662A-14H-3, 119	121.39	84.9	4.8	10.3	0.94
108-662A-14H-3, 131	121.51	85.1	4.9	9.9	0.94
108-662A-14H-3, 139	121.59	82.7	5.7	11.6	0.94
108-662A-14H-3, 146	121.66	80.1	6.3	13.6	0.94
108-662A-14H-4, 11	121.81	76.9	8.0	15.1	0.88
108-662A-14H-4, 19	121.89	61.6	11.0	27.3	0.79
108-662A-14H-4, 29	121.99	64.2	10.0	25.8	0.88
108-662A-14H-4, 41	122.11	81.7	5.7	12.7	0.92
108-662A-14H-4, 50	122.20	80.3	6.1	13.6	1.00
108-662A-14H-4, 59	122.29	84.7	4.8	10.5	0.94
108-662A-14H-4, 71	122.41	85.0	4.1	10.9	1.00
108-662A-14H-4, 79	122.49	87.1	3.6	9.3	1.05
108-662A-14H-4, 89	122.59	88.2	2.8	9.1	1.03
108-662A-14H-4, 101	122.71	84.8	2.8	12.4	0.96
108-662A-14H-4, 110	122.80	86.7	3.8	9.5	1.02
108-662A-14H-4, 119	122.89	84.1	4.8	11.1	0.95
108-662A-14H-4, 131	123.01	82.1	5.7	12.1	0.90
108-662A-14H-4, 139	123.09	77.0	4.6	18.4	0.90
108-662A-14H-4, 146	123.16	81.6	3.1	15.3	1.03
108-662A-14H-5, 11	123.31	87.3	3.0	9.8	1.00
108-662A-14H-5, 19	123.39	82.3	3.5	14.2	1.01
108-662A-14H-5, 29	123.49	85.3	3.5	11.2	0.98
108-662A-14H-5, 41	123.61	84.2	3.9	11.9	0.94
108-662A-14H-5, 50	123.70	83.2	4.9	11.9	0.98
108-662A-14H-5, 59	123.79	73.3	7.1	19.6	0.90
108-662A-14H-5, 71	123.91	71.0	11.1	17.9	0.76
108-662A-14H-5, 79	123.99	68.5	7.5	24.0	0.84
108-662A-14H-5, 89	124.09	78.3	6.7	15.1	0.89
108-662A-14H-5, 101	124.21	79.8	6.2	14.0	0.89
108-662A-14H-5, 110	124.30	84.9	4.8	10.4	0.99
108-662A-14H-5, 119	124.39	82.9	4.6	12.5	0.97
108-662A-14H-5, 131	124.51	85.6	3.3	11.0	0.95
108-662A-14H-5, 139	124.59	90.9	2.9	6.2	0.96
108-662A-14H-5, 146	124.66	89.1	2.8	8.1	1.00
108-662A-14H-6, 11	124.81	88.3	3.0	8.6	1.00
108-662A-14H-6, 19	124.89	87.8	3.0	9.1	0.92
108-662A-14H-6, 29	124.99	87.7	2.8	9.5	0.98
108-662A-14H-6, 41	125.11	86.8	2.9	10.3	0.94
108-662A-14H-6, 50	125.20	86.0	3.4	10.6	1.09
108-662A-14H-6, 59	125.29	81.8	4.9	13.3	0.93
108-662A-14H-6, 71	125.41	84.6	3.6	11.8	0.93
108-662A-14H-6, 79	125.49	82.6	4.6	12.8	0.92
108-662A-14H-6, 89	125.59	86.4	4.5	9.1	1.00
108-662A-14H-6, 101	125.71	84.8	4.0	11.2	0.98
108-662A-14H-6, 110	125.80	74.8	5.9	19.3	0.95
108-662A-14H-6, 119	125.89	87.1	3.3	9.6	1.03
108-662A-14H-6, 131	126.01	88.2	3.4	8.4	1.02
108-662A-14H-6, 139	126.09	85.5	3.7	10.8	1.00
108-662A-14H-6, 146	126.16	75.4	5.0	19.6	0.96
108-662A-14H-7, 11	126.31	86.6	2.9	10.5	1.01
108-662A-14H-7, 14	126.34	89.2	2.7	8.1	1.01
108-662A-15H-1, 11	126.81	86.6	4.5	8.8	0.87
108-662A-15H-1, 19	126.89	82.3	3.7	14.0	0.90
108-662A-15H-1, 29	126.99	84.7	4.3	11.0	0.92
108-662A-15H-1, 41	127.11	85.4	4.2	10.4	0.92
108-662A-15H-1, 50	127.20	83.8	5.5	10.8	0.97
108-662A-15H-1, 59	127.29	87.6	3.3	9.1	0.93
108-662A-15H-1, 71	127.41	87.5	3.1	9.4	0.92
108-662A-15H-1, 79	127.49	86.8	3.7	9.5	0.94
108-662A-15H-1, 89	127.59	81.4	2.8	15.7	1.03
108-662A-15H-1, 101	127.71	88.1	3.0	9.0	0.96
108-662A-15H-1, 110	127.80	85.3	3.8	10.9	1.05
108-662A-15H-1, 119	127.89	87.1	3.4	9.6	1.00
108-662A-15H-1, 131	128.01	88.5	3.5	8.0	0.96
108-662A-15H-1, 139	128.09	87.9	3.1	9.0	0.94
108-662A-15H-1, 146	128.16	79.9	4.8	15.3	0.95
108-662A-15H-2, 11	128.31	79.2	4.6	16.1	0.96

Table 4 (continued).

Core, section, interval (cm)	Depth (mbsf)	CaCO ₃ (%)	SiO ₂ (%)	Terrigenous fraction (%)	Dry-bulk density (g/cm ³)
108-662A-15H-2, 19	128.39	80.5	5.4	14.1	0.93
108-662A-15H-2, 29	128.49	87.2	3.3	9.6	1.01
108-662A-15H-2, 41	128.61	89.0	2.4	8.7	1.02
108-662A-15H-2, 50	128.70	86.5	2.9	10.6	1.08
108-662A-15H-2, 59	128.79	87.6	2.2	10.2	1.00
108-662A-15H-2, 71	128.91	75.7	4.6	19.8	0.94
108-662A-15H-2, 79	128.99	81.7	4.3	14.0	0.93
108-662A-15H-2, 89	129.09	72.8	5.3	21.9	0.95
108-662A-15H-2, 101	129.21	65.1	7.0	27.9	0.92
108-662A-15H-2, 110	129.30	78.3	6.7	15.0	0.98
108-662A-15H-2, 119	129.39	83.4	5.4	11.2	0.99
108-662A-15H-2, 131	129.51	88.3	3.5	8.2	1.02
108-662A-15H-2, 139	129.59	85.7	3.2	11.1	1.00
108-662A-15H-2, 146	129.66	79.9	2.8	17.3	1.02
108-662A-15H-3, 11	129.81	83.2	4.3	12.5	0.96
108-662A-15H-3, 19	129.89	84.1	4.3	11.6	0.95
108-662A-15H-3, 29	129.99	85.8	4.4	9.8	1.00
108-662A-15H-3, 41	130.11	73.8	5.9	20.3	0.91
108-662A-15H-3, 50	130.20	82.0	4.5	13.6	1.02
108-662A-15H-3, 59	130.29	82.2	4.5	13.3	1.00
108-662A-15H-3, 71	130.41	81.1	4.5	14.4	0.97
108-662A-15H-3, 79	130.49	84.1	4.6	11.3	0.96
108-662A-15H-3, 139	130.59	92.1	2.5	5.4	1.04
108-662A-15H-3, 101	130.71	92.7	2.3	5.1	1.01
108-662A-15H-3, 110	130.80	91.1	1.9	7.1	1.08
108-662A-15H-3, 119	130.89	92.4	2.0	5.6	1.03
108-662A-15H-4, 131	131.01	91.0	2.7	6.3	1.01
108-662A-15H-4, 139	131.09	90.2	2.5	7.3	1.00
108-662A-15H-4, 146	131.16	88.2	2.7	9.1	1.03
108-662A-15H-4, 11	131.31	81.8	3.5	14.6	0.98
108-662A-15H-4, 19	131.39	89.0	2.2	8.8	1.06
108-662A-15H-4, 29	131.49	84.6	3.5	11.8	1.05
108-662A-15H-4, 41	131.61	86.9	2.0	11.2	1.05
108-662A-15H-4, 50	131.70	90.3	2.5	7.2	1.12
108-662A-15H-4, 59	131.79	87.5	2.9	9.6	1.09
108-662A-15H-4, 71	131.91	89.8	2.9	7.3	1.05
108-662A-15H-4, 79	131.99	87.4	3.6	9.0	1.02
108-662A-15H-4, 89	132.09	87.8	2.9	9.2	1.12
108-662A-15H-4, 101	132.11	86.1	3.2	10.8	1.04
108-662A-15H-4, 110	132.21	86.5	3.2	8.5	0.97
108-662A-15H-4, 119	132.31	91.6	1.7	6.7	1.03
108-662A-15H-4, 131	132.39	81.7	5.6	12.7	1.03
108-662A-15H-4, 139	132.49	84.2	4.8	11.1	1.07
108-662A-15H-5, 41	133.11	88.2	3.0	8.8	1.08
108-662A-15H-5, 50	133.20	88.8	2.2	9.0	1.11
108-662A-15H-5, 59	133.29	91.1	1.4	7.5	1.11
108-662A-15H-5, 71	133.41	91.6	1.7	6.7	1.03
108-662A-15H-5, 79	133.49	91.7	1.7	6.6	1.08
108-662A-15H-5, 89	133.59	91.5	1.5	7.1	1.16
108-662A-15H-5, 101	133.71	91.1	1.6	7.4	1.12
108-662A-15H-5, 110	133.80	87.3	2.4	10.3	1.10
108-662A-15H-5, 119	133.89	87.1	3.2	9.7	1.03
108-662A-15H-5, 131	134.01	77.1	5.8	17.2	0.95
108-662A-15H-5, 139	134.09	76.6	6.2	17.2	0.94
108-662A-15H-5, 146	134.16	73.1	7.7	19.2	0.93
108-662A-15H-6, 11	134.31	76.0	5.5	18.5	0.96
108-662A-15H-6, 19	134.89	80.0	5.4	14.7	0.96
108-662A-15H-6, 29	134.49	80.2	6.9	12.8	0.99
108-662A-15H-6, 41	134.61	81.4	7.1	11.5	0.95
108-662A-15H-6, 50	134.70	82.2	6.5	11.3	1.04
108-662A-15H-6, 59	134.79	87.3	3.4	9.3	1.13
108-662A-15H-6, 71	134.91	87.2	3.2	9.6	1.06
108-662A-15H-6, 79	134.99	88.5	2.9	8.6	1.00
108-662A-15H-6, 89	135.09	88.3	3.4	8.3	1.06
108-662A-15H-6, 101	135.21	82.2	4.6	13.2	1.03
108-662A-15H-6, 110	135.30	82.9	5.1	12.0	1.06
108-662A-15H-6, 119	135.39	82.8	5.2	11.9	1.02
108-662A-15H-6, 131	135.51	79.8	4.9	15.3	1.01
108-662A-15H-6, 139	135.59	75.8	4.9	19.3	0.98
108-662A-15H-6, 146	135.66	75.5	6.		

Table 4 (continued).

Core, section, interval (cm)	Depth (mbsf)	CaCO ₃ (%)	SiO ₂ (%)	Terrigenous fraction (%)	Dry-bulk density (g/cm ³)
108-662A-15H-7, 19	135.89	89.2	3.1	7.7	1.09
108-662A-15H-7, 29	135.99	88.8	2.3	8.9	1.11
108-662A-15H-7, 41	136.11	88.7	2.6	8.7	1.04
108-662A-16H-1, 3	136.23	76.7	5.0	18.3	0.94
108-662A-16H-1, 29	136.49	79.7	4.5	15.8	1.03
108-662A-16H-1, 31	136.51	79.2	4.8	16.0	0.94
108-662A-16H-1, 41	136.61	72.5	5.8	21.7	0.93
108-662A-16H-1, 50	136.70	78.7	5.0	16.2	1.03
108-662A-16H-1, 59	136.79	84.0	4.9	11.1	1.00
108-662A-16H-1, 71	136.91	86.9	3.9	9.2	1.00
108-662A-16H-1, 79	136.99	89.1	3.0	8.0	1.05
108-662A-16H-1, 89	137.09	88.4	2.8	8.8	1.09
108-662A-16H-1, 101	137.21	91.7	2.1	6.1	1.03
108-662A-16H-1, 110	137.30	90.5	2.6	6.9	1.03
108-662A-16H-1, 119	137.39	90.6	2.5	6.8	1.06
108-662A-16H-1, 131	137.51	87.8	2.5	9.7	1.02
108-662A-16H-1, 139	137.59	88.5	3.0	8.5	0.97
108-662A-16H-1, 145	137.65	88.0	3.0	9.0	1.00
108-662A-16H-2, 11	137.81	88.6	3.2	8.1	1.01
108-662A-16H-2, 19	137.89	88.3	3.0	8.7	0.95
108-662A-16H-2, 29	137.99	85.7	7.5	6.8	1.02
108-662A-16H-2, 41	138.11	85.5	3.7	10.8	0.98
108-662A-16H-2, 50	138.20	88.8	3.3	7.9	1.02
108-662A-16H-2, 59	138.29	85.5	3.9	10.6	0.99
108-662A-16H-2, 71	138.41	81.2	5.5	13.3	0.98
108-662A-16H-2, 79	138.49	80.9	5.4	13.7	0.95
108-662A-16H-2, 89	138.59	66.0	7.7	26.3	0.87
108-662A-16H-2, 101	138.71	81.9	5.0	13.1	0.98
108-662A-16H-2, 110	138.80	81.2	5.3	13.5	0.95
108-662A-16H-2, 119	138.89	81.8	5.0	13.3	0.99
108-662A-16H-2, 131	139.01	82.9	5.5	11.6	0.95
108-662A-16H-2, 139	139.09	82.3	5.2	12.6	0.94
108-662A-16H-2, 146	139.16	84.9	3.4	11.7	1.07
108-662A-16H-3, 11	139.31	89.7	2.5	7.9	1.04
108-662A-16H-3, 19	139.39	90.3	2.5	7.2	1.00
108-662A-16H-3, 29	139.49	89.5	2.6	7.9	0.99
108-662A-16H-3, 41	139.61	90.5	2.5	7.0	1.05
108-662A-16H-3, 50	139.70	90.4	2.4	7.2	1.06
108-662A-16H-3, 59	139.79	89.9	2.6	7.5	1.11
108-662A-16H-3, 71	139.91	86.7	3.3	9.9	1.04
108-662A-16H-3, 79	139.99	77.5	3.9	18.6	1.02
108-662A-16H-3, 89	140.09	84.8	4.0	11.2	1.02
108-662A-16H-3, 101	140.21	86.4	3.8	9.8	1.05
108-662A-16H-3, 110	140.30	88.4	3.1	8.4	1.02
108-662A-16H-3, 119	140.39	88.3	2.8	9.0	1.10
108-662A-16H-3, 131	140.51	85.8	2.4	11.8	1.09
108-662A-16H-3, 139	140.59	89.0	2.8	8.1	1.07
108-662A-16H-3, 146	140.66	88.4	3.0	8.6	1.10
108-662A-16H-4, 11	140.81	86.1	3.4	10.5	1.04
108-662A-16H-4, 19	140.89	80.5	5.4	14.1	1.01
108-662A-16H-4, 29	140.99	78.6	6.5	14.9	1.00
108-662A-16H-4, 41	141.11	77.6	7.0	15.4	0.97
108-662A-16H-4, 50	141.20	82.2	5.1	12.7	1.02
108-662A-16H-4, 59	141.29	81.7	5.9	12.4	1.14
108-662A-16H-4, 71	141.41	79.3	5.9	14.8	0.99
108-662A-16H-4, 79	141.49	80.5	5.6	13.8	1.00
108-662A-16H-4, 89	141.59	80.3	4.6	15.2	1.09
108-662A-16H-4, 101	141.71	89.4	2.5	8.2	1.08
108-662A-16H-4, 110	141.80	91.9	2.3	5.8	1.04
108-662A-16H-4, 119	141.89	90.4	2.1	7.4	1.13
108-662A-16H-4, 131	142.01	89.2	1.9	8.9	1.05
108-662A-16H-4, 139	142.09	92.2	2.3	5.5	1.06
108-662A-16H-4, 146	142.16	90.7	2.1	7.1	1.05
108-662A-16H-5, 11	142.31	87.4	2.9	9.6	1.05
108-662A-16H-5, 19	142.39	76.4	5.0	18.7	0.99
108-662A-16H-5, 29	142.49	87.0	3.5	9.4	1.04
108-662A-16H-5, 41	142.61	89.3	3.3	7.4	0.99
108-662A-16H-5, 50	142.70	87.9	3.7	8.4	0.98
108-662A-16H-5, 59	142.79	89.4	3.0	7.6	1.05
108-662A-16H-5, 71	142.91	88.8	4.8	6.5	1.05
108-662A-16H-5, 79	142.99	87.6	3.6	8.8	1.01
108-662A-16H-5, 89	143.09	88.5	3.2	8.3	1.04
108-662A-16H-5, 101	143.21	85.6	3.7	10.7	1.02
108-662A-16H-5, 110	143.30	86.7	3.3	10.0	1.02
108-662A-16H-5, 119	143.39	83.9	4.1	12.1	1.02
108-662A-16H-5, 131	143.51	91.4	2.4	6.2	1.08

Table 4 (continued).

Core, section, interval (cm)	Depth (mbsf)	CaCO ₃ (%)	SiO ₂ (%)	Terrigenous fraction (%)	Dry-bulk density (g/cm ³)
108-662A-16H-5, 139	143.59	85.7	2.3	12.0	1.02
108-662A-16H-6, 11	143.81	90.3	2.2	7.4	1.03
108-662A-16H-6, 19	143.89	89.8	2.5	7.6	1.05
108-662A-16H-6, 29	143.99	91.0	2.5	6.5	1.13
108-662A-16H-6, 41	144.11	89.6	2.1	8.3	1.07
108-662A-16H-6, 50	144.20	93.9	2.2	3.8	1.08
108-662A-16H-6, 59	144.29	91.3	1.9	6.9	1.10
108-662A-16H-6, 71	144.41	92.0	1.9	6.1	1.05
108-662A-16H-6, 79	144.49	92.0	2.1	5.9	1.10
108-662A-16H-6, 89	144.59	88.2	2.2	9.6	1.09
108-662A-16H-6, 101	144.71	92.2	2.2	5.6	1.04
108-662A-16H-6, 110	144.80	92.7	2.5	4.8	1.07
108-662A-16H-6, 119	144.89	90.6	2.2	7.1	1.09
108-662A-16H-6, 131	145.01	91.0	2.3	6.7	1.07
108-662A-16H-6, 139	145.09	89.7	2.5	7.8	1.03
108-662A-16H-6, 146	145.16	90.4	2.1	7.4	1.05
108-662A-16H-7, 11	145.31	89.4	2.4	8.2	1.06
108-662A-16H-7, 19	145.39	91.9	2.0	6.1	1.02
108-662A-16H-7, 29	145.49	90.0	1.9	8.2	1.05
108-662A-16H-7, 41	145.61	91.3	2.3	6.5	1.06
108-662A-16H-7, 51	145.71	91.3	1.3	7.4	1.06
108-662A-17H-1, 11	145.81	77.5	5.0	17.5	0.96
108-662A-17H-1, 19	145.89	81.7	4.6	13.8	0.99
108-662A-17H-1, 29	145.99	89.8	1.9	8.3	1.06
108-662A-17H-1, 41	146.11	91.3	1.7	7.0	1.01
108-662A-17H-1, 42	146.12	91.8	2.7	5.6	1.01
108-662A-17H-1, 50	146.20	87.1	5.7	7.3	0.96
108-662A-17H-1, 59	146.29	85.0	6.3	8.8	0.96
108-662A-17H-1, 71	146.41	85.4	5.4	9.1	0.96
108-662A-17H-1, 79	146.49	81.5	9.5	9.0	0.90
108-662A-17H-1, 89	146.59	86.2	6.8	7.1	0.98
108-662A-17H-1, 101	146.71	87.1	2.9	10.0	1.01
108-662A-17H-1, 110	146.80	88.6	3.2	8.2	1.01
108-662A-17H-1, 119	146.89	90.2	2.5	7.3	1.07
108-662A-17H-1, 130	147.00	88.5	2.6	8.8	1.03
108-662A-17H-1, 139	147.09	85.7	3.5	10.8	0.97
108-662A-17H-1, 142	147.12	89.2	3.5	7.3	1.00
108-662A-17H-1, 146	147.16	81.8	2.6	15.6	1.10
108-662A-17H-2, 9	147.29	70.9	4.6	24.5	0.91
108-662A-17H-2, 13	147.33	65.2	8.3	26.5	0.87
108-662A-17H-2, 19	147.39	64.4	7.8	27.8	0.85
108-662A-17H-2, 29	147.49	85.4	3.7	10.9	1.05
108-662A-17H-2, 38	147.58	87.5	2.9	9.6	1.01
108-662A-17H-2, 41	147.61	87.8	3.7	8.4	0.98
108-662A-17H-2, 50	147.70	88.0	2.9	9.1	1.00
108-662A-17H-2, 59	147.79	90.7	2.5	6.8	1.09
108-662A-17H-2, 71	147.91	88.9	1.9	9.2	1.05
108-662A-17H-2, 79	147.99	88.8	1.9	9.3	1.00
108-662A-17H-2, 89	148.09	90.5	2.0	7.5	1.01
108-662A-17H-2, 101	148.21	90.8	2.1	7.1	1.01
108-662A-17H-2, 110	148.30	90.8	2.0	7.1	1.03
108-662A-17H-2, 119	148.39	90.2	1.8	8.0	1.02
108-662A-17H-2, 130	148.50	88.8	2.2	8.9	1.00
108-662A-17H-2, 139	148.59	88.1	2.5	9.3	1.01
108-662A-17H-2, 142	148.62	90.0	2.2	7.8	1.06
108-662A-17H-2, 145	148.65	89.2	2.1	8.7	1.08
108-662A-17H-3, 12	148.82	88.6	2.3	9.2	1.00
108-662A-17H-3, 14	148.84	90.5	2.3	7.2	1.08
108-662A-17H-3, 17	148.87	87.0	2.7	10.2	0.96
108-662A-17H-3, 32	149.02	73.8	6.8	19.4	0.90
108-662A-17H-3, 41	149.11	81.2	5.9	12.9	0.97
108-662A-17H-3, 43	149.13	85.0	3.2	11.8	1.04
108-662A-17H-3, 50	149.20	84.8	3.7	11.6	1.04
108-662A-17H-3, 59	149.29	63.5	6.8	29.7	1.08
108-662A-17H-3, 71	149.41	69.2	1.4	29.3	1.04
108-662A-17H-3, 79	149.49	78.8	4.0	17.2	0.98
108-662A-17H-3, 89	149.59	84.3	4.4	11.3	1.05
108-662A-17H-3, 101	149.71	76.0	3.2	20.7	1.02
108-662A-17H-3, 118	149.88	90.7			

Table 4 (continued).

Core, section, interval (cm)	Depth (mbsf)	CaCO ₃ (%)	SiO ₂ (%)	Terrigenous fraction (%)	Dry-bulk density (g/cm ³)
108-662A-17H-4, 59	150.79	62.0	3.8	34.3	1.02
108-662A-17H-4, 71	150.91	82.7	3.7	13.7	0.99
108-662A-17H-4, 79	150.99	83.3	3.6	13.1	0.97
108-662A-17H-4, 89	151.09	88.1	3.5	8.4	1.01
108-662A-17H-4, 110	151.30	85.8	3.1	11.1	1.05
108-662A-17H-4, 101	151.21	85.3	4.6	10.1	1.01
108-662A-17H-4, 119	151.39	85.2	3.2	11.7	1.06
108-662A-17H-4, 130	151.50	81.3	3.3	15.4	1.06
108-662A-17H-4, 139	151.59	68.3	7.2	24.5	0.93
108-662A-17H-4, 142	151.62	72.5	5.9	21.6	0.99
108-662A-17H-4, 146	151.66	84.0	4.6	11.4	1.03
108-662A-17H-5, 11	151.81	89.4	3.4	7.2	1.09
108-662A-17H-5, 14	151.83	88.4	2.8	8.9	1.03
108-662A-17H-5, 19	151.89	87.5	2.9	9.6	1.02
108-662A-17H-5, 29	151.99	91.1	2.3	6.6	1.32
108-662A-17H-5, 41	152.11	89.5	2.8	7.7	1.04
108-662A-17H-5, 50	152.20	88.0	1.9	10.1	1.04
108-662A-17H-5, 59	152.29	89.2	2.2	8.6	1.05
108-662A-17H-5, 71	152.41	87.4	2.3	10.3	1.02
108-662A-17H-5, 79	152.49	90.2	2.3	7.5	0.99
108-662A-17H-5, 89	152.59	87.5	3.0	9.4	1.04
108-662A-17H-5, 101	152.71	87.6	2.7	9.8	1.03
108-662A-17H-5, 110	152.80	87.8	2.9	9.3	1.03
108-662A-17H-5, 119	152.89	87.1	3.3	9.7	1.17
108-662A-17H-5, 130	153.00	88.5	3.1	8.4	1.12
108-662A-17H-5, 139	153.09	87.8	3.0	9.2	0.99
108-662A-17H-5, 142	153.12	87.8	2.6	9.6	1.14
108-662A-17H-5, 146	153.16	85.4	2.5	12.1	1.22
108-662A-17H-6, 11	153.31	88.7	2.3	9.0	1.02
108-662A-17H-6, 14	153.33	90.2	2.2	7.6	1.14
108-662A-17H-6, 19	153.39	88.5	2.7	8.8	1.00
108-662A-17H-6, 29	153.49	87.8	3.0	9.2	1.04
108-662A-17H-6, 41	153.61	84.3	4.1	11.6	1.02
108-662A-17H-6, 50	153.70	84.6	3.7	11.6	1.12
108-662A-17H-6, 59	153.79	90.0	2.3	7.7	1.04
108-662A-17H-6, 71	153.91	92.9	2.1	5.0	1.04
108-662A-17H-6, 79	153.99	92.4	1.9	5.8	1.00
108-662A-17H-6, 89	154.09	92.3	2.1	5.6	1.04
108-662A-17H-6, 101	154.21	91.8	2.6	5.6	1.04
108-662A-17H-6, 110	154.30	86.4	3.0	10.6	1.12
108-662A-17H-6, 119	154.39	78.4	5.4	16.2	0.99
108-662A-17H-6, 124	154.44	72.9	5.1	22.0	1.04
108-662A-17H-6, 129	154.49	78.6	3.8	17.6	0.99
108-662A-18H-1, 11	155.31	91.5	2.1	6.4	0.96
108-662A-18H-1, 19	155.39	92.7	1.8	5.5	0.98
108-662A-18H-1, 29	155.49	90.0	2.4	7.6	0.98
108-662A-18H-1, 41	155.61	90.0	2.7	7.3	1.04
108-662A-18H-1, 50	155.70	89.6	2.3	8.1	1.12
108-662A-18H-1, 59	155.79	89.6	2.5	7.9	0.73
108-662A-18H-1, 71	155.91	89.8	2.5	7.7	0.98
108-662A-18H-1, 79	155.99	76.4	2.5	21.1	0.96
108-662A-18H-1, 89	156.09	87.1	2.2	10.8	1.00
108-662A-18H-1, 101	156.21	90.7	2.2	7.2	0.98
108-662A-18H-1, 110	156.30	84.6	3.7	11.7	1.14
108-662A-18H-1, 119	156.39	88.5	4.1	7.4	0.93
108-662A-18H-1, 131	156.51	87.0	4.0	9.1	0.98
108-662A-18H-1, 139	156.59	83.4	4.4	12.3	0.95
108-662A-18H-1, 147	156.67	82.5	4.6	12.9	0.99
108-662A-18H-2, 11	156.81	85.2	4.0	10.8	1.01
108-662A-18H-2, 19	156.89	86.6	2.8	10.7	1.01
108-662A-18H-2, 41	157.11	93.6	1.8	4.6	1.00
108-662A-18H-2, 50	157.20	92.5	1.7	5.8	1.09
108-662A-18H-2, 59	157.29	93.2	1.6	5.2	1.02
108-662A-18H-2, 71	157.41	90.3	2.2	7.5	0.99
108-662A-18H-2, 79	157.49	87.4	2.6	10.0	0.92
108-662A-18H-2, 89	157.59	91.5	2.3	6.2	1.01
108-662A-18H-2, 101	157.71	87.3	2.5	10.1	1.04
108-662A-18H-2, 110	157.80	86.8	2.8	10.4	1.05
108-662A-18H-2, 119	157.89	86.2	5.7	8.1	1.00
108-662A-18H-2, 131	158.01	85.5	3.9	10.6	1.02
108-662A-18H-2, 139	158.09	89.1	2.8	8.1	1.02
108-662A-18H-2, 144	158.14	89.2	2.6	8.2	1.09
108-662A-18H-3, 11	158.31	90.8	2.6	6.6	1.02
108-662A-18H-3, 19	158.39	90.7	2.5	6.8	1.01
108-662A-18H-3, 29	158.49	91.2	2.0	6.8	1.16
108-662A-18H-3, 41	158.61	90.9	1.8	7.4	1.06

Table 4 (continued).

Core, section, interval (cm)	Depth (mbsf)	CaCO ₃ (%)	SiO ₂ (%)	Terrigenous fraction (%)	Dry-bulk density (g/cm ³)
108-662A-18H-3, 50	158.70	93.7	1.5	4.9	1.08
108-662A-18H-3, 59	158.79	93.7	1.5	4.8	1.02
108-662A-18H-3, 71	158.91	94.5	1.6	4.0	1.05
108-662A-18H-3, 79	158.99	93.4	1.4	5.2	1.00
108-662A-18H-3, 89	159.09	90.9	1.6	7.4	1.00
108-662A-18H-3, 101	159.21	92.3	1.9	5.8	0.99
108-662A-18H-3, 110	159.30	92.7	1.8	5.5	1.03
108-662A-18H-3, 119	159.39	93.9	1.9	4.2	0.98
108-662A-18H-3, 131	159.51	94.7	1.5	3.8	0.97
108-662A-18H-3, 139	159.59	92.0	1.6	6.3	0.91
108-662A-18H-3, 147	159.67	94.0	1.6	4.5	0.97
108-662A-18H-4, 11	159.81	91.0	1.9	7.2	1.02
108-662A-18H-4, 19	159.89	86.9	1.6	11.5	0.98
108-662A-18H-4, 29	159.99	93.1	1.6	5.3	1.05
108-662A-18H-4, 41	160.11	92.5	1.7	5.8	0.99
108-662A-18H-4, 50	160.20	92.5	1.9	5.7	1.05
108-662A-18H-4, 59	160.29	90.9	2.1	7.0	1.0
108-662A-18H-4, 71	160.41	88.9	2.4	8.7	1.02
108-662A-18H-4, 79	160.49	88.4	2.4	9.2	1.00
108-662A-18H-4, 139	161.09	93.7	1.6	4.7	1.04
108-662A-18H-4, 147	161.17	92.9	1.9	5.1	1.08
108-662A-18H-5, 11	161.31	89.8	1.9	8.3	1.07
108-662A-18H-5, 19	161.39	92.3	1.8	5.9	1.02
108-662A-18H-5, 131	161.61	93.7	1.7	4.6	1.07
108-662A-18H-5, 141	161.61	93.5	1.8	4.8	1.08
108-662A-18H-5, 150	161.70	91.1	1.8	7.1	1.11
108-662A-18H-5, 160	162.30	90.5	1.6	7.9	1.17
108-662A-18H-5, 169	162.39	90.6	2.0	7.3	1.01
108-662A-18H-5, 171	162.51	88.2	1.9	9.9	1.02
108-662A-18H-5, 189	162.59	92.4	2.0	5.6	1.01
108-662A-18H-5, 197	162.67	93.0	1.7	5.4	1.05
108-662A-18H-6, 11	162.81	92.6	1.7	5.7	1.04
108-662A-18H-6, 19	162.89	93.5	1.6	4.9	1.06
108-662A-18H-6, 29	162.99	92.1	1.5	6.4	1.05
108-662A-18H-6, 41	163.11	93.1	1.6	5.3	1.06
108-662A-18H-6, 50	163.20	91.0	1.5	7.5	1.10
108-662A-18H-6, 59	163.29	92.9	1.0	6.0	1.06
108-662A-18H-6, 71	163.41	93.9	0.2	6.0	1.05
108-662A-18H-6, 79	163.49	93.1	1.5	5.4	1.02
108-662A-18H-6, 89	163.59	92.5	1.6	5.8	1.10
108-662A-18H-6, 101	163.71	92.0	1.6	6.4	1.09
108-662A-18H-6, 110	163.80	92.7	1.6	5.8	1.09
108-662A-18H-6, 119	163.89	95.1	0.9	4.0	0.99
108-662A-18H-6, 131	164.01	92.9	0.2	6.8	1.00
108-662A-18H-6, 139	164.09	92.5	0.3	7.2	0.98
108-662A-18H-6, 147	164.17	95.1	1.8	3.0	1.02
108-662A-18H-7, 11	164.31	93.3	0.4	6.3	1.01
108-662A-18H-7, 19	164.39	91.2	1.9	6.9	1.02
108-662A-18H-7, 29	164.49	91.2	0.3	8.5	1.07
108-662A-18H-7, 41	164.49	92.4	1.9	5.7	1.01
108-662A-19H-1, 41	165.11	90.3	0.3	9.4	1.00
108-662A-19H-1, 50	165.20	87.0	1.9	11.1	1.04
108-662A-19H-1, 59	165.29	89.6	2.0	8.5	1.02
108-662A-19H-1, 71	165.41	88.6	1.9	9.6	1.02
108-662A-19H-1, 79	165.49	91.4	1.5	7.1	1.01
108-662A-19H-1, 89	165.59	89.2	1.7	9.1	1.07
108-662A-19H-1, 101	165.71	88.9	2.1	8.9	1.03
108-662A-19H-1, 110	165.80	71.2	2.0	26.8	1.06
108-662A-19H-1, 119	165.89	82.2	3.1	14.7	1.04
108-662A-19H-1, 131	166.01	78.0	3.9	18.1	0.96
108-662A-19H-1, 139	166.09	79.5	4.3	16.3	0.94
108-662A-19H-1, 146	166.16	87.5	2.2	10.3	1.04
108-662A-19H-2, 11	166.31	89.2	1.8	9.0	1.01
108-662A-19H-2, 19	166.39	92.0	1.3	6.7	1.02
108-662A-19H-2, 29	166.49	91.6	1.7	6.7	1.06
108-662A-19H-2, 41	166.61	91.2	2.0	6.8	1.02

Table 4 (continued).

Core, section, interval (cm)	Depth (mbsf)	CaCO ₃ (%)	SiO ₂ (%)	Terrigenous fraction (%)	Dry-bulk density (g/cm ³)
108-662A-19H-2, 50	166.70	87.7	1.8	10.5	1.02
108-662A-19H-2, 59	166.79	89.6	1.8	8.6	1.06
108-662A-19H-2, 71	166.91	88.7	1.7	9.7	1.04
108-662A-19H-2, 79	166.99	92.3	0.3	7.4	1.01
108-662A-19H-2, 89	167.09	90.3	1.6	8.1	1.05
108-662A-19H-2, 101	167.21	88.6	2.4	9.0	1.01
108-662A-19H-2, 110	167.30	88.0	3.1	8.9	1.03
108-662A-19H-2, 119	167.39	87.0	2.6	10.4	1.01
108-662A-19H-2, 131	167.51	91.5	1.7	6.8	1.03
108-662A-19H-2, 139	167.59	91.2	1.9	6.9	0.75
108-662A-19H-3, 11	167.81	90.3	2.1	7.6	1.03
108-662A-19H-3, 19	167.89	89.3	2.0	8.7	0.98
108-662A-19H-3, 29	167.99	89.4	2.6	8.0	1.03
108-662A-19H-3, 41	168.11	89.2	2.5	8.3	1.02
108-662A-19H-3, 50	168.20	81.0	1.9	17.1	1.07
108-662A-19H-3, 59	168.29	90.1	2.0	7.9	1.15
108-662A-19H-3, 71	168.41	89.1	1.7	9.2	1.03
108-662A-19H-3, 79	168.49	89.3	2.3	8.3	1.00
108-662A-19H-3, 89	168.59	90.5	2.5	7.0	1.03
108-662A-19H-3, 101	168.71	78.7	3.8	17.6	0.95
108-662A-19H-3, 110	168.80	77.6	3.2	19.2	0.96
108-662A-19H-3, 119	168.89	86.8	3.1	10.1	0.94
108-662A-19H-3, 131	169.01	87.8	1.8	10.4	1.03
108-662A-19H-3, 139	169.09	88.6	2.0	9.4	1.05
108-662A-19H-3, 146	169.16	88.6	2.4	9.0	1.02
108-662A-19H-4, 11	169.31	73.7	3.4	22.8	1.09
108-662A-19H-4, 19	169.39	72.2	4.5	23.2	0.95
108-662A-19H-4, 29	169.49	83.8	3.3	12.9	0.92
108-662A-19H-4, 41	169.61	88.5	2.2	9.2	1.03
108-662A-19H-4, 50	169.70	89.8	1.5	8.6	1.07
108-662A-19H-4, 59	169.79	88.4	2.4	9.1	1.05
108-662A-19H-4, 71	169.91	80.2	3.5	16.3	1.04
108-662A-19H-4, 79	169.99	82.4	4.1	13.6	0.99
108-662A-19H-4, 89	170.09	86.5	2.5	11.0	1.03
108-662A-19H-4, 101	170.21	88.8	2.2	8.9	1.03
108-662A-19H-4, 110	170.30	89.2	1.6	9.2	1.05
108-662A-19H-4, 119	170.39	84.7	2.5	12.9	1.05
108-662A-19H-4, 131	170.51	85.0	3.8	11.2	1.02
108-662A-19H-4, 139	170.59	87.1	3.4	9.6	1.00
108-662A-19H-4, 146	170.66	88.8	2.5	8.7	1.07
108-662A-19H-5, 11	170.81	89.2	1.9	8.9	1.05
108-662A-19H-5, 19	170.89	89.0	1.9	9.1	1.03
108-662A-19H-5, 29	170.99	88.8	2.3	8.8	1.06
108-662A-19H-5, 41	171.11	89.1	1.9	9.0	1.07
108-662A-19H-5, 50	171.20	88.6	2.4	9.0	1.05
108-662A-19H-5, 59	171.29	89.6	2.9	7.5	1.04
108-662A-19H-5, 71	171.41	86.8	2.6	10.6	1.02
108-662A-19H-5, 79	171.50	88.8	2.9	8.3	1.02
108-662A-19H-5, 89	171.59	87.4	2.2	10.4	1.03
108-662A-19H-5, 101	171.71	90.7	2.0	7.3	1.01
108-662A-19H-5, 110	171.80	87.3	1.9	10.8	1.03
108-662A-19H-5, 119	171.89	82.4	3.2	14.4	1.07
108-662A-19H-5, 131	172.01	76.0	3.9	20.2	0.99
108-662A-19H-5, 139	172.09	85.7	3.7	10.5	1.01
108-662A-19H-5, 146	172.16	88.0	2.2	9.8	1.08
108-662A-19H-6, 11	172.31	90.9	2.5	6.6	1.01
108-662A-19H-6, 19	172.39	90.0	3.0	7.1	0.98
108-662A-19H-6, 29	172.49	87.4	3.2	9.4	1.00
108-662A-19H-6, 41	172.61	82.6	4.0	13.4	0.97
108-662A-19H-6, 50	172.70	87.8	3.2	9.0	1.00
108-662A-19H-6, 59	172.79	88.9	2.5	8.6	1.03
108-662A-19H-6, 71	172.91	89.9	2.2	7.9	1.00
108-662A-19H-6, 79	172.99	88.7	2.2	9.1	0.99
108-662A-19H-6, 89	173.09	90.8	2.0	7.2	1.02
108-662A-19H-6, 101	173.21	90.0	0.4	9.6	1.01
108-662A-19H-6, 110	173.30	87.1	3.0	9.9	1.00
108-662A-19H-6, 119	173.39	85.0	3.7	11.3	0.97
108-662A-19H-6, 131	173.51	89.3	3.1	7.6	0.98
108-662A-19H-6, 139	173.59	91.1	2.5	6.3	0.98
108-662A-19H-6, 146	173.66	90.0	2.5	7.4	1.02
108-662A-19H-7, 11	173.81	90.2	2.6	7.2	1.02
108-662A-19H-7, 19	173.89	90.7	2.0	7.2	1.04
108-662A-19H-7, 29	173.99	90.4	2.5	7.1	1.10
108-662A-20H-1, 11	174.31	91.3	2.6	6.1	0.98
108-662A-20H-1, 19	174.39	89.3	2.3	8.4	0.94
108-662A-20H-1, 29	174.49	91.0	2.7	6.2	1.02

Table 4 (continued).

Core, section, interval (cm)	Depth (mbsf)	CaCO ₃ (%)	SiO ₂ (%)	Terrigenous fraction (%)	Dry-bulk density (g/cm ³)
108-662A-20H-1, 41	174.61	90.9	2.7	6.5	0.98
108-662A-20H-1, 50	174.70	90.4	2.1	7.5	0.97
108-662A-20H-1, 59	174.79	92.2	2.1	5.6	0.97
108-662A-20H-1, 71	174.91	91.5	2.5	6.1	0.94
108-662A-20H-1, 79	174.99	90.3	2.8	6.9	0.93
108-662A-20H-1, 89	175.09	87.7	2.7	9.6	0.75
108-662A-20H-1, 101	175.21	90.4	2.5	7.1	0.93
108-662A-20H-1, 110	175.30	89.2	1.8	9.0	0.93
108-662A-20H-1, 119	175.39	90.5	2.2	7.3	0.93
108-662A-20H-1, 131	175.51	90.2	2.3	7.5	0.94
108-662A-20H-1, 139	175.59	89.8	2.6	7.6	0.94
108-662A-20H-1, 145	175.65	91.1	2.3	6.7	0.97
108-662A-20H-2, 11	175.81	89.8	2.3	7.8	1.00
108-662A-20H-2, 19	175.89	90.9	2.9	6.2	0.94
108-662A-20H-2, 29	175.99	90.2	2.0	7.8	1.00
108-662A-20H-2, 41	176.11	87.3	3.2	9.5	0.97
108-662A-20H-2, 50	176.20	87.1	2.7	10.2	0.95
108-662A-20H-2, 59	176.29	88.8	3.0	8.2	1.00
108-662A-20H-2, 71	176.41	87.9	3.3	8.8	0.99
108-662A-20H-2, 79	176.49	88.7	2.9	8.4	0.97
108-662A-20H-2, 131	177.01	88.5	2.6	8.9	1.00
108-662A-20H-2, 139	177.09	88.4	3.0	8.6	1.00
108-662A-20H-2, 146	177.16	88.5	3.3	8.2	1.04
108-662A-20H-3, 11	177.21	90.0	1.9	8.1	1.02
108-662A-20H-3, 110	176.80	89.8	1.4	8.8	1.00
108-662A-20H-3, 119	176.89	89.2	2.3	8.5	1.00
108-662A-20H-3, 19	177.39	92.6	2.2	5.1	1.00
108-662A-20H-3, 29	177.49	91.4	2.0	6.6	1.04
108-662A-20H-3, 41	177.61	90.2	2.5	7.2	1.07
108-662A-20H-3, 50	177.70	91.6	2.3	6.1	1.04
108-662A-20H-3, 59	177.79	89.5	2.8	7.7	1.02
108-662A-20H-3, 71	177.91	91.5	2.4	6.0	1.02
108-662A-20H-3, 79	177.99	91.6	2.2	6.2	0.99
108-662A-20H-3, 89	178.09	92.4	1.8	5.8	1.03
108-662A-20H-3, 101	178.21	91.9	2.0	6.1	1.00
108-662A-20H-4, 11	178.30	88.7	2.7	8.6	0.99
108-662A-20H-4, 119	178.39	86.9	2.8	10.4	1.06
108-662A-20H-4, 131	178.51	86.6	3.3	10.1	1.10
108-662A-20H-4, 139	178.59	88.7	3.2	8.1	0.97
108-662A-20H-4, 146	178.66	89.3	2.8	7.9	1.03
108-662A-20H-4, 149	178.76	89.3	2.3	6.1	1.04
108-662A-20H-4, 151	178.86	90.3	1.7	8.0	1.03
108-662A-20H-4, 171	179.41	92.0	2.1	5.9	1.07
108-662A-20H-4, 179	179.49	92.2	2.2	5.6	1.00
108-662A-20H-4, 189	179.59	90.2	2.6	7.2	1.03
108-662A-20H-4, 201	179.71	90.5	2.2	7.3	1.02
108-662A-20H-4, 209	179.79	92.3	1.9	5.9	1.05
108-662A-20H-4, 211	179.80	90.3	1.7	8.0	1.03
108-662A-20H-4, 219	179.89	92.8	2.1	5.1	1.08
108-662A-20H-4, 231	179.98	92.0	2.2	5.6	1.00
108-662A-20H-4, 249	180.01	93.5	1.8	4.8	1.05
108-662A-20H-4, 251	180.09	92.7	2.2	5.1	1.01
108-662A-20H-4, 269	180.16	90.4	2.5	7.2	1.04
108-662A-20H-4, 271	180.31	88.6	3.0	8.4	1.04
108-662A-20H-4, 289	180.39	91.8	2.2	6.0	1.02
108-662A-20H-5, 29	180.49	93.1	2.0	4.9	1.14
108-662A-20H-5, 41	180.61	92.3	2.0	5.7	1.04
108-662A-20H-5, 50	180.70	93.4	1.7	4.9	1.03
108-662A-20H-5, 59	180.79	91.1	2.3	6.6	1.04
108-662A-20H-5, 71	180.91	84.4	3.3	12.3	1.06
108-662A-20H-5, 79	180.99	82.6	3.1	14.3	1.02
108-662A-20H-5, 89	181.09	85.5	3.3	11.2	1.34
108-662A-20H-5, 101	181.21	91.8	2.3	5.9	1.03
108-662A-20H-5, 113	181.33	91.9	1.7	6.5	1.06
108-662A-20H-5, 119	181.39	93.1	1.8	5.1	1.09
108-662A-20H-5, 119	181.81	88.4	2.6	9.1	1.03
108-662A-20H-6, 11	181.89	85.5	2.3	12.1	1.01
108-662A-20H-6, 29	181.99	92.2	2.0	5.8	1.06
108-662A-20H-6, 41	182.11	91.0	2.0		

Table 4 (continued).

Core, section, interval (cm)	Depth (mbsf)	CaCO ₃ (%)	SiO ₂ (%)	Terrigenous fraction (%)	Dry-bulk density (g/cm ³)
108-662A-20H-6, 79	182.49	87.3	3.4	9.3	1.02
108-662A-20H-6, 89	182.59	87.1	3.1	9.9	1.03
108-662A-20H-6, 101	182.71	90.2	3.3	6.5	0.97
108-662A-20H-6, 110	182.80	91.2	3.1	5.7	1.01
108-662A-20H-6, 119	182.89	92.1	2.7	5.2	1.02
108-662A-20H-6, 131	183.01	92.8	2.2	5.0	1.03
108-662A-20H-6, 139	183.09	92.6	2.2	5.2	1.00
108-662A-20H-6, 146	183.16	92.7	1.8	5.5	1.04
108-662A-20H-7, 11	183.31	88.9	1.9	9.2	1.07
108-662A-20H-7, 19	183.39	92.2	1.9	5.9	1.07
108-662A-20H-7, 29	183.49	91.4	1.9	6.7	1.25
108-662A-20H-7, 41	183.61	92.1	2.3	5.5	1.06
108-662A-21H-1, 11	183.81	86.8	2.8	10.4	
108-662A-21H-1, 19	183.89	89.1	2.6	8.3	0.99
108-662A-21H-1, 29	183.99	90.9	1.2	7.9	
108-662A-21H-1, 41	184.11	92.9	1.3	5.8	
108-662A-21H-1, 50	184.20	93.2	1.3	5.5	
108-662A-21H-1, 59	184.29	91.4	1.9	6.8	
108-662A-21H-1, 71	184.41	88.7	2.1	9.2	
108-662A-21H-1, 79	184.49	88.6	2.2	9.2	1.01
108-662A-21H-1, 89	184.59	91.3	1.6	7.1	
108-662A-21H-1, 101	184.71	92.3	1.3	6.4	
108-662A-21H-1, 108	184.78	93.3	1.1	5.7	
108-662A-21H-1, 119	184.89	91.2	1.3	7.4	
108-662A-21H-1, 131	185.01	93.7	1.3	5.0	
108-662A-21H-1, 139	185.09	87.6	2.2	10.2	1.00
108-662A-21H-1, 146	185.16	91.9	1.8	6.3	
108-662A-21H-2, 11	185.31	90.9	2.4	6.7	
108-662A-21H-2, 19	185.39	89.2	2.3	8.5	0.99
108-662A-21H-2, 29	185.49	91.1	2.0	6.9	
108-662A-21H-2, 41	185.61	91.2	1.6	7.2	
108-662A-21H-2, 50	185.70	91.4	1.5	7.1	
108-662A-21H-2, 59	185.79	93.2	1.7	5.1	
108-662A-21H-2, 71	185.91	91.8	1.7	6.5	
108-662A-21H-2, 79	185.99	92.9	1.7	5.5	0.99
108-662A-21H-2, 89	186.09	93.0	1.3	5.7	
108-662A-21H-2, 101	186.21	90.7	1.2	8.1	
108-662A-21H-2, 108	186.28	92.9	1.1	5.9	
108-662A-21H-2, 119	186.39	93.6	1.1	5.3	
108-662A-21H-2, 131	186.51	93.0	1.2	5.8	
108-662A-21H-2, 139	186.59	91.7	2.0	6.3	1.01
108-662A-21H-2, 146	186.66	91.4	1.9	6.7	
108-662A-21H-3, 11	186.81	90.5	2.2	7.3	
108-662A-21H-3, 19	186.89	89.5	1.9	8.5	1.01
108-662A-21H-3, 29	186.99	92.2	1.9	5.9	
108-662A-21H-3, 41	187.11	91.3	1.7	7.0	
108-662A-21H-3, 50	187.20	92.1	1.5	6.4	
108-662A-21H-3, 59	187.29	91.0	1.8	7.2	
108-662A-21H-3, 71	187.41	89.6	1.9	8.5	
108-662A-21H-3, 79	187.49	89.8	2.1	8.1	0.99
108-662A-21H-3, 89	187.59	93.2	1.1	5.8	
108-662A-21H-3, 101	187.71	94.3	1.0	4.7	
108-662A-21H-3, 108	187.78	94.3	1.3	4.4	
108-662A-21H-3, 119	187.89	93.7	1.0	5.3	
108-662A-21H-3, 131	188.01	92.3	1.6	6.1	
108-662A-21H-3, 139	188.09	92.1	1.6	6.4	1.02
108-662A-21H-3, 146	188.16	81.3	1.5	17.1	
108-662A-21H-4, 11	188.31	91.5	1.5	7.0	
108-662A-21H-4, 19	188.39	90.5	1.7	7.8	1.07
108-662A-21H-4, 29	188.49	88.8	2.3	8.9	
108-662A-21H-4, 41	188.61	86.7	3.1	10.2	
108-662A-21H-4, 50	188.70	86.8	2.5	10.8	
108-662A-21H-4, 59	188.79	91.2	1.6	7.1	
108-662A-21H-4, 71	188.91	92.4	1.3	6.4	
108-662A-21H-4, 79	188.99	92.1	1.3	6.6	0.98
108-662A-21H-4, 89	189.09	92.8	1.5	5.7	
108-662A-21H-4, 101	189.21	85.8	1.5	12.8	
108-662A-21H-4, 108	189.28	93.0	1.6	5.4	
108-662A-21H-4, 119	189.39	93.1	1.0	5.9	
108-662A-21H-4, 131	189.51	91.7	1.2	7.1	
108-662A-21H-4, 139	189.59	93.6	1.0	5.4	1.03
108-662A-21H-4, 146	189.66	91.4	1.1	7.4	
108-662A-21H-5, 11	189.81	92.3	0.8	6.9	
108-662A-21H-5, 19	189.89	91.5	1.1	7.3	1.01
108-662A-21H-5, 29	189.99	85.8	0.9	13.3	
108-662A-21H-5, 41	190.11	87.1	1.0	11.9	

Table 4 (continued).

Core, section, interval (cm)	Depth (mbsf)	CaCO ₃ (%)	SiO ₂ (%)	Terrigenous fraction (%)	Dry-bulk density (g/cm ³)
108-662A-21H-5, 50	190.20	92.6	1.4	6.0	
108-662A-21H-5, 59	190.29	91.3	1.0	7.7	
108-662A-21H-5, 71	190.41	90.8	1.4	7.8	
108-662A-21H-5, 79	190.49	90.3	1.3	8.3	1.02
108-662A-21H-5, 89	190.59	92.9	1.1	6.0	
108-662A-21H-5, 101	190.71	91.4	1.3	7.3	
108-662A-21H-5, 108	190.78	92.2	1.6	6.3	
108-662A-21H-5, 119	190.89	92.3	1.4	6.3	
108-662A-21H-5, 131	191.01	88.5	1.3	10.2	
108-662A-21H-5, 136	191.06	91.0	1.5	7.5	1.00
108-662A-21H-5, 138	191.08	90.8	1.6	7.7	
108-662A-21H-6, 11	191.31	92.0	1.9	6.1	
108-662A-21H-6, 19	191.39	71.3	2.1	26.6	1.02
108-662A-21H-6, 29	191.49	88.9	2.0	9.1	
108-662A-21H-6, 39	191.59	88.5	2.0	9.6	
108-662A-21H-6, 50	191.70	88.7	2.6	8.7	
108-662A-21H-6, 59	191.79	93.2	1.7	5.1	
108-662A-21H-6, 71	191.91	87.5	1.9	10.7	
108-662A-21H-6, 79	191.99	92.3	1.6	6.1	1.01
108-662A-21H-6, 89	192.09	93.5	1.3	5.1	
108-662A-21H-6, 101	192.21	92.0	1.7	6.3	
108-662A-21H-6, 108	192.28	92.3	1.9	5.8	
108-662A-21H-6, 119	192.39	92.9	1.6	5.5	
108-662A-21H-6, 131	192.51	95.7	1.5	2.8	
108-662A-21H-6, 139	192.59	77.7	1.5	20.8	1.23
108-662A-21H-6, 144	192.64	90.6	1.4	8.0	
108-662A-21H-7, 11	192.81	89.0	1.3	9.8	
108-662A-21H-7, 29	192.99	91.5	1.7	6.8	
108-662A-21H-7, 39	193.09	88.2	1.3	10.5	
108-662A-22H-1, 50	193.70	90.3	1.8	7.9	
108-662A-22H-1, 59	193.79	90.5			
108-662A-22H-1, 71	193.91	92.5	1.3	6.3	
108-662A-22H-1, 79	193.99	91.7	1.3	7.1	0.96
108-662A-22H-1, 89	194.09	92.0	1.3	6.7	
108-662A-22H-1, 101	194.21	91.8	1.3	6.9	
108-662A-22H-1, 110	194.30	92.7	1.6	5.7	
108-662A-22H-1, 119	194.39	91.6	1.3	7.2	
108-662A-22H-1, 131	194.51	88.8	1.4	9.8	
108-662A-22H-1, 139	194.59	91.5	1.6	7.0	1.01
108-662A-22H-1, 146	194.66	86.5	1.4	12.1	
108-662A-22H-2, 11	194.81	90.2	1.6	8.3	
108-662A-22H-2, 19	194.89	88.8	1.4	9.8	1.01
108-662A-22H-2, 29	194.99	91.3	1.3	7.5	
108-662A-22H-2, 41	195.11	92.5	1.0	6.6	
108-662A-22H-2, 50	195.20	91.5	1.2	7.3	
108-662A-22H-2, 59	195.29	92.6	1.1	6.3	
108-662A-22H-2, 71	195.41	90.2	1.2	8.6	
108-662A-22H-2, 110	195.49	91.7	1.4	6.9	
108-662A-22H-2, 131	195.49	91.6	0.9	7.5	
108-662A-22H-2, 146	196.16	91.4	1.1	7.5	
108-662A-22H-3, 11	196.31	90.3	1.3	8.4	
108-662A-22H-3, 19	196.39	91.4	1.2	7.4	1.02
108-662A-22H-3, 29	196.49	90.4	1.0	8.6	
108-662A-22H-3, 41	196.61	93.7	1.3	5.0	
108-662A-22H-3, 50	196.70	94.8	1.2	4.0	
108-662A-22H-3, 59	196.79	94.3	1.3	4.4	
108-662A-22H-3, 71	196.91	92.2	1.5	6.2	
108-662A-22H-3, 79	196.99	85.7	1.3	13.0	1.01
108-662A-22H-3, 89	197.09	92.8	1.6	5.6	
108-662A-22H-3, 101	197.21	94.2	2.1	3.8	
108-662A-22H-3, 110	197.30	92.5	1.7	5.7	
108-662A-22H-3, 119	197.39	93.1	1.6	5.4	
108-662A-22H-3, 131	197.51	78.6	1.7	19.7	
108-662A-22H-3, 139	197.59	93.8	1.7	4.6	1.00
108-662A-22H-3, 146	197.66	94.0	1.6	4.4	
108-662A-22H-4, 11	197.81	92.2	1.9	5.9	
108-662A-22H-4, 19	197.89	92.2	1.5	6.3	1.04
108-662A-22H-4, 29	197.99	90.5	2.2	7.3	
108-662A-22H-4, 41	198.11	91.4	2.1	6.5	
108-662A-22H-4, 50	198.20	91.2	1.4	7.4	
108-662A-22H-4, 59	198.29	92.7	1.7	5.6	

Table 4 (continued).

Core, section, interval (cm)	Depth (mbsf)	CaCO ₃ (%)	SiO ₂ (%)	Terrigenous fraction (%)	Dry-bulk density (g/cm ³)
108-662A-22H-4, 71	198.41	93.1	1.7	5.2	
108-662A-22H-4, 79	198.49	91.2	1.5	7.3	0.98
108-662A-22H-4, 89	198.59	93.0	1.5	5.6	
108-662A-22H-4, 101	198.71	92.3	1.4	6.3	
108-662A-22H-4, 110	198.80	91.7	1.3	7.0	
108-662A-22H-4, 119	198.89	91.6	1.4	7.0	
108-662A-22H-4, 131	199.01	89.9	1.4	8.6	
108-662A-22H-4, 139	199.09	90.8	1.8	7.3	0.99
108-662A-22H-4, 146	199.16	92.3	1.5	6.2	
108-662A-22H-5, 11	199.31	90.8	1.5	7.7	
108-662A-22H-5, 19	199.39	91.3	1.3	7.4	0.99
108-662A-22H-5, 29	199.49	91.0	1.1	7.9	
108-662A-22H-5, 41	199.61	91.2	1.3	7.6	
108-662A-22H-5, 50	199.70	91.1	1.4	7.5	
108-662A-22H-5, 59	199.79	95.0	0.8	4.3	
108-662A-22H-5, 71	199.91	87.6	1.3	11.1	
108-662A-22H-5, 79	199.99	84.3	1.9	13.8	1.01
108-662A-22H-5, 89	200.09	82.4	1.7	15.9	
108-662A-22H-5, 101	200.21	85.5	1.6	13.0	
108-662A-22H-5, 110	200.30	87.9	1.5	10.6	
108-662A-22H-5, 119	200.39	90.7	1.1	8.2	
108-662A-22H-5, 131	200.51	90.4	0.9	8.7	
108-662A-22H-5, 139	200.59	91.5	1.3	7.2	
108-662A-22H-5, 146	200.66	91.4	1.1	7.5	
108-662A-22H-6, 11	200.81	90.4	1.3	8.2	
108-662A-22H-6, 19	200.89	90.0	1.8	8.2	1.01
108-662A-22H-6, 29	200.99	85.0	1.5	13.6	
108-662A-22H-6, 41	201.11	86.7	1.5	11.8	
108-662A-22H-6, 50	201.20	90.8	1.5	7.6	
108-662A-22H-6, 59	201.29	91.3	1.1	7.7	
108-662A-22H-6, 71	201.41	91.9	1.2	6.9	
108-662A-22H-6, 79	201.49	91.3	1.2	7.5	1.00
108-662A-22H-6, 89	201.59	93.8	1.3	4.9	
108-662A-22H-6, 101	201.71	91.7	1.5	6.8	
108-662A-22H-6, 110	201.80	92.4	1.5	6.1	
108-662A-22H-6, 119	201.89	91.8	1.8	6.4	
108-662A-22H-6, 131	202.01	91.7	1.5	6.8	
108-662A-22H-6, 139	202.09	91.4	1.5	7.1	1.00
108-662A-22H-6, 146	202.16	92.1	1.4	6.4	
108-662A-22H-7, 11	202.31	92.1	1.3	6.6	
108-662A-22H-7, 19	202.39	92.4	1.5	6.1	0.97
108-662A-22H-7, 29	202.49	91.5	1.7	6.8	
108-662A-22H-7, 41	202.61	93.3	1.8	4.9	
108-662A-22H-7, 50	202.70	94.3	1.9	3.8	
108-662A-22H-7, 59	202.79	91.7	1.7	6.6	

Table 5 (continued).

Core, section, interval (cm)	Depth (mbsf)	CaCO ₃ (%)	SiO ₂ (%)	Terrigenous fraction (%)	Dry-bulk density (g/cm ³)
108-663A-1H-2, 71	2.21	77.5	5.1	17.4	0.62
108-663A-1H-2, 79	2.29	75.0	3.1	21.8	0.62
108-663A-1H-2, 89	2.39	80.7	4.4	14.9	0.71
108-663A-1H-2, 101	2.51	80.7	4.8	14.5	0.69
108-663A-1H-2, 110	2.60	78.1	5.3	16.6	0.74
108-663A-1H-2, 119	2.69	75.9	6.1	18.1	0.63
108-663A-1H-2, 131	2.81	72.2	6.7	21.1	0.59
108-663A-1H-2, 139	2.89	70.4	6.9	22.6	0.54
108-663A-1H-3, 11	3.11	70.5	7.5	22.0	0.57
108-663A-1H-3, 19	3.19	71.7	6.4	22.0	0.55
108-663A-1H-3, 29	3.29	63.2	7.4	29.4	0.57
108-663A-1H-3, 41	3.41	75.7	4.7	19.6	0.66
108-663A-1H-3, 50	3.50	84.6	3.1	12.3	0.72
108-663A-1H-3, 59	3.59	86.8	3.0	10.3	0.73
108-663A-1H-3, 71	3.71	76.4	5.4	18.1	0.68
108-663A-1H-3, 79	3.79	84.4	3.0	12.6	0.71
108-663A-1H-3, 89	3.89	83.6	3.2	13.2	0.70
108-663A-1H-3, 101	4.01	74.4	3.5	22.1	0.69
108-663A-1H-3, 110	4.10	85.0	3.3	11.7	0.72
108-663A-1H-3, 119	4.19	85.9	2.8	11.3	0.77
108-663A-1H-3, 131	4.31	81.3	2.8	15.8	0.74
108-663A-1H-3, 139	4.39	83.6	3.1	13.4	0.66
108-663A-1H-3, 146	4.46	83.1	3.5	13.4	0.67
108-663A-2H-1, 11	4.81	75.4	6.6	18.0	0.55
108-663A-2H-1, 21	4.91	64.8	8.4	26.8	0.48
108-663A-2H-1, 29	4.99	66.2	7.3	26.5	0.49
108-663A-2H-1, 40	5.09	66.1	7.1	26.8	0.52
108-663A-2H-1, 50	5.19	85.2	3.5	11.3	0.72
108-663A-2H-1, 59	5.29	86.1	3.5	10.3	0.71
108-663A-2H-1, 71	5.41	77.0	3.7	19.3	0.68
108-663A-2H-1, 79	5.49	76.2	3.7	20.2	0.70
108-663A-2H-1, 89	5.59	85.3	4.3	10.4	0.68
108-663A-2H-1, 101	5.71	72.1	4.5	23.4	0.59
108-663A-2H-1, 110	5.80	76.7	5.0	18.4	0.68
108-663A-2H-1, 119	5.89	73.9	6.0	20.1	0.54
108-663A-2H-1, 131	6.01	83.8	5.6	10.6	0.56
108-663A-2H-1, 139	6.09	75.8	4.6	19.6	0.64
108-663A-2H-2, 11	6.31	66.2	6.1	27.7	0.61
108-663A-2H-2, 19	6.39	85.4	3.3	11.4	0.76
108-663A-2H-2, 29	6.49	88.8	2.1	9.1	0.76
108-663A-2H-2, 41	6.61	78.5	3.8	17.7	0.71
108-663A-2H-2, 50	6.70	80.2	4.0	15.8	0.78
108-663A-2H-2, 59	6.79	80.3	3.7	16.0	0.62
108-663A-2H-2, 71	6.91	86.6	3.0	10.4	0.77
108-663A-2H-2, 79	6.99	86.5	3.2	10.3	0.78
108-663A-2H-2, 89	7.09	79.6	3.1	17.3	0.71
108-663A-2H-2, 101	7.21	81.0	4.4	14.6	0.63
108-663A-2H-2, 110	7.30	68.9	5.5	25.6	0.64
108-663A-2H-2, 119	7.39	63.7	6.2	30.0	0.53
108-663A-2H-2, 131	7.51	71.0	5.6	23.4	0.56
108-663A-2H-2, 139	7.59	82.7	4.5	12.8	0.68
108-663A-2H-2, 146	7.66	83.5	4.5	12.0	0.67
108-663A-2H-3, 11	7.81	88.9	3.2	7.8	0.72
108-663A-2H-3, 19	7.89	74.9	5.3	19.7	0.64
108-663A-2H-3, 29	7.99	80.4	4.5	15.0	0.72
108-663A-2H-3, 41	8.11	78.6	4.5	16.9	0.66
108-663A-2H-3, 50	8.20	77.2	4.9	18.0	0.66
108-663A-2H-3, 59	8.29	81.9	4.6	13.5	0.64
108-663A-2H-3, 71	8.41	82.8	3.6	13.6	0.66
108-663A-2H-3, 79	8.49	82.1	4.3	13.6	0.70
108-663A-2H-3, 89	8.59	78.4	4.7	16.9	0.67
108-663A-2H-3, 101	8.71	69.0	6.1	25.0	0.61
108-663A-2H-3, 110	8.80	74.8	7.2	18.0	0.68
108-663A-2H-3, 119	8.89	77.5	5.6	16.9	0.63
108-663A-2H-3, 131	9.01	72.4	6.5	21.1	0.55
108-663A-2H-3, 139	9.09	65.7	8.2	26.2	0.48
108-663A-2H-3, 146	9.16	67.5	7.5	25.0	0.54
108-663A-2H-4, 11	9.31	68.3	6.4	25.3	0.60
108-663A-2H-4, 19	9.39	78.1	4.1	17.9	0.72
108-663A-2H-4, 29	9.49	83.5	3.5	13.0	0.74
108-663A-2H-4, 41	9.61	87.9	3.7	8.4	0.71
108-663A-2H-4, 50	9.70	86.6	3.3	10.1	0.81
108-663A-2H-4, 59	9.79	86.2	2.8	11.0	0.80
108-663A-2H-4, 71	9.91	84.0	3.6	12.4	0.77
108-663A-2H-4, 79	9.99	84.4	2.9	12.7	0.75
108-663A-2H-4, 89	10.09	78.4	3.8	17.8	0.73
108-663A-2H-4, 101	10.21	81.1	3.7	15.3	0.75

Table 5 (continued).

Core, section, interval (cm)	Depth (mbsf)	CaCO ₃ (%)	SiO ₂ (%)	Terrigenous fraction (%)	Dry-bulk density (g/cm ³)
108-663A-2H-4, 110	10.30	82.2	4.0	13.8	0.77
108-663A-2H-4, 119	10.39	76.9	5.5	17.6	0.66
108-663A-2H-4, 131	10.51	84.1	3.2	12.6	0.78
108-663A-2H-4, 139	10.59	82.9	2.3	14.8	0.80
108-663A-2H-4, 146	10.66	86.7	2.7	10.6	0.81
108-663A-2H-5, 11	10.81	73.1	5.1	21.8	0.69
108-663A-2H-5, 19	10.89	82.6	4.6	12.8	0.74
108-663A-2H-5, 29	10.99	85.3	3.8	10.9	0.82
108-663A-2H-5, 41	11.11	88.7	3.0	8.3	0.82
108-663A-2H-5, 50	11.20	78.4	2.9	18.7	0.85
108-663A-2H-5, 59	11.29	83.1	3.7	13.2	0.83
108-663A-2H-5, 71	11.41	64.5	6.8	28.7	0.63
108-663A-2H-5, 79	11.49	64.6	5.7	29.7	0.59
108-663A-2H-5, 89	11.59	67.2	6.3	26.5	0.59
108-663A-2H-5, 101	11.71	77.1	5.5	17.5	0.66
108-663A-2H-5, 110	11.80	81.6	5.1	13.3	0.69
108-663A-2H-5, 118	11.88	79.4	4.5	16.1	0.68
108-663A-2H-6, 11	12.31	64.3	5.0	30.7	0.70
108-663A-2H-6, 19	12.39	78.0	5.2	16.8	0.68
108-663A-2H-6, 29	12.49	79.7	4.7	15.6	0.84
108-663A-2H-6, 41	12.61	80.1	6.1	13.9	0.69
108-663A-2H-6, 50	12.70	82.4	4.5	13.1	0.73
108-663A-2H-6, 59	12.79	81.0	4.7	14.3	0.70
108-663A-2H-6, 71	12.91	81.8	3.8	14.4	0.72
108-663A-2H-6, 79	12.99	80.3	4.5	15.2	0.78
108-663A-2H-6, 89	13.09	85.5	3.9	10.7	0.81
108-663A-2H-6, 101	13.21	80.7	2.3	17.0	0.84
108-663A-2H-6, 110	13.30	89.3	2.7	8.0	0.88
108-663A-2H-6, 119	13.39	83.7	3.9	12.4	0.77
108-663A-2H-6, 131	13.51	90.7	1.8	7.5	0.89
108-663A-2H-6, 139	13.59	88.2	2.1	9.7	0.91
108-663A-2H-6, 146	13.66	90.4	2.2	7.4	0.84
108-663A-2H-7, 11	13.81	84.3	3.2	12.6	0.82
108-663A-2H-7, 19	13.89	83.0	4.0	13.1	0.75
108-663A-2H-7, 29	13.99	69.0	5.1	25.9	0.65
108-663A-3H-1, 19	14.39	88.0	2.1	9.9	0.87
108-663A-3H-1, 29	14.49	85.8	2.5	11.7	0.90
108-663A-3H-1, 41	14.61	64.1	6.6	29.3	0.61
108-663A-3H-1, 50	14.70	75.6	5.5	18.9	0.69
108-663A-3H-1, 57	14.77	76.6	5.6	17.8	0.71
108-663A-3H-1, 71	14.91	82.9	4.7	12.4	0.70
108-663A-3H-1, 79	14.99	81.0	4.7	14.3	0.70
108-663A-3H-1, 89	15.09	74.5	6.0	19.5	0.73
108-663A-3H-1, 101	15.21	74.1	7.3	18.6	0.61
108-663A-3H-1, 110	15.30	81.1	4.1	14.8	0.72
108-663A-3H-1, 119	15.39	81.6	3.6	14.9	0.71
108-663A-3H-1, 131	15.51	88.9	2.9	8.2	0.80
108-663A-3H-1, 139	15.59	88.0	2.6	9.4	0.80
108-663A-3H-1, 146	15.66	83.4	3.5	13.2	0.76
108-663A-3H-2, 11	15.81	77.4	5.0	17.6	0.69
108-663A-3H-2, 19	15.89	66.6	5.8	27.7	0.60
108-663A-3H-2, 29	15.99	79.7	4.4	15.9	0.69
108-663A-3H-2, 41	16.11	83.8	4.1	12.1	0.72
108-663A-3H-2, 50	16.20	75.3	5.8	18.9	0.67
108-663A-3H-2, 59	16.29	86.3	3.7	10.0	0.75
108-663A-3H-2, 71	16.41	84.6	3.4	12.0	0.77
108-663A-3H-2, 79	16.49	80.3	5.0	14.7	0.73
108-663A-3H-2, 89	16.59	79.8	5.1	15.1	0.68
108-663A-3H-2, 101	16.71	78.8	4.6	16.6	0.69
108-663A-3H-2, 110	16.80	69.7	5.1	25.1	0.66
108-663A-3H-2, 119	16.89	65.3	7.5	27.3	0.59
108-663A-3H-2, 131	17.01	89.5	3.0	7.5	0.83
108-663A-3H-2, 139	17.09	86.7	4.0	9.4	0.84
108-663A-3H-2, 146	17.16	89.8	2.1	8.1	0.89
108-663A-3H-3, 11	17.31	90.8	2.3	7.0	0.90
108-663A-3H-3, 19	17.39	84.3	2.7	12.9	0.86
108-663A-3H-3, 29	17.49	91.1	2.1	6.8	0.94
108-663A-3H-3, 41	17.61	87.8	2.7	9.5	0.89
108-663A-3H-3, 50	17.70	89.5	2.4	8.1	0.91
108-663A-3H-3, 59	17.79	86.9	2.7	10.3	0.88
108-663A-3H-3, 71	17.91	87.0	2.8	10.3	0.88
108-663A-3H-3, 79	17.99	86.6	2.7	10.7	0.88
108-663A-3H-3, 89	18.09	85.6	2.9	11.5	0.88
108-663A-3H-3, 101	18.21	87.5	2.8	9.7	0.87
108-663A-3H-3, 110	18.30	87.2	3.0	9.8	0.86
108-663A-3H-3, 119	18.39	88.5	3.0	8.5	0.83

Table 5 (continued).

Core, section, interval (cm)	Depth (mbsf)	CaCO ₃ (%)	SiO ₂ (%)	Terrigenous fraction (%)	Dry-bulk density (g/cm ³)
108-663A-3H-3, 131	18.51	89.1	2.6	8.3	0.87
108-663A-3H-3, 139	18.59	89.5	2.4	8.1	0.86
108-663A-3H-3, 146	18.66	92.6	2.1	5.2	0.87
108-663A-3H-4, 11	18.81	86.2	2.5	11.4	0.89
108-663A-3H-4, 19	18.89	90.3	2.4	7.3	0.86
108-663A-3H-4, 29	18.99	90.1	2.5	7.4	0.87
108-663A-3H-4, 41	19.11	84.4	3.8	11.8	0.84
108-663A-3H-4, 50	19.20	87.2	3.7	9.1	0.79
108-663A-3H-4, 59	19.29	85.5	3.4	11.1	0.64
108-663A-3H-4, 71	19.41	87.7	3.1	9.3	0.80
108-663A-3H-4, 79	19.49	89.8	3.2	7.0	0.81
108-663A-3H-4, 89	19.59	79.9	5.5	14.6	0.71
108-663A-3H-4, 101	19.71	86.8	3.4	9.8	0.79
108-663A-3H-4, 110	19.80	87.2	3.0	9.8	0.84
108-663A-3H-4, 119	19.89	84.4	3.3	12.3	0.81
108-663A-3H-4, 131	20.01	85.5	4.3	10.3	0.78
108-663A-3H-4, 139	20.09	83.4	3.8	12.8	0.79
108-663A-3H-4, 146	20.16	82.9	4.2	12.9	0.78
108-663A-3H-5, 11	20.31	75.3	3.9	20.8	0.71
108-663A-3H-5, 19	20.39	86.9	3.3	9.8	0.88
108-663A-3H-5, 29	20.49	84.3	4.0	11.7	0.87
108-663A-3H-5, 41	20.61	86.1	3.7	10.1	0.84
108-663A-3H-5, 50	20.70	87.1	2.5	10.5	1.27
108-663A-3H-5, 59	20.79	86.9	3.5	9.6	0.85
108-663A-3H-5, 71	20.91	82.9	4.3	12.9	0.81
108-663A-3H-5, 79	20.99	81.8	4.6	13.5	0.77
108-663A-3H-6, 11	21.09	82.8	3.7	13.6	0.79
108-663A-3H-6, 131	21.51	82.3	4.2	13.5	0.79
108-663A-3H-6, 139	21.59	87.3	3.5	9.2	0.84
108-663A-3H-6, 146	21.66	86.5	4.0	9.5	0.83
108-663A-3H-6, 157	21.74	78.3	4.9	16.8	0.72
108-663A-3H-6, 71	21.81	86.5	2.9	10.6	0.86
108-663A-3H-6, 19	21.89	80.2	4.4	15.4	0.77
108-663A-3H-6, 29	21.99	73.9	6.7	19.4	0.67
108-663A-3H-6, 41	22.11	75.0	6.6	18.4	0.67
108-663A-3H-6, 50	22.20	80.7	5.5	13.9	0.71
108-663A-3H-6, 59	22.29	78.3	4.9	16.8	0.72
108-663A-3H-6, 71	22.41	74.7	6.8	18.5	0.69
108-663A-3H-6, 79	22.49	76.6	5.9	17.5	0.69
108-663A-3H-6, 89	22.59	83.8	4.4	11.8	0.74
108-663A-3H-6, 101	22.71	84.3	4.2	11.6	0.76
108-663A-3H-6, 110	22.80	83.5	2.8	13.7	1.03
108-663A-3H-6, 119	22.89	88.4	3.3	8.3	0.83
108-663A-3H-6, 131	23.01	85.3	3.4	11.4	0.81
108-663A-3H-6, 139	23.09	85.5	4.2	10.3	0.77
108-663A-3H-6, 146	23.16	85.4	3.9	10.7	0.80
108-663A-3H-7, 11	23.31	79.4	5.7	14.9	0.72
108-663A-3H-7, 19	23.39	79.2	5.9	14.9	0.68
108-663A-3H-7, 41	23.61	71.9	6.3	21.8	0.67
108-663A-4H-1, 11	23.81	89.1	2.6	8.3	0.83
108-663A-4H-1, 19	23.89	89.4	2.1	8.6	0.79
108-663A-4H-1, 29	23.98	85.7	2.9	11.4	0.81
108-663A-4H-1, 41	24.09	84.7	2.9	12.4	0.80
108-663A-4H-1, 50	24.29	87.1	2.1	10.8	0.81
108-663A-4H-1, 59	24.29	87.1	2.1	10.8	0.81
108-663A-4H-1, 71	24.41	75.4	5.2	19.4	0.73
108-663A-4H-1, 79	24.49	67.7	7.6	24.7	0.61
108-663A-4H-1, 89	24.59	76.6	5.9	17.5	0.66
108-663A-4H-1, 101	24.71	81.5	5.6	12.9	0.71
108-663A-4H-1, 110	24.80	83.0	4.1	12.9	0.78
108-663A-4H-1, 119	24.89	86.3	3.7	10.0	0.76
108-663A-4H-1, 131	25.01	88.1	2.8	9.0	0.85
108-663A-4H-1, 137	25.07	88.1	2.9	9.0	0.85
108-663A-4H-2, 11	25.31	90.3	2.6	7.1	0.85
108-663A-4H-2, 19	25.39	84.7	2.7	12.6	0.83
108-663A-4H-2, 29	25.49	88.6	2.7	8.7	0.85
108-663A-4H-2, 41	25.61	85.8	3.4	10.9	0.80
108-663A-4H-2, 50	25.70	77.9	5.8	16.3	0.79
108-663A-4H-2, 59	25.79	70.4	7.9	21.7	0.64
108-663A-4H-2, 71	25.91	84.4	4.2	11.4	0.79
108-663A-4H-2, 79	25.99	84.3	3.3	12.4	0.83
108-663A-4H-2, 89	26.09	84.8	4.0	11.2	

Table 5 (continued).

Core, section, interval (cm)	Depth (mbsf)	CaCO ₃ (%)	SiO ₂ (%)	Terrigenous fraction (%)	Dry-bulk density (g/cm ³)
108-663A-4H-2, 119	26.39	80.1	4.6	15.2	0.75
108-663A-4H-2, 131	26.51	70.7	7.7	21.6	0.65
108-663A-4H-2, 139	26.59	86.4	4.1	9.5	0.77
108-663A-4H-2, 146	26.66	81.7	4.2	14.1	0.76
108-663A-4H-3, 11	26.81	85.5	4.8	9.7	0.90
108-663A-4H-3, 19	26.89	79.7	5.4	14.8	0.72
108-663A-4H-3, 29	26.99	87.7	4.0	8.3	0.76
108-663A-4H-3, 41	27.11	87.8	2.6	9.5	0.77
108-663A-4H-3, 50	27.20	83.2	4.0	12.8	0.78
108-663A-4H-3, 59	27.29	70.1	9.6	20.3	0.63
108-663A-4H-3, 71	27.41	54.7	2.4	42.9	0.55
108-663A-4H-3, 79	27.49	53.3	11.1	35.6	0.53
108-663A-4H-3, 89	27.59	82.7	5.8	11.5	0.71
108-663A-4H-3, 101	27.71	81.9	7.3	10.8	0.69
108-663A-4H-3, 110	27.80	82.0	4.7	13.3	0.76
108-663A-4H-3, 119	27.89	78.1	6.1	15.8	0.69
108-663A-4H-3, 131	28.01	81.7	5.4	12.9	0.73
108-663A-4H-3, 139	28.09	84.0	4.4	11.6	0.77
108-663A-4H-3, 146	28.16	83.3	4.5	12.2	0.77
108-663A-4H-4, 11	28.31	79.5	6.1	14.4	0.72
108-663A-4H-4, 19	28.39	84.4	4.1	11.5	0.78
108-663A-4H-4, 41	28.61	87.1	3.5	9.4	0.82
108-663A-4H-4, 50	28.70	70.7	4.3	24.9	0.80
108-663A-4H-4, 59	28.79	87.2	4.4	8.4	0.80
108-663A-4H-4, 79	28.99	77.7	5.2	17.1	0.71
108-663A-4H-4, 89	29.09	57.1	6.3	36.6	0.59
108-663A-4H-4, 101	29.21	86.0	3.9	10.1	0.74
108-663A-4H-4, 110	29.30	86.7	3.9	9.5	0.83
108-663A-4H-4, 119	29.39	84.4	3.9	11.7	0.82
108-663A-4H-4, 131	29.51	75.1	6.8	18.1	0.73
108-663A-4H-4, 139	29.59	82.2	4.3	13.6	0.80
108-663A-4H-4, 146	29.66	85.7	4.3	10.0	0.86
108-663A-4H-5, 11	29.81	84.4	3.4	12.3	0.80
108-663A-4H-5, 19	29.89	81.9	3.7	14.5	0.81
108-663A-4H-5, 29	29.99	65.7	5.9	28.4	0.65
108-663A-4H-5, 41	30.11	69.8	5.5	24.8	0.68
108-663A-4H-5, 50	30.20	69.5	8.8	21.7	0.66
108-663A-4H-5, 59	30.29	77.4	6.5	16.1	0.77
108-663A-4H-5, 79	30.49	81.7	2.2	16.1	0.74
108-663A-4H-5, 89	30.59	79.3	5.3	15.4	0.77
108-663A-4H-5, 101	30.71	79.4	5.8	14.8	0.69
108-663A-4H-5, 110	30.80	67.1	8.0	24.9	0.66
108-663A-4H-5, 119	30.89	63.3	9.6	27.1	0.60
108-663A-4H-5, 131	31.01	69.8	8.1	22.1	0.65
108-663A-4H-5, 139	31.09	78.2	6.3	15.5	0.68
108-663A-4H-5, 146	31.16	80.9	5.3	13.8	0.72
108-663A-4H-6, 11	31.31	85.0	4.2	10.8	0.73
108-663A-4H-6, 19	31.39	82.9	4.2	12.9	0.72
108-663A-4H-6, 29	31.49	83.7	4.3	12.0	0.76
108-663A-4H-6, 41	31.61	85.8	3.8	10.4	0.74
108-663A-4H-6, 50	31.70	79.4	4.8	15.8	0.75
108-663A-4H-6, 59	31.79	67.7	8.0	24.3	0.68
108-663A-4H-6, 71	31.91	80.5	6.8	12.7	0.70
108-663A-4H-6, 79	31.99	76.9	6.1	17.0	0.71

Table 6 (continued).

Core, section, interval (cm)	Depth (mbsf)	CaCO ₃ (%)	SiO ₂ (%)	Terrigenous fraction (%)	Dry-bulk density (g/cm ³)
108-664B-1H-2, 11	1.61	80.7	2.0	17.3	0.77
108-664B-1H-2, 19	1.69	74.0	2.5	23.5	0.78
108-664B-1H-2, 29	1.79	62.8	2.8	34.4	0.69
108-664B-1H-2, 41	1.91	72.1	4.0	23.9	0.69
108-664B-1H-2, 59	2.09	67.5	4.0	28.5	0.68
108-664B-1H-2, 71	2.21	67.5	2.7	29.8	0.62
108-664B-1H-2, 79	2.29	75.3	1.7	23.0	0.67
108-664B-1H-2, 89	2.39	73.6	2.8	23.6	0.65
108-664B-1H-2, 101	2.51	86.1	1.5	12.4	0.76
108-664B-1H-2, 119	2.69	68.0	2.5	29.5	0.79
108-664B-1H-2, 126	2.76	80.0	1.4	18.6	0.81
108-664B-1H-2, 139	2.89	85.1	1.7	13.3	0.82
108-664B-1H-2, 146	2.96	83.5	1.9	14.6	0.72
108-664B-1H-3, 11	3.11	84.0	1.3	14.7	0.87
108-664B-1H-3, 19	3.19	85.9	1.7	12.3	0.86
108-664B-1H-3, 29	3.29	80.6	1.6	17.8	0.80
108-664B-1H-3, 41	3.41	74.0	1.8	24.2	0.83
108-664B-1H-3, 59	3.59	81.6	1.9	16.6	0.74
108-664B-1H-3, 71	3.71	81.8	1.7	16.5	0.83
108-664B-1H-3, 79	3.79	77.0	1.4	21.6	0.71
108-664B-1H-3, 89	3.89	72.1	2.0	26.0	0.82
108-664B-1H-4, 101	4.01			3.7	0.81
108-664B-1H-4, 119	4.19	75.7	2.5	21.9	0.67
108-664B-1H-4, 126	4.26	75.9	2.6	21.4	0.66
108-664B-1H-4, 139	4.39	74.9	3.3	21.9	0.67
108-664B-1H-4, 146	4.46	80.2	2.9	16.9	0.65
108-664B-1H-4, 11	4.61	76.2	3.3	20.5	0.72
108-664B-1H-4, 19	4.69	76.0	2.7	21.3	0.69
108-664B-1H-4, 29	4.79			3.2	0.68
108-664B-1H-4, 41	4.91			3.3	0.67
108-664B-1H-4, 59	5.09	76.3	3.2	20.6	0.68
108-664B-1H-4, 71	5.21	65.5	2.5	32.0	0.62
108-664B-1H-4, 79	5.29	62.5	2.9	34.7	0.55
108-664B-1H-4, 89	5.39	72.7	3.6	23.7	
108-664B-1H-4, 101	5.51	82.6	1.7	15.7	0.83
108-664B-1H-4, 119	5.69	79.6	2.0	18.4	0.78
108-664B-1H-4, 126	5.76	80.8	1.9	17.3	0.79
108-664B-1H-4, 139	5.89	74.6	2.9	22.5	0.72
108-664B-1H-4, 146	5.96	64.9	2.2	33.0	0.83
108-664B-1H-5, 11	6.11	75.2	1.5	23.2	0.71
108-664B-1H-5, 19	6.19	74.0	2.8	23.2	0.67
108-664B-1H-5, 29	6.29	73.9	2.2	24.0	0.77
108-664B-1H-5, 41	6.41	53.1	1.3	45.7	0.72
108-664B-1H-5, 59	6.59	89.7	2.5	7.8	0.86
108-664B-1H-5, 71	6.71	79.7	2.0	18.3	0.83
108-664B-1H-5, 79	6.79	72.6	2.5	24.9	0.76
108-664B-1H-5, 89	6.89	84.8	2.3	13.0	0.84
108-664B-1H-5, 101	7.01	83.7	2.1	14.1	0.85
108-664B-1H-5, 119	7.19	85.1	1.9	13.1	0.91
108-664B-1H-5, 126	7.26	77.9	1.9	20.2	0.82
108-664B-1H-5, 139	7.39	75.2	2.1	22.7	0.72
108-664B-1H-6, 11	7.61	66.4	3.0	30.7	0.75
108-664B-1H-6, 19	7.69	75.0	2.2	22.8	0.71
108-664B-1H-6, 29	7.79	85.4	1.8	12.8	0.79
108-664B-1H-6, 41	7.91	86.7	1.4	11.8	0.82
108-664B-1H-6, 59	8.09	80.4	2.0	17.5	0.82
108-664B-1H-6, 71	8.21	66.9	2.2	30.9	0.77
108-664B-1H-6, 79	8.29	80.1	1.5	18.4	0.77
108-664B-1H-6, 89	8.39	74.0	3.1	22.9	0.76
108-664B-1H-6, 101	8.51	80.0	1.4	18.6	0.76
108-664B-1H-6, 119	8.69	86.0	2.0	12.0	0.84
108-664B-1H-6, 126	8.76	82.1	1.8	16.1	0.81
108-664B-1H-6, 139	8.89	79.1	2.0	18.9	0.75
108-664B-1H-6, 146	8.96	73.5	2.1	24.4	0.79
108-664B-1H-7, 11	9.11	63.5	2.0	34.5	0.75
108-664B-1H-7, 19	9.19	75.1	3.2	21.7	0.69
108-664B-1H-7, 29	9.29	71.7	3.0	25.4	0.66
108-664B-1H-7, 41	9.41	69.8	3.5	26.7	0.70
108-664B-2H-1, 11	9.61	69.6	3.1	27.2	0.63
108-664B-2H-1, 19	9.69	0.8			0.76
108-664B-2H-1, 29	9.79	83.1	1.1	15.9	0.86
108-664B-2H-1, 41	9.91	78.0	1.5	20.5	0.88
108-664B-2H-1, 59	10.09	84.8	1.9	13.3	0.98
108-664B-2H-1, 71	10.21	66.2	1.3	32.5	0.91
108-664B-2H-1, 79	10.29	88.6	1.3	10.0	0.90
108-664B-2H-1, 89	10.39	83.6	1.7	14.7	0.90
108-664B-2H-1, 101	10.51	64.8	2.7	32.5	0.72

Table 6 (continued).

Core, section, interval (cm)	Depth (mbsf)	CaCO ₃ (%)	SiO ₂ (%)	Terrigenous fraction (%)	Dry-bulk density (g/cm ³)
108-664B-2H-1, 119	10.69	53.2	2.7	44.1	
108-664B-2H-1, 126	10.76	56.2	2.5	41.3	0.63
108-664B-2H-1, 139	10.89	73.6	3.0	23.4	0.70
108-664B-2H-1, 146	10.96	76.9	2.1	20.9	0.73
108-664B-2H-2, 11	11.11	82.9	2.0	15.1	0.79
108-664B-2H-2, 19	11.19	83.1	1.8	15.1	0.81
108-664B-2H-2, 29	11.29	79.8	1.2	19.0	0.80
108-664B-2H-2, 41	11.41	77.7	2.3	20.0	0.79
108-664B-2H-2, 59	11.59	79.4	1.4	19.2	0.81
108-664B-2H-2, 71	11.71	80.9	0.6	18.5	0.83
108-664B-2H-2, 79	11.79	78.0	2.1	19.9	0.73
108-664B-2H-2, 89	11.89	79.8	2.2	18.1	0.80
108-664B-2H-2, 101	12.01	70.1	1.3	28.6	0.90
108-664B-2H-2, 119	12.19	79.6	1.3	19.1	0.87
108-664B-2H-2, 126	12.26	79.5	1.2	19.3	0.92
108-664B-2H-2, 139	12.39	87.4	1.0	11.7	0.93
108-664B-2H-2, 146	12.46	78.5	1.2	20.3	0.92
108-664B-2H-3, 11	12.61	87.4	0.8	11.8	0.98
108-664B-2H-3, 19	12.69	83.0	0.7	16.2	0.97
108-664B-2H-3, 29	12.79	86.7	0.8	12.5	0.93
108-664B-2H-3, 41	12.91	74.4	1.2	24.4	0.95
108-664B-2H-3, 59	13.09	65.7	1.5	32.8	0.83
108-664B-2H-3, 71	13.21	85.3	1.3	13.4	0.87
108-664B-2H-3, 79	13.29	90.0	1.1	8.9	0.94
108-664B-2H-3, 89	13.39	93.0	0.9	6.1	0.96
108-664B-2H-3, 101	13.51	91.9	0.9	7.1	1.07
108-664B-2H-3, 119	13.69	90.9	0.9	8.2	0.96
108-664B-2H-3, 126	13.76	89.7	0.6	9.7	1.10
108-664B-2H-3, 139	13.89	86.8	0.9	12.3	0.87
108-664B-2H-3, 146	13.96	79.7	1.5	18.8	0.90
108-664B-2H-4, 11	14.11	51.3	2.4	46.2	0.72
108-664B-2H-4, 19	14.19	54.1	2.1	43.7	0.63
108-664B-2H-4, 29	14.29	65.4	2.4	32.2	0.75
108-664B-2H-4, 41	14.41	80.6	2.3	17.0	0.76
108-664B-2H-4, 59	14.59	71.0	1.7	27.3	0.72
108-664B-2H-4, 71	14.71	82.3	1.7	16.0	0.80
108-664B-2H-4, 79	14.79	84.2	2.3	13.5	0.77
108-664B-2H-4, 89	14.89	86.2	1.4	12.4	0.90
108-664B-2H-4, 101	15.01	88.5	1.0	10.4	0.90
108-664B-2H-4, 119	15.19	78.3	1.5	20.2	0.82
108-664B-2H-4, 126	15.26	64.1	2.0	33.8	0.71
108-664B-2H-4, 139	15.39	82.9	2.0	15.1	0.79
108-664B-2H-4, 146	15.46	80.4	1.6	18.0	0.83
108-664B-2H-5, 11	15.61	76.2	1.7	22.1	0.82
108-664B-2H-5, 19	15.69	85.5	1.5	13.1	0.83
108-664B-2H-5, 29	15.79	82.7	1.7	15.7	0.86
108-664B-2H-5, 41	15.91	78.2	2.3	19.5	0.80
108-664B-2H-5, 59	16.09	74.0	1.8	24.3	0.81
108-664B-2H-5, 71	16.21	60.4	1.9	37.7	0.85
108-664B-2H-5, 79	16.29	88.7	1.0	10.3	0.91
108-664B-2H-5, 89	16.39	78.1	1.5	20.4	0.91
108-664B-2H-5, 101	16.51	90.2	1.2	8.6	0.97
108-664B-2H-5, 119	16.69	86.1	1.0	12.9	0.95
108-664B-2H-6, 11	17.11	86.9	0.9	12.2	0.98
108-664B-2H-6, 19	17.19	85.6	1.0	13.4	0.93
108-664B-2H-6, 29	17.29	87.8	0.9	11.3	1.02
108-664B-2H-6, 41	17.41	88.9	1.1	10.0	0.98
108-664B-2H-6, 59	17.59	84.2	0.7	15.0	0.94
108-664B-2H-6, 71	17.71	86.7	0.8	12.5	1.01
108-664B-2H-6, 79	17.79	90.1	1.0	8.9	0.99
108-664B-2H-6, 89	17.89	87.2	1.1	11.7	1.03
108-664B-2H-6, 101	18.01	89.7	0.9	9.4	1.04
108-664B-2H-6, 119	18.19	78.0	1.1	20.9	0.88
108-664B-2H-6, 126	18.26	85.5	1.5	13.0	0.91
108-664B-2H-6, 139	18.39	90.1	1.2	8.7	0.90
108-664B-2H-6, 146	18.46	80.4	1.0	18.6	0.92
108-664B-3H-1, 11	19.11	82.5	1.1	16.4	0.88
108-664B-3H-1, 19	19.19	75.8	1.4	22.8	0.73
108-664B-3H-1, 29	19.29	87.2	1.7	11.1	0.96
108-664B-3H-1, 41	19.41	86.3	1.1	12.6	0.97
108-664B-3H-1, 59	19.59	76.8	1.3	21.9	0.89
108-664B-3H-1, 71	19.71	78.1	1.7	20.3	0.86
108-664B-3H-1, 79	19.79	83.4	1.2	15.4	0.92
108-664B-3H-1, 89	19.89	70.8	1.6	27.6	0.88
108-664B-3H-1, 101	20.01	84.5	0.8	14.8	0.90
108-664B-3H-1, 119	20.19	85.2	1.1	13.7	0.93
108-664B-3H-1, 126	20.26	86.6	1.2	12.2	0.94

Table 6 (continued).

Core, section, interval (cm)	Depth (mbsf)	CaCO ₃ (%)	SiO ₂ (%)	Terrigenous fraction (%)	Dry-bulk density (g/cm ³)
108-664B-3H-1, 139	20.39	85.3	1.6	13.2	0.87
108-664B-3H-1, 145	20.45	84.0	1.4	14.6	0.94
108-664B-3H-2, 11	20.61	82.9	1.8	15.4	0.96
108-664B-3H-2, 19	20.69	71.8	1.8	26.4	0.72
108-664B-3H-2, 29	20.79	60.6	2.1	37.2	0.77
108-664B-3H-2, 41	20.91	64.6	1.9	33.5	0.69
108-664B-3H-2, 59	21.09	79.2	1.5	19.3	0.85
108-664B-3H-2, 71	21.21	69.9	1.7	28.4	0.79
108-664B-3H-2, 79	21.29	82.3	1.7	16.0	0.82
108-664B-3H-2, 89	21.39	79.4	1.9	18.8	0.84
108-664B-3H-2, 101	21.51	85.7	1.3	13.0	0.96
108-664B-3H-2, 119	21.69	82.9	2.2	14.9	0.91
108-664B-3H-2, 126	21.76	81.7	1.3	16.9	0.94
108-664B-3H-2, 139	21.89	78.8	2.2	19.1	0.79
108-664B-3H-2, 146	21.96	78.9	2.1	19.0	0.81
108-664B-3H-3, 11	22.11	72.3	2.4	25.3	0.78
108-664B-3H-3, 19	22.19	61.1	2.8	36.1	0.69
108-664B-3H-3, 29	22.29	67.3	1.9	30.8	0.83
108-664B-3H-3, 41	22.41	82.6	1.8	15.6	0.87
108-664B-3H-3, 59	22.59	81.1	2.6	16.3	0.86
108-664B-3H-3, 71	22.71	85.8	1.8	12.4	0.90
108-664B-3H-3, 79	22.79	80.9	2.1	17.0	0.81
108-664B-3H-3, 89	22.89	66.0	3.0	31.0	0.76
108-664B-3H-3, 101	23.01	62.2	2.3	35.4	0.74
108-664B-3H-3, 119	23.19	87.1	1.7	11.2	0.91
108-664B-3H-3, 126	23.26	91.0	1.8	7.2	0.92
108-664B-3H-3, 139	23.39	87.6	1.1	11.3	0.88
108-664B-3H-4, 11	23.51	86.9	1.4	11.7	0.98
108-664B-3H-4, 29	23.79	87.3	1.4	11.3	0.92
108-664B-3H-4, 41	23.91	84.2	1.5	14.4	0.89
108-664B-3H-4, 59	24.09	53.4	2.4	44.2	0.74
108-664B-3H-4, 71	24.21	58.6	2.9	38.5	0.70
108-664B-3H-4, 79	24.29	67.6	1.9	30.5	0.72
108-664B-3H-4, 89	24.39	81.8	1.7	16.6	0.85
108-664B-3H-4, 101	24.51	81.0	2.1	16.9	0.89
108-664B-3H-4, 129	24.79	87.7	1.5	10.8	0.95
108-664B-3H-4, 134	24.84	88.5	1.6	10.0	0.97
108-664B-3H-4, 146	24.96	89.2	1.3	11.1	0.94
108-664B-3H-5, 11	25.11	86.9	1.4	11.7	0.98
108-664B-3H-5, 19	25.19	87.3	1.3	11.4	0.89
108-664B-3H-5, 29	25.29	86.7	1.5	11.8	0.93
108-664B-3H-5, 41	25.41	81.6	1.9	16.5	0.94
108-664B-3H-5, 59	25.59	61.9	2.6	35.5	0.77
108-664B-3H-5, 71	25.71	84.7	1.4	13.9	0.86
108-664B-3H-5, 79	25.79	83.8	1.4	14.9	0.85
108-664B-3H-5, 89	25.89	85.7	1.9	12.5	0.94
108-664B-3H-5, 101	26.01	84.1	2.1	13.9	0.93
108-664B-3H-5, 119	26.19	78.1	2.2	19.7	0.84
108-664B-3H-5, 126	26.26	82.3	1.9	15.9	0.84
108-664B-3H-5, 139	26.39	73.0	2.6	24.5	0.72
108-664B-3H-5, 146	26.46	83.3	1.3	15.4	0.88
108-664B-3H-6, 11	26.61	81.4	2.3	16.3	0.83
108-664B-3H-6, 19	26.69	79.8	2.0	18.2	0.83
108-664B-3H-6, 29	26.79	81.7	2.2	16.1	0.84
108-664B-3H-6, 41	26.91	81.2	1.9	16.9	0.94
108-664B-3H-6, 59	27.09	84.0	1.9	14.1	0.88
108-664B-3H-6, 71	27.21	64.5	2.2	33.3	0.76
108-664B-3H-6, 79	27.29	49.4	3.3	47.3	0.65
108-664B-3H-6, 89	27.39	49.5	4.0	46.6	0.64
108-664B-3H-6, 101	27.51	46.9	2.8	50.3	0.99
108-664B-3H-6, 119	27.69	71.3	3.2	25.5	0.77
108-664B-3H-6, 126	27.76	89.8	3.0	7.2	0.83
108-664B-3H-6, 139	27.89	81.6	2.6	15.8	0.75
108-664B-3H-6, 144	27.94	74.7	2.5	22.9	0.83
108-664B-4H-1, 11	28.61	80.0	2.0	18.0	0.79
108-664B-4H-1, 19	28.69	76.5	1.9	21.6	0.76
108-664B-4H-1, 29	28.79	83.2	1.8	15.0	0.85
108-664B-4H-1, 41	28.91	80.3	1.7	17.9	0.81
108-664B-4H-1, 59	29.09	81.3	1.9	16.9	0.89
108-664B-4H-1, 71	29.21	69.8	2.3	27.9	0.85
108-664B-4H-1, 79	29.29</td				

Table 6 (continued).

Core, section, interval (cm)	Depth (mbsf)	CaCO_3 (%)	SiO_2 (%)	Terrigenous fraction (%)	Dry-bulk density (g/cm^3)
108-664B-4H-1, 126	29.76	50.0	4.4	45.6	0.67
108-664B-4H-1, 139	29.89	55.0	3.6	41.4	0.63
108-664B-4H-1, 145	29.95	62.7	3.2	34.1	0.69
108-664B-4H-2, 11	30.11	60.0	2.7	37.3	0.69
108-664B-4H-2, 19	30.19	75.1	3.4	21.5	0.70
108-664B-4H-2, 29	30.29	76.5	2.7	20.8	0.76
108-664B-4H-2, 41	30.41	78.8	2.8	18.4	0.79
108-664B-4H-2, 59	30.59	60.6	2.9	36.5	0.78
108-664B-4H-2, 71	30.71	55.5	3.5	40.9	0.71
108-664B-4H-2, 79	30.79	64.1	3.5	32.4	0.71
108-664B-4H-2, 89	30.89	80.4	2.6	17.0	0.99
108-664B-4H-2, 101	31.01	77.5	2.1	20.4	0.82
108-664B-4H-2, 119	31.19	91.2	0.5	8.3	0.78
108-664B-4H-2, 126	31.26	78.0	3.4	18.6	0.70
108-664B-4H-2, 139	31.39	86.3	2.4	11.3	0.72
108-664B-4H-2, 145	31.45	83.8	2.1	14.0	0.79
108-664B-4H-3, 11	31.61	85.1	1.9	13.1	0.79
108-664B-4H-3, 19	31.69	84.2	2.2	13.6	0.72
108-664B-4H-3, 29	31.79	87.9	1.4	10.6	0.80
108-664B-4H-3, 41	31.91	84.1	2.3	13.6	0.79
108-664B-4H-3, 59	32.09	59.9	2.6	37.5	0.80
108-664B-4H-3, 71	32.21	78.9	3.2	17.9	0.78
108-664B-4H-3, 79	32.29	78.8	3.0	18.2	0.74
108-664B-4H-3, 89	32.39	73.9	2.9	23.2	0.89
108-664B-4H-3, 101	32.51	77.3	2.0	20.7	1.13
108-664B-4H-3, 119	32.69	65.1	1.4	33.5	0.82
108-664B-4H-3, 126	32.76	59.2	2.5	38.3	0.75
108-664B-4H-3, 139	32.89	78.4	2.2	19.5	0.85
108-664B-4H-3, 145	32.95	84.4	1.3	14.2	0.94
108-664B-4H-4, 11	33.11	83.9	1.9	14.3	1.00
108-664B-4H-4, 19	33.19	88.2	1.7	10.1	0.95
108-664B-4H-4, 29	33.29	89.1	1.6	9.3	1.01
108-664B-4H-4, 41	33.41	87.8	1.7	10.4	1.08
108-664B-4H-4, 59	33.59	90.0	1.5	8.4	1.08
108-664B-4H-4, 71	33.71	78.7	2.1	19.1	0.91
108-664B-4H-4, 79	33.79	70.4	2.7	26.9	0.77
108-664B-4H-4, 89	33.89	72.5	3.0	24.6	0.86
108-664B-4H-4, 101	34.01	86.2	1.2	12.6	0.84
108-664B-4H-4, 119	34.19	84.5	1.3	14.2	0.91
108-664B-4H-4, 126	34.26	85.6	1.4	12.9	1.06
108-664B-4H-4, 139	34.39	87.6	1.5	10.9	0.91
108-664B-4H-4, 145	34.45	87.4	1.4	11.2	1.01
108-664B-4H-5, 8	34.58	84.7	1.5	13.8	1.01
108-664B-4H-5, 19	34.69	84.5	1.4	14.0	0.91
108-664B-4H-5, 29	34.79	77.3	1.8	20.9	0.92
108-664B-4H-5, 41	34.91	81.8	1.6	16.6	0.94
108-664B-4H-5, 59	35.08	87.8	1.6	10.6	1.31
108-664B-4H-5, 71	35.21	87.8	1.7	10.5	0.90
108-664B-4H-5, 79	35.29	89.3	1.1	9.5	0.94
108-664B-4H-5, 89	35.39	90.7	1.1	8.2	1.06
108-664B-4H-5, 101	35.51	87.6	0.8	11.7	1.11
108-664B-4H-5, 119	35.69	85.2	1.3	13.4	1.02
108-664B-4H-5, 126	35.76	81.6	1.5	16.9	1.01
108-664B-4H-5, 139	35.89	83.3	1.3	15.4	0.90
108-664B-4H-5, 145	35.95	67.6	1.6	30.8	1.03
108-664B-4H-6, 11	36.11	79.1	1.8	19.1	0.99
108-664B-4H-6, 19	36.19	71.2	3.1	25.6	0.84
108-664B-4H-6, 29	36.29	60.3	3.0	36.8	0.85
108-664B-4H-6, 41	36.41	88.5	1.4	10.1	1.34
108-664B-4H-6, 59	36.59	89.9	1.3	8.9	1.23
108-664B-4H-6, 71	36.71	83.1	1.5	15.4	1.04
108-664B-4H-6, 79	36.79	89.0	1.1	9.9	1.03
108-664B-4H-6, 89	36.89	87.2	0.7	12.1	1.29
108-664B-4H-6, 101	37.01	81.0	1.3	17.7	1.09
108-664B-4H-6, 119	37.19	77.7	0.9	21.3	0.95
108-664B-4H-6, 126	37.26	81.4	1.3	17.3	0.93
108-664B-4H-6, 139	37.39	77.6	2.1	20.3	0.86
108-664B-4H-6, 145	37.45	78.0	2.0	20.0	0.97
108-664B-4H-7, 11	37.61	75.5	2.8	21.7	0.84
108-664B-4H-7, 19	37.69	81.3	2.2	16.5	0.82
108-664B-4H-7, 29	37.79	83.4	1.7	14.8	0.97
108-664B-4H-7, 41	37.91	89.5	1.4	9.1	1.01
108-664B-5H-1, 59	38.59	68.8	2.2	29.0	0.86
108-664B-5H-1, 71	38.71	63.1	2.3	34.6	0.75
108-664B-5H-1, 79	38.79	73.5	1.4	25.1	0.74
108-664B-5H-1, 89	38.89	61.4	2.2	36.4	0.76

Table 6 (continued).

Core, section, interval (cm)	Depth (mbsf)	CaCO_3 (%)	SiO_2 (%)	Terrigenous fraction (%)	Dry-bulk density (g/cm^3)
108-664B-5H-1, 101	39.01	84.1	1.4	14.5	0.90
108-664B-5H-1, 119	39.19	85.2	1.7	13.2	1.04
108-664B-5H-1, 126	39.26	83.9	1.6	14.5	0.98
108-664B-5H-1, 139	39.39	72.1	1.7	26.2	0.79
108-664B-5H-1, 146	39.46	56.8	2.4	40.8	0.78
108-664B-5H-2, 11	39.61	82.7	1.6	15.7	0.96
108-664B-5H-2, 19	39.69	78.5	1.9	19.6	0.85
108-664B-5H-2, 29	39.79	83.2	1.1	15.6	0.95
108-664B-5H-2, 41	39.91	80.1	2.0	17.9	0.90
108-664B-5H-2, 59	40.09	52.1	2.4	45.5	0.79
108-664B-5H-2, 71	40.21	72.6	1.5	25.9	0.92
108-664B-5H-2, 79	40.29	76.0	1.4	22.5	0.88
108-664B-5H-2, 89	40.39	86.4	1.4	12.2	1.27
108-664B-5H-2, 101	40.51	84.5	1.5	13.9	0.93
108-664B-5H-2, 119	40.69	89.4	1.5	9.1	1.02
108-664B-5H-2, 126	40.76	88.0	1.6	10.4	0.99
108-664B-5H-2, 139	40.89	85.0	1.4	13.6	1.03
108-664B-5H-2, 146	40.96	89.0	1.5	9.5	0.99
108-664B-5H-3, 11	41.11	87.2	1.3	11.4	1.01
108-664B-5H-3, 19	41.19	85.0	1.4	13.7	0.88
108-664B-5H-3, 29	41.29	85.0	1.4	13.6	1.03
108-664B-5H-3, 41	41.41	85.5	1.6	13.0	1.03
108-664B-5H-3, 59	41.59	85.1	1.5	13.4	1.11
108-664B-5H-3, 71	41.71	86.3	1.3	12.4	1.01
108-664B-5H-3, 79	41.79	87.2	1.2	11.6	0.90
108-664B-5H-3, 89	41.89	88.3	1.0	10.6	1.01
108-664B-5H-3, 101	42.01	85.1	1.1	13.8	0.96
108-664B-5H-3, 119	42.19	78.2	2.2	19.6	0.88
108-664B-5H-3, 126	42.26	79.8	1.0	19.2	0.90
108-664B-5H-3, 139	42.39	86.4	1.7	11.9	0.82
108-664B-5H-3, 146	42.46	87.4	1.7	10.9	0.91
108-664B-5H-4, 11	42.61	87.5	1.4	11.2	1.03
108-664B-5H-4, 19	42.69	83.1	1.1	15.9	0.79
108-664B-5H-4, 29	42.79	80.7	1.1	18.3	0.86
108-664B-5H-4, 41	42.91	62.4	2.7	34.9	0.81
108-664B-5H-4, 59	43.09	49.4	2.0	48.7	0.79
108-664B-5H-4, 71	43.21	61.7	1.7	36.7	0.86
108-664B-5H-4, 79	43.29	75.1	1.0	23.9	0.82
108-664B-5H-4, 89	43.39	90.3	1.0	8.7	1.07
108-664B-5H-5, 11	44.11	67.4	2.5	30.0	0.82
108-664B-5H-5, 19	44.19	48.9	2.5	48.5	0.64
108-664B-5H-5, 29	44.29	64.6	3.0	32.4	0.93
108-664B-5H-5, 41	44.41	78.0	2.2	19.7	0.88
108-664B-5H-5, 59	44.59	74.3	2.3	23.5	0.89
108-664B-5H-5, 71	44.71	83.7	2.1	14.1	0.93
108-664B-5H-5, 79	44.79	81.8	1.9	16.3	0.84
108-664B-5H-5, 89	44.89	67.4	2.6	29.9	0.86
108-664B-5H-5, 101	45.01	77.7	2.0	20.3	0.97
108-664B-5H-5, 119	45.19	85.2	1.7	13.1	0.98
108-664B-5H-5, 126	45.31	71.8	1.6	26.6	1.00
108-664B-5H-5, 139	45.49	73.7	2.1	14.1	0.93
108-664B-5H-5, 145	45.59	81.8	1.9	16.3	0.84
108-664B-5H-6, 19	45.69	78.4	1.6	20.0	0.82
108-664B-5H-6, 29	45.79	81.5	1.4	17.1	0.92
108-664B-5H-6, 41	45.91	72.4	2.4	25.2	0.94
108-664B-5H-6, 59	46.09	68.1	3.1	28.9	0.90
108-664B-5H-6, 71	46.21	68.7	2.4	28.9	0.87
108-664B-5H-6, 79	46.29	72.5	2.4	25.2	0.77
108-664B-5H-6, 89	46.39	74.9	2.7	22.4	0.85
108-664B-5H-6, 101	46.51	54.6	3.4	42.0	0.80
108-664B-5H-6, 119	46.69	84.0	1.9	14.1	0.99
108-664B-5H-6, 126	46.76	70.6	2.2	27.3	0.92
108-664B-5H-6, 139	46.89	89.2	1.5	9.2	0.92
108-664B-5H-6, 145	46.95	92.6	1.9	5.6	1.05
108-664B-5H-7, 11	47.11	87.2	1.7	11.2	1.06
108-664B-5H-7, 19	47.19	89.0	1.7	9.3	0.88
108-664B-5H-7, 29	47.29	86.1	2.1	11.8	0.95
108-664B-5H-7, 41	47.41	88.1	1.8	10.1	0.96
108-664B-5H-7, 49	47.79	83.5	2.7	13.8	1.04
108-664B-5H-7, 59	47.91	86.8	2.0	11.2	1.05
108-664B-5H-7, 71	48.09	89.9	1.2	8.9	1.1

Table 6 (continued).

Core, section, interval (cm)	Depth (mbsf)	CaCO ₃ (%)	SiO ₂ (%)	Terrigenous fraction (%)	Dry-bulk density (g/cm ³)
108-664B-6H-1, 89	48.39	87.9	1.5	10.6	0.99
108-664B-6H-1, 101	48.51	84.2	1.7	14.1	1.02
108-664B-6H-1, 119	48.69	84.0	1.1	14.9	0.94
108-664B-6H-1, 126	48.76	87.4	1.4	11.2	1.06
108-664B-6H-1, 139	48.89	85.5	1.5	13.0	0.95
108-664B-6H-1, 146	48.95	82.6	1.7	15.7	1.09
108-664B-6H-2, 11	49.11	83.5	1.4	15.1	1.13
108-664B-6H-2, 19	49.19	87.1	1.4	11.5	0.91
108-664B-6H-2, 29	49.29	83.2	1.6	15.2	
108-664B-6H-2, 41	49.41	70.6	2.5	25.9	0.98
108-664B-6H-2, 59	49.59	85.6	2.2	12.2	1.31
108-664B-6H-2, 71	49.71	87.4	1.5	11.1	1.16
108-664B-6H-2, 79	49.79	90.9	1.2	7.9	0.99
108-664B-6H-2, 89	49.89	88.2	1.1	10.8	1.60
108-664B-6H-2, 101	50.01	89.3	1.0	9.7	1.18
108-664B-6H-2, 119	50.19	89.3	1.1	9.6	1.09
108-664B-6H-2, 126	50.26	83.6	1.2	15.2	1.06
108-664B-6H-2, 139	50.39	82.4	1.5	16.1	0.90
108-664B-6H-2, 146	50.46	83.4	1.4	15.1	1.26
108-664B-6H-3, 11	50.61	77.7	1.5	20.8	1.04
108-664B-6H-3, 19	50.69		1.3		0.95
108-664B-6H-3, 29	50.79	71.0	2.0	26.9	1.13
108-664B-6H-3, 41	50.91	82.2	1.1	16.7	0.98
108-664B-6H-3, 59	51.09	89.6	1.0	9.5	1.10
108-664B-6H-3, 71	51.21	86.0	1.1	12.9	1.29
108-664B-6H-3, 79	51.29	87.3	1.1	11.6	0.91
108-664B-6H-3, 89	51.39	86.5	1.1	12.4	1.21
108-664B-6H-3, 101	51.51	87.7	1.2	11.1	1.17
108-664B-6H-3, 119	51.69	86.3	1.1	12.6	0.98
108-664B-6H-3, 126	51.76	78.6	1.5	19.9	1.25
108-664B-6H-3, 146	51.96	83.5	1.1	15.4	1.20

Table 7 . Percentages of carbonate, opal, and terrigenous fraction, and dry-bulk densities at Hole 664D.

Core, section, interval (cm)	Depth (mbsf)	CaCO ₃ (%)	SiO ₂ (%)	Terrigenous fraction (%)	Dry-bulk density (g/cm ³)
108-664D-11H-1, 11	87.91	92.2	1.4	6.4	1.38
108-664D-11H-1, 19	87.99	84.1	2.3	13.6	1.00
108-664D-11H-1, 29	88.09	82.2	1.8	16.0	1.25
108-664D-11H-1, 41	88.21	81.6	2.0	16.4	1.32
108-664D-11H-1, 59	88.39	84.5	1.5	14.1	1.22
108-664D-11H-1, 71	88.51	90.6	1.4	7.9	1.35
108-664D-11H-1, 79	88.59	68.4	1.4	30.2	1.03
108-664D-11H-1, 89	88.69	88.0	1.4	10.6	1.19
108-664D-11H-1, 101	88.81	85.3	1.7	13.0	1.32
108-664D-11H-1, 119	88.89	85.9	1.7	12.4	1.19
108-664D-11H-1, 126	88.96	73.9	1.9	24.2	1.25
108-664D-11H-1, 139	89.09	86.4	1.4	12.2	1.00
108-664D-11H-1, 146	89.16	85.3	1.7	13.0	1.32
108-664D-11H-2, 11	89.41	89.2	1.3	9.5	
108-664D-11H-2, 19	89.49	91.2	1.0	7.8	1.07
108-664D-11H-2, 29	89.59	92.4	1.0	6.6	1.37
108-664D-11H-2, 41	89.71	90.8	1.1	8.1	1.35
108-664D-11H-2, 59	89.89	90.2	1.3	8.6	1.36
108-664D-11H-2, 71	90.01	87.6	1.2	11.2	1.19
108-664D-11H-2, 79	90.09	82.9	1.3	15.8	1.10
108-664D-11H-2, 89	90.19	86.5	1.1	12.4	1.27
108-664D-11H-2, 101	90.31	83.4	1.6	15.0	1.41
108-664D-11H-2, 119	90.49	88.1	1.6	10.4	1.23
108-664D-11H-2, 126	90.56	88.0	1.7	10.3	1.22
108-664D-11H-2, 139	90.69	87.0	1.5	11.5	1.00
108-664D-11H-2, 146	90.76	82.6	2.2	15.2	1.18
108-664D-11H-3, 11	90.91	81.4	1.6	17.0	1.39
108-664D-11H-3, 19	90.99	86.4	1.5	12.1	1.04
108-664D-11H-3, 29	91.09	84.3	1.6	14.2	1.29
108-664D-11H-3, 41	91.21	80.1	1.9	18.1	1.36
108-664D-11H-3, 59	91.39	90.8	1.4	7.7	1.27
108-664D-11H-3, 71	91.51	85.3	1.7	13.1	1.28
108-664D-11H-3, 79	91.59	89.4	1.4	9.2	1.06
108-664D-11H-3, 89	91.69	91.7	1.1	7.2	1.44

Table 7 (continued).

Core, section, interval (cm)	Depth (mbsf)	CaCO ₃ (%)	SiO ₂ (%)	Terrigenous fraction (%)	Dry-bulk density (g/cm ³)
108-664D-11H-3, 101	91.81	92.0	1.0	6.9	1.44
108-664D-11H-3, 119	91.89	88.4	1.0	10.6	1.26
108-664D-11H-3, 126	91.96	85.9	0.8	13.3	1.44
108-664D-11H-3, 139	92.09	89.1	1.1	9.9	1.05
108-664D-11H-3, 146	92.16	88.9	1.0	10.0	1.28
108-664D-11H-4, 11	92.41	83.0	1.6	15.4	1.32
108-664D-11H-4, 19	92.49	80.8	2.0	17.3	1.02
108-664D-11H-4, 29	92.59	82.4	2.1	15.5	1.33
108-664D-11H-4, 41	92.71	85.7	1.8	12.5	1.36
108-664D-11H-4, 59	92.89	90.6	1.2	8.2	1.66
108-664D-11H-4, 71	93.01	90.8	1.2	8.0	1.21
108-664D-11H-4, 79	93.09	85.4	1.3	13.3	1.03
108-664D-11H-4, 89	93.19	77.0	1.7	21.3	1.25
108-664D-11H-4, 101	93.31	85.9	1.7	12.3	1.30
108-664D-11H-4, 119	93.49	80.2	2.4	17.4	1.18
108-664D-11H-4, 126	93.56	82.7	2.0	15.3	1.23
108-664D-11H-4, 139	93.69	89.1	1.1	9.8	1.03
108-664D-11H-4, 146	93.76	89.0	1.3	9.7	1.30
108-664D-11H-5, 11	93.91	91.0	1.1	7.8	1.39
108-664D-11H-5, 19	93.99	87.2	1.1	11.7	1.06
108-664D-11H-5, 29	94.09	79.9	1.7	18.4	1.56
108-664D-11H-5, 41	94.21	84.4	1.3	14.3	1.35
108-664D-11H-5, 59	94.39	72.0	2.3	25.6	1.21
108-664D-11H-5, 71	94.51	84.5	2.3	13.2	1.35
108-664D-11H-5, 79	94.59	84.4	2.4	13.2	1.05
108-664D-11H-5, 89	94.69	85.9	1.9	12.2	1.30
108-664D-11H-5, 101	94.81	88.8	1.4	9.8	
108-664D-11H-5, 119	94.99	89.3	1.4	9.4	1.29
108-664D-11H-5, 126	95.06	91.3	1.1	7.6	1.51
108-664D-11H-6, 11	95.41	91.7	1.3	7.1	1.65
108-664D-11H-6, 19	95.49	89.9	1.4	8.7	1.12
108-664D-11H-6, 29	95.59	89.7	1.4	8.9	1.46
108-664D-11H-6, 41	95.71	88.9	1.4	9.7	1.46
108-664D-11H-6, 59	95.89	84.7	1.3	13.9	1.39
108-664D-11H-6, 89	96.19	83.8	1.9	14.4	1.33
108-664D-11H-6, 101	96.31	88.3	1.6	10.2	1.45
108-664D-11H-6, 119	96.49	82.3	1.6	16.2	1.34
108-664D-11H-6, 126	96.56	69.0	2.5	28.5	1.36
108-664D-11H-7, 11	96.91	84.2	1.6	14.2	1.23
108-664D-11H-7, 19	96.99	86.6	1.9	11.5	1.06
108-664D-11H-7, 29	97.09	68.0	1.6	30.5	1.42
108-664D-11H-7, 41	97.21	91.2	1.3	7.5	1.63
108-664D-11H-7, 59	97.39	89.2	1.2	9.6	1.52
108-664D-12H-2, 11	98.91	88.6	1.3	10.2	1.53
108-664D-12H-2, 19	98.99	86.2	1.1	12.7	1.09
108-664D-12H-2, 29	99.09	71.3	1.8	27.0	
108-664D-12H-2, 41	99.21	90.2	1.0	8.8	1.27
108-664D-12H-2, 59	99.39	91.6	1.1	7.3	
108-664D-12H-2, 71	99.51	83.8	1.6	14.6	1.32
108-664D-12H-2, 79	99.59	88.7	1.2	10.1	1.04
108-664D-12H-2, 89	99.69	89.6	1.2	9.2	1.28
108-664D-12H-2, 101	99.81	85.1	1.8	13.1	1.19
108-664D-12H-2, 119	99.99	92.5	1.2	6.3	1.38
108-664D-12H-2, 126	100.06	89.3	1.1	9.5	1.52
108-664D-12H-2, 139	100.19	91.6	1.1	7.3	1.07
108-664D-12H-2, 145	100.25	89.9	1.1	9.0	1.35
108-664D-12H-3, 11	100.41	90.4	1.2	8.5	1.43
108-664D-12H-3, 19	100.49	89.6	1.2	9.2	1.07
108-664D-12H-3, 29	100.59	92.8	1.3	5.9	1.50
108-664D-12H-3, 41	100.71	93.4	1.1	5.5	1.53
108-664D-12H-3, 59	100.89	90.5	1.0	8.5	1.31
108-664D-12H-3, 71	101.01	88.9	1.1	10.0	1.37
108-664D-12H-3, 79	101.09	92.4	1.0	6.6	1.10
108-664D-12H-3, 89	101.19	91.8	1.0	7.2	1.32
108-664D-12H-3, 101	101.31	93.4	1.0	5.7	1.34
108-664D-12H-3, 119	101.49	91.2	1.0	7.7	
108-664D-12H-3, 126	101.56	93.9	0.9	5.2	1.33
108-664D-12H-3, 139	101.69	86.2	0.9	12.9	1.11
108-664D-12H-3, 145	101.75	93.2	1.0	5.8	
108-664D-12H-4, 11	101.91	92.4	0.9	6.8	1.53
108-664D-12H-4, 19	101.99	91.6	1.0	7.4	1.06
108-664D-12H-4, 29	102.09	89.8	1.0	9.2	1.40
108-664D-12H-4, 41	102.21	90.0	1.1	8.9	1.60
108-664D-12H-4, 59	102.39	75.4	1.9	22.8	1.20
108-664D-12H-4, 71	102.51	88.4	0.7	10.9	1.23
108-664D-12H-4, 79					

Table 7 (continued).

Core, section, interval (cm)	Depth (mbsf)	CaCO ₃ (%)	SiO ₂ (%)	Terrigenous fraction (%)	Dry-bulk density (g/cm ³)
108-664D-12H-4, 89	102.69	91.3	1.0	7.7	1.35
108-664D-12H-4, 101	102.81	87.9	1.0	11.1	1.16
108-664D-12H-4, 119	102.99	91.0	1.1	7.9	1.18
108-664D-12H-4, 126	103.06	77.6	1.6	20.9	1.31
108-664D-12H-4, 139	103.19	86.8	1.3	11.9	0.99
108-664D-12H-4, 145	103.25	91.0	1.2	7.8	1.55
108-664D-12H-5, 11	103.41	90.3	1.0	8.7	1.48
108-664D-12H-5, 19	103.49	85.5	1.0	13.5	1.04
108-664D-12H-5, 29	103.59	60.6	3.4	36.0	1.18
108-664D-12H-5, 41	103.71	89.0	1.3	9.8	1.30
108-664D-12H-5, 59	103.89	89.2	0.8	10.0	1.36
108-664D-12H-5, 71	104.01	94.1	0.9	5.0	1.25
108-664D-12H-5, 79	104.09	93.8	1.0	5.2	1.25
108-664D-12H-5, 89	104.19	93.5	0.8	5.7	1.03
108-664D-12H-5, 101	104.31	92.1	1.1	6.9	1.29
108-664D-12H-5, 119	104.49	90.4	1.1	8.4	1.34
108-664D-12H-5, 126	104.56	91.1	1.1	7.8	1.48
108-664D-12H-5, 139	104.69	91.8	1.2	7.0	1.05
108-664D-12H-5, 143	104.73	91.0	1.3	7.7	
108-664D-12H-6, 11	104.91	87.6	1.1	11.3	
108-664D-12H-6, 19	104.99	75.1	1.4	23.5	0.94
108-664D-12H-6, 29	105.09	56.0	2.8	41.2	1.25
108-664D-12H-6, 41	105.21	89.7	1.8	8.6	1.39
108-664D-12H-6, 59	105.39	81.6	1.3	17.2	1.22
108-664D-12H-6, 71	105.51	75.6	2.0	22.4	1.23
108-664D-12H-6, 79	105.59	84.9	1.3	13.8	1.03
108-664D-12H-6, 89	105.69	93.1	1.1	5.7	1.29
108-664D-12H-6, 101	105.81	92.9	1.0	6.1	1.25
108-664D-12H-6, 119	105.99	90.4	1.1	8.5	1.41
108-664D-12H-6, 126	106.06	73.5	1.1	25.4	1.27
108-664D-12H-6, 139	106.19	88.9	1.2	9.9	1.05
108-664D-12H-6, 145	106.25	86.5	1.3	12.2	1.44
108-664D-12H-7, 11	106.41	68.2	2.3	29.6	1.14
108-664D-12H-7, 19	106.49	86.4	1.8	11.8	0.98
108-664D-12H-7, 29	106.59	84.2	1.3	14.6	1.18
108-664D-12H-7, 41	106.71	84.1	1.3	14.6	
108-664D-12H-7, 59	106.89	85.8	1.8	12.4	1.23
108-664D-14H-3, 19	119.49	93.1	0.8	6.1	1.06
108-664D-14H-3, 29	119.59	93.6	0.6	5.8	1.29
108-664D-14H-3, 59	119.89	89.9	1.1	9.1	1.21
108-664D-14H-3, 79	120.09	88.5	1.6	10.0	1.02
108-664D-14H-3, 89	120.19	90.2	1.6	8.2	1.31
108-664D-14H-3, 119	120.39	93.3	1.0	5.7	1.27
108-664D-14H-3, 139	120.59	92.7	1.1	6.1	1.03
108-664D-14H-3, 146	120.66	90.8	1.1	8.2	1.28
108-664D-14H-4, 19	120.99	93.2	0.9	5.9	1.07
108-664D-14H-4, 29	121.09	89.2	0.8	10.0	1.38
108-664D-14H-4, 59	121.39	90.0	1.0	9.0	1.24
108-664D-14H-4, 77	121.57	89.7	0.7	9.5	1.03
108-664D-14H-4, 89	121.69	86.8	1.3	11.9	1.56
108-664D-14H-4, 119	121.99	88.4	1.6	9.9	1.27
108-664D-14H-4, 139	122.19	91.8	0.9	7.3	1.09
108-664D-14H-4, 146	122.26	93.8	0.8	5.4	1.27
108-664D-14H-5, 19	122.49	92.4	0.9	6.7	1.01
108-664D-14H-5, 29	122.59	90.2	0.8	9.0	1.39
108-664D-14H-5, 59	122.89	85.9	1.3	12.8	1.23
108-664D-14H-5, 79	123.09	91.3	1.2	7.5	1.04
108-664D-14H-5, 89	123.19	90.9	0.7	8.4	1.37
108-664D-14H-5, 119	123.49	92.0	1.0	7.0	1.31
108-664D-14H-5, 139	123.69	90.7	1.0	8.3	1.01
108-664D-14H-5, 146	123.76	94.3	0.9	4.8	1.38
108-664D-14H-6, 19	123.99	91.5	0.8	7.6	1.02
108-664D-14H-6, 29	124.09	93.8	0.8	5.4	1.30
108-664D-14H-6, 59	124.39	91.9	0.9	7.3	1.27
108-664D-14H-6, 79	124.59	93.5	0.8	5.7	1.00
108-664D-14H-6, 89	124.69	92.3	0.9	6.7	
108-664D-14H-6, 119	124.99	92.6	1.3	6.2	1.22
108-664D-14H-6, 139	125.19	69.4	0.9	29.7	1.03
108-664D-14H-6, 144	125.24	92.6	1.0	6.4	1.29
108-664D-14H-7, 11	125.41	90.8	1.1	8.1	12.5
108-664D-14H-7, 19	125.49	87.3	1.1	11.5	1.02
108-664D-14H-7, 29	125.59	88.9	1.3	9.9	1.30
108-664D-15H-1, 70	126.50	92.0	1.0	7.0	
108-664D-15H-1, 80	126.60	93.8	1.0	5.2	
108-664D-15H-1, 89	126.69	91.2			
108-664D-15H-1, 100	126.80	92.8	0.9	6.3	

Table 7 (continued).

Core, section, interval (cm)	Depth (mbsf)	CaCO ₃ (%)	SiO ₂ (%)	Terrigenous fraction (%)	Dry-bulk density (g/cm ³)
108-664D-15H-1, 110	126.90	92.0	0.4	7.6	
108-664D-15H-1, 120	127.00	92.7	0.5	6.8	
108-664D-15H-1, 130	127.10	93.9	1.0	5.1	
108-664D-15H-2, 10	127.40	93.0	1.1	6.0	
108-664D-15H-2, 29	127.59	93.9	1.1	4.9	
108-664D-15H-2, 30	127.70	93.4	0.9	5.7	
108-664D-15H-2, 50	127.80	92.7	0.8	6.5	
108-664D-15H-2, 60	127.90	93.4	0.6	6.0	
108-664D-15H-2, 70	128.00	93.6	0.7	5.8	
108-664D-15H-2, 90	128.20	93.3	0.4	6.3	
108-664D-15H-2, 100	128.30	92.6	0.7	6.7	
108-664D-15H-2, 110	128.40	92.1	0.7	7.2	
108-664D-15H-2, 120	128.50	91.8	0.6	7.6	
108-664D-15H-2, 130	128.60	92.0	0.9	7.1	
108-664D-15H-2, 147	128.77	91.7	1.0	7.3	
108-664D-15H-3, 10	128.90	91.3	0.9	7.8	
108-664D-15H-3, 30	129.10	89.8	0.8	9.4	
108-664D-15H-3, 40	129.20	92.7	1.0	6.3	
108-664D-15H-3, 50	129.30	91.6	0.8	7.6	
108-664D-15H-3, 60	129.40	91.8	0.7	7.5	
108-664D-15H-3, 70	129.50	95.0	0.6	4.4	
108-664D-15H-3, 90	129.70	90.3	0.3	9.5	
108-664D-15H-3, 100	129.80	90.0	0.7	9.2	
108-664D-15H-3, 110	129.90	91.1	0.6	8.4	
108-664D-15H-3, 120	130.0	89.5	0.6	9.8	
108-664D-15H-3, 130	130.10	92.2	0.6	7.2	
108-664D-15H-3, 149	130.29	19.5	0.4	8.1	
108-664D-15H-4, 10	130.40	90.7	0.6	8.7	
108-664D-15H-4, 28	130.58	84.8	1.3	13.9	
108-664D-15H-4, 40	130.70	89.0	0.8	10.2	
108-664D-15H-4, 50	130.80	90.9	0.7	8.4	
108-664D-15H-4, 60	130.90	92.1	0.6	7.3	
108-664D-15H-4, 70	131.00	92.1	0.6	7.3	
108-664D-15H-4, 90	131.20	90.1	0.8	9.1	
108-664D-15H-4, 100	131.30	90.2	0.9	9.0	
108-664D-15H-4, 110	131.40	91.2	0.6	8.2	
108-664D-15H-4, 119	131.49	91.8	0.8	7.3	
108-664D-15H-4, 130	131.60	92.4	1.0	6.6	
108-664D-15H-4, 148	131.78	93.8	1.0	5.3	
108-664D-15H-5, 10	131.90	91.8	0.8	7.4	
108-664D-15H-5, 28	132.08	85.8	1.0	13.3	
108-664D-15H-5, 40	132.20	84.5	1.4	14.1	
108-664D-15H-5, 50	132.30	89.8	1.0	9.1	
108-664D-15H-5, 60	132.40	91.9	1.3	6.8	
108-664D-15H-5, 70	132.50	92.8	1.0	6.2	
108-664D-15H-5, 90	132.70	92.5	0.6	6.9	
108-664D-15H-5, 100	132.80	92.4	1.0	6.6	
108-664D-15H-5, 110	132.90	92.6	1.1	6.3	
108-664D-15H-5, 119	132.99	92.0	1.1	6.9	
108-664D-15H-5, 130	133.10	91.9	1.1	7.0	
108-664D-15H-5, 148	133.28	90.1	0.9	9.0	
108-664D-15H-6, 10	133.40	85.8	1.1	13.1	
108-664D-15H-6, 28	133.58	91.6	1.0	7.5	
108-664D-15H-6, 40	133.70	91.0	0.9	8.0	
108-664D-15H-6, 60	133.80	91.1	0.8	8.1	
108-664D-15H-6, 60	133.90	92.7	1.0	6.4	
108-664D-15H-6, 70	134.00	92.8	0.8	6.3	
108-664D-15H-6, 90	134.20	90.5	1.1	8.4	
108-664D-15H-6, 100	134.30	86.1	1.6	12.3	
108-664D-15H-6, 110	134.40	81.0	1.7	17.3	
108-664D-15H-6, 119	134.49	83.7	1.4	14.9	
108-664D-15H-6, 130	134.60	90.6	1.1	8.3	
108-664D-15H-6, 148	134.78	89.1	1.0	9.9	
108-664D-15H-6, 70	134.90	90.8	1.1	8.1	
108-664D-15H-7, 28	135.08	90.6	1.1	8.3	
108-664D-15H-7, 40	135.20	92.7	1.2	6.1	
108-664D-15H-7, 50	135.30	85.7	1.3	13.0	
108-664D-15H-7, 55	135.35	86.5	1.4	12.1	
108-664D-16H-2, 10	136.90	90.5	0.7	8.9	
108-664D-16H-2, 27	137.07	89.1	1.1	9.8	
108-664D-16H-2, 40	137.20	89.1	0.9	10.1	
108-664D-16H-2, 50	137.30	90.7	0.9	8.3	
108-664D-16H-2, 60	137.40	89.3	1.0	9.7	
108-664D-16H-2, 70	137.50	88.2	1.1	10.7	
108-664D-16H-2, 90	137.70	91.0			

Table 7 (continued).

Core, section, interval (cm)	Depth (mbfs)	CaCO ₃ (%)	SiO ₂ (%)	Terrigenous fraction (%)	Dry-bulk density (g/cm ³)
108-664D-16H-2, 110	137.90	90.0	0.9	9.1	
108-664D-16H-2, 120	138.00	88.6	1.0	10.5	
108-664D-16H-2, 129	138.09	89.8	0.9	9.2	
108-664D-16H-2, 150	138.30	81.8	1.9	16.3	
108-664D-16H-3, 10	138.40	86.1	1.3	12.6	
108-664D-16H-3, 27	138.57	90.8	0.9	8.3	
108-664D-16H-3, 40	138.70	91.6	1.0	7.4	
108-664D-16H-3, 50	138.80	91.8	1.0	7.2	
108-664D-16H-3, 60	138.90	89.3	1.2	9.6	
108-664D-16H-3, 70	139.00	87.4	1.3	11.4	
108-664D-16H-3, 90	139.20	90.2	0.9	8.9	
108-664D-16H-3, 100	139.30	92.4	1.0	6.6	
108-664D-16H-3, 110	139.40	90.4	1.0	8.6	
108-664D-16H-3, 120	139.50	93.4	0.4	6.2	
108-664D-16H-3, 133	139.63	90.6	0.5	8.9	
108-664D-16H-3, 140	139.70	90.3			
108-664D-16H-3, 149	139.79	91.4			
108-664D-16H-4, 10	139.90	90.7			
108-664D-16H-4, 30	140.10	92.7			
108-664D-16H-5, 30	141.60	91.5			
108-664D-16H-5, 40	141.70	94.5			
108-664D-16H-5, 50	141.80	93.3			
108-664D-16H-5, 60	141.90	94.6			
108-664D-16H-5, 70	142.00	93.0	0.3	6.7	
108-664D-16H-5, 90	142.20	94.5	0.3	5.2	
108-664D-16H-5, 100	142.30	91.8	0.4	7.8	
108-664D-16H-5, 110	142.40	93.7	0.4	5.9	
108-664D-16H-5, 119	142.49	93.7	0.3	6.1	
108-664D-16H-5, 133	142.63	96.4	0.3	3.3	
108-664D-16H-5, 149	142.79	91.9	0.4	7.6	
108-664D-16H-6, 10	142.90	91.0	0.4	8.6	
108-664D-16H-6, 27	143.07	90.2	0.4	9.4	
108-664D-16H-6, 40	143.20	91.0	0.1	8.9	
108-664D-16H-6, 50	143.30	91.4	0.4	8.2	
108-664D-16H-6, 60	143.40	92.9	0.2	7.0	
108-664D-16H-6, 70	143.50	91.1	0.3	8.6	
108-664D-16H-6, 90	143.70	92.0	0.1	7.9	
108-664D-16H-6, 100	143.80	91.2	0.4	8.4	
108-664D-16H-6, 110	143.90	90.7	0.2	9.1	
108-664D-16H-6, 120	144.00	91.0	0.5	8.5	
108-664D-16H-6, 133	144.13	92.1	0.6	7.3	
108-664D-16H-6, 149	144.29	88.4	0.3	11.3	
108-664D-16H-7, 10	144.40	87.5	0.4	12.1	
108-664D-16H-7, 27	144.57	91.7	0.5	7.8	
108-664D-16H-7, 40	144.70	92.7	0.2	7.1	
108-664D-16H-7, 50	144.80	91.9	0.6	7.5	
108-664D-16H-7, 60	144.90	90.9	0.1	8.9	
108-664D-16H-7, 70	145.00	92.6	0.2	7.2	
108-664D-16H-7, 79	145.09	91.1	0.4	8.5	
108-664D-17H-1, 40	145.20	93.1	0.2	6.6	
108-664D-17H-1, 50	145.30	92.8	0.2	7.1	
108-664D-17H-1, 60	145.40	91.8	0.5	7.7	
108-664D-17H-1, 70	145.50	91.2	0.2	8.6	
108-664D-17H-1, 90	145.70	92.5	0.2	7.3	
108-664D-17H-1, 100	145.80	92.7	0.1	7.2	
108-664D-17H-1, 110	145.90	92.7	0.1	7.3	
108-664D-17H-1, 120	146.00	93.2	0.2	6.6	
108-664D-17H-1, 133	146.13	93.4	0.1	6.5	
108-664D-17H-1, 149	150.79	93.9	0.1	6.0	
108-664D-17H-5, 10	150.90	94.1	0.1	5.8	
108-664D-17H-5, 27	151.07	92.1	0.1	7.7	
108-664D-17H-5, 40	151.20	90.9	0.1	9.0	
108-664D-17H-5, 50	151.30	90.9	0.6	8.4	
108-664D-17H-5, 60	151.40	91.0	0.8	8.2	
108-664D-17H-5, 70	151.50	92.8	0.7	6.5	
108-664D-17H-5, 90	151.70	94.9	0.3	4.8	
108-664D-17H-5, 100	151.80	93.6	0.6	5.8	
108-664D-17H-5, 110	151.90	93.2	0.6	6.2	
108-664D-17H-5, 120	152.00	92.7	0.5	6.8	
108-664D-17H-5, 123	152.03	94.0	0.5	5.5	
108-664D-17H-5, 146	152.26	92.1	0.6	7.3	
108-664D-17H-6, 10	152.40	93.6	0.6	5.8	
108-664D-17H-6, 27	152.57	93.5	0.3	6.3	
108-664D-17H-6, 40	152.70	93.7	0.6	5.7	
108-664D-17H-6, 50	152.80	93.2	0.8	6.0	
108-664D-17H-6, 60	152.90	88.9	0.9	10.2	

Table 7 (continued).

Core, section, interval (cm)	Depth (mbfs)	CaCO ₃ (%)	SiO ₂ (%)	Terrigenous fraction (%)	Dry-bulk density (g/cm ³)
108-664D-17H-6, 70	153.00	89.2	1.1	9.7	
108-664D-17H-6, 90	153.20	94.8	0.6	4.7	
108-664D-17H-6, 100	153.30	94.5	0.5	5.0	
108-664D-17H-6, 110	153.40	93.4	0.6	6.0	
108-664D-17H-6, 120	153.50	94.3	0.7	5.0	
108-664D-17H-6, 130	153.60	90.9	0.8	8.2	
108-664D-17H-6, 149	153.79	94.6	0.6	4.8	
108-664D-17H-7, 10	153.90	95.0	0.6	4.5	
108-664D-17H-7, 27	154.07	93.5	0.6	5.9	
108-664D-17H-7, 40	154.20	93.8	0.4	5.9	
108-664D-17H-7, 48	154.28	92.3	0.9	6.8	
108-664D-18H-1, 1	154.31	92.1	0.8	7.1	
108-664D-18H-1, 10	154.40	93.7	0.8	5.5	
108-664D-18H-1, 20	154.50	93.9	0.3	5.8	
108-664D-18H-1, 30	154.60	94.4	0.5	5.1	
108-664D-18H-1, 40	154.70	94.8	0.8	4.4	
108-664D-18H-1, 49	154.79	95.0	0.7	4.3	
108-664D-18H-1, 60	154.90	94.6	0.7	4.7	
108-664D-18H-1, 70	155.00	94.3	0.7	4.9	
108-664D-18H-1, 80	155.10	93.8	0.8	5.4	
108-664D-18H-1, 90	155.20	94.0	0.8	5.2	
108-664D-18H-1, 100	155.30	93.4	0.2	6.4	
108-664D-18H-1, 110	155.40	92.2	0.7	7.1	
108-664D-18H-1, 120	155.50	91.5	0.6	7.9	
108-664D-18H-1, 130	155.60	92.4	0.2	7.3	
108-664D-18H-1, 139	155.69	93.5	0.6	5.9	
108-664D-18H-2, 10	155.90	94.5	0.3	5.2	
108-664D-18H-2, 20	156.00	92.4	0.7	7.0	
108-664D-18H-2, 30	156.10	93.5	0.7	5.8	
108-664D-18H-2, 40	156.20	92.7	0.6	6.6	
108-664D-18H-2, 49	156.29	92.5	0.3	7.1	
108-664D-18H-2, 60	156.40	94.8	0.3	4.8	
108-664D-18H-2, 70	156.50	94.7	0.6	4.8	
108-664D-18H-2, 80	156.60	94.8	0.2	5.0	
108-664D-18H-2, 90	156.70	95.1	0.6	4.4	
108-664D-18H-2, 100	156.80	95.3	0.3	4.4	
108-664D-18H-2, 110	156.90	94.3	0.3	5.4	
108-664D-18H-2, 120	157.00	93.0	0.1	6.8	
108-664D-18H-2, 130	157.10	93.1	0.1	6.8	
108-664D-18H-2, 140	157.20	93.5	0.1	6.4	
108-664D-18H-3, 10	157.40	94.1	0.1	5.7	
108-664D-18H-3, 20	157.50	91.5	0.3	8.2	
108-664D-18H-3, 30	157.60	90.7	0.8	8.4	
108-664D-18H-3, 40	157.70	90.5	0.5	9.1	
108-664D-18H-3, 49	157.79	91.7	0.6	7.7	
108-664D-18H-3, 60	157.90	94.9	0.3	4.8	
108-664D-18H-3, 70	158.00	94.1	0.2	5.6	
108-664D-18H-3, 80	158.10	94.6	0.4	4.9	
108-664D-18H-3, 90	158.20	94.1	0.8	5.1	
108-664D-18H-3, 100	158.30	94.2	0.6	5.1	
108-664D-18H-3, 110	158.40	93.6	0.7	5.7	
108-664D-18H-3, 120	158.50	93.2	0.7	6.1	
108-664D-18H-3, 130	158.60	91.3	0.7	8.1	
108-664D-18H-3, 140	158.70	90.6	0.7	8.8	
108-664D-18H-3, 149	158.79	93.8	0.5	5.7	
108-664D-18H-4, 10	158.90	92.2	0.2	7.5	
108-664D-18H-4, 20	159.00	92.9	0.7	6.3	
108-664D-18H-4, 30	159.10	93.7	0.6	5.8	
108-664D-18H-4, 40	159.20	92.3	0.6	7.1	
108-664D-18H-4, 49	159.29	88.3	0.9	10.8	
108-664D-18H-4, 60	159.40	87.2	1.1	11.6	
108-664D-18H-4, 70	159.50	89.1	0.8	10.0	
108-664D-18H-4, 80	159.60	94.0	0.5	5.5	
108-664D-18H-4, 90	159.70	93.1	0.4	6.5	
108-664D-18H-4, 100	159.80	94.4	0.4	5.2	
108-664D-18H-4, 110	159.90	93.7	0.1	6.2	
108-664D-18H-4, 120	160.00	93.6	0.5	5.9	
108-664D-18H-4, 130	160.10	94.4	0.3	5.3	
108-664D-18H-4, 140	160.20	93.1	0.7	6.2	
108-664D-18H-4, 149	160.29	92.1	0.7	7.2	
108-664D-18H-5, 10	160.40	93.9	0.7	5.4	
108-664D-18H-5, 20	160.50	93.5	0.6	5.9	
108-664D-18H-5, 30	160.60	95.2	0.1	4.7	
108-664D-18H-5, 40	160.70	93.0	0.9	6.0	
108-664D-18H-5, 49	160.79	93.7	0.8	5.5	
108-664D-18H-5, 60	160.90	94.3	0.8	4.9	

Table 7 (continued).

Core, section, interval (cm)	Depth (mbsf)	CaCO ₃ (%)	SiO ₂ (%)	Terrigenous fraction (%)	Dry-bulk density (g/cm ³)
108-664D-18H-5, 70	161.00	94.1	0.7	5.2	
108-664D-18H-5, 80	161.10	93.7	0.9	5.4	
108-664D-18H-5, 90	161.20	90.9	0.9	8.2	
108-664D-18H-5, 100	161.30	92.4	0.9	6.6	
108-664D-18H-5, 110	161.40	92.3	0.8	6.8	
108-664D-18H-5, 120	161.50	94.3	0.7	5.0	
108-664D-18H-5, 130	161.60	94.9	0.4	4.7	
108-664D-18H-5, 140	161.70	94.7	0.7	4.6	
108-664D-18H-5, 149	161.79	94.5	0.7	4.8	
108-664D-18H-6, 10	161.90	94.7	0.6	4.8	
108-664D-18H-6, 20	162.00	94.9	0.5	4.6	
108-664D-18H-6, 30	162.10	93.3	0.5	6.2	
108-664D-18H-6, 40	162.20	94.6	0.6	4.8	
108-664D-18H-6, 49	162.29	94.3	0.8	4.9	
108-664D-18H-6, 60	162.40	94.4	0.7	4.8	
108-664D-18H-6, 70	162.50	91.5	0.7	7.8	
108-664D-18H-6, 80	162.60	91.2	0.7	8.1	
108-664D-18H-6, 90	162.70	91.8	0.5	7.6	
108-664D-18H-6, 100	162.80	91.4	0.6	8.0	
108-664D-18H-6, 110	162.90	93.7	0.5	5.8	
108-664D-18H-6, 120	163.00	92.7	0.4	6.9	
108-664D-18H-6, 129	163.09	94.6	0.6	4.8	
108-664D-19H-1, 10	163.90	88.4	0.8	10.8	
108-664D-19H-1, 20	164.00	82.6	1.2	16.2	
108-664D-19H-1, 30	164.10	85.6	1.1	13.3	
108-664D-19H-1, 40	164.20	91.4	0.6	8.0	
108-664D-19H-1, 49	164.29	92.3	0.5	7.3	
108-664D-19H-1, 60	164.40	88.8	0.6	10.5	
108-664D-19H-1, 70	164.50	93.1	0.6	6.4	
108-664D-19H-1, 80	164.60	92.2	0.5	7.3	
108-664D-19H-1, 90	164.70	94.0	0.7	5.3	
108-664D-19H-1, 100	164.80	95.0	0.6	4.4	
108-664D-19H-1, 110	164.90	94.4	0.6	4.9	
108-664D-19H-1, 120	165.00	90.0	0.2	9.7	
108-664D-19H-1, 130	165.10	91.5	0.8	7.7	
108-664D-19H-1, 140	165.20	93.2	0.7	6.2	
108-664D-19H-2, 10	165.40	92.6	0.6	6.8	
108-664D-19H-2, 20	165.50	94.0	0.5	5.5	
108-664D-19H-2, 30	165.60	93.2	0.4	6.4	
108-664D-19H-2, 40	165.70	92.2	0.9	6.9	
108-664D-19H-2, 49	165.79	92.6	0.9	6.5	
108-664D-19H-2, 60	165.90	92.7	0.4	6.8	
108-664D-19H-2, 70	166.00	91.8	1.1	7.1	
108-664D-19H-2, 80	166.10	89.2	0.8	10.0	
108-664D-19H-2, 90	166.20	89.5	1.0	9.6	
108-664D-19H-2, 100	166.30	92.6	0.9	6.5	
108-664D-19H-2, 110	166.40	92.6	0.8	6.6	
108-664D-19H-2, 120	166.50	91.5	0.6	7.9	
108-664D-19H-2, 130	166.60	91.4	0.6	8.0	
108-664D-19H-2, 140	166.70	92.5	0.6	6.8	
108-664D-19H-2, 149	166.79	93.4	0.2	6.4	
108-664D-19H-3, 10	166.90	94.4	0.8	4.7	
108-664D-19H-3, 20	167.00	94.1	0.6	5.3	
108-664D-19H-3, 30	167.10	93.2	0.2	6.6	
108-664D-19H-3, 40	167.20	93.4	0.9	5.7	
108-664D-19H-3, 49	167.29	92.8	0.8	6.4	

Table 7 (continued).

Core, section, interval (cm)	Depth (mbsf)	CaCO ₃ (%)	SiO ₂ (%)	Terrigenous fraction (%)	Dry-bulk density (g/cm ³)
108-664D-19H-3, 60	167.40	92.3	0.7	6.9	
108-664D-19H-3, 70	167.50	93.7	0.4	6.0	
108-664D-19H-3, 80	167.60	92.3	0.7	7.0	
108-664D-19H-3, 90	167.70	93.7	0.6	5.7	
108-664D-19H-3, 100	167.80	93.6	0.4	5.9	
108-664D-19H-3, 110	167.90	92.4	0.8	6.9	
108-664D-19H-3, 120	168.00	91.1	0.9	7.9	
108-664D-19H-3, 130	168.10	86.7	1.1	12.2	
108-664D-19H-3, 140	168.20	84.9	1.3	13.8	
108-664D-19H-3, 149	168.29	87.2	1.1	11.7	
108-664D-19H-4, 10	168.40	93.1	0.6	6.3	
108-664D-19H-4, 20	168.50	95.1	0.7	4.2	
108-664D-19H-4, 30	168.60	92.5	0.6	6.9	
108-664D-19H-4, 40	168.70	93.6	0.7	5.7	
108-664D-19H-4, 49	168.79	91.6	0.7	7.7	
108-664D-19H-4, 60	168.90	90.9	0.7	8.4	
108-664D-19H-4, 70	169.00	89.8	0.8	9.4	
108-664D-19H-4, 80	169.10	90.1	1.0	8.9	
108-664D-19H-4, 90	169.20	87.5	1.1	11.4	
108-664D-19H-4, 100	169.30	90.3	0.5	9.1	
108-664D-19H-4, 110	169.40	93.6	0.6	5.8	
108-664D-19H-4, 120	169.50	94.1	0.6	5.2	
108-664D-19H-4, 130	169.60	94.4	0.7	5.0	
108-664D-19H-4, 140	169.70	94.4	0.8	4.8	
108-664D-19H-4, 149	169.79	95.4	0.8	3.8	
108-664D-19H-5, 10	169.90	94.6	0.8	4.7	
108-664D-19H-5, 20	170.00	92.6	0.8	6.6	
108-664D-19H-5, 30	170.10	92.6	0.9	6.5	
108-664D-19H-5, 40	170.20	93.5	0.6	5.9	
108-664D-19H-5, 49	170.29	91.5	0.7	7.8	
108-664D-19H-5, 60	170.40	93.2	0.8	5.9	
108-664D-19H-5, 70	170.50	93.4	0.8	5.8	
108-664D-19H-5, 80	170.60	91.6	0.7	7.7	
108-664D-19H-5, 90	170.70	92.7	0.8	6.5	
108-664D-19H-5, 100	170.80	91.8	0.8	7.4	
108-664D-19H-5, 110	170.90	92.9	0.8	6.3	
108-664D-19H-5, 120	171.00	92.4	0.7	6.9	
108-664D-19H-5, 130	171.10	92.7	0.7	6.7	
108-664D-19H-5, 140	171.20	92.2	0.7	7.1	
108-664D-19H-5, 149	171.29	92.9	0.9	6.2	
108-664D-19H-6, 10	171.40	91.5	0.6	7.9	
108-664D-19H-6, 20	171.50	93.1	0.8	6.0	
108-664D-19H-6, 30	171.60	92.9	0.8	6.3	
108-664D-19H-6, 40	171.70	93.3	0.9	5.8	
108-664D-19H-6, 49	171.79	93.2	0.9	5.9	
108-664D-19H-6, 60	171.90	92.8	0.8	6.4	
108-664D-19H-6, 70	172.00	94.1	0.7	5.2	
108-664D-19H-6, 80	172.10	93.3	0.8	5.9	
108-664D-19H-6, 90	172.20	93.5	0.8	5.7	
108-664D-19H-6, 100	172.30	93.3	0.8	5.9	
108-664D-19H-6, 110	172.40	93.6	0.4	5.9	

Note: Average shipboard-measured dry-bulk densities (in g/cm³) used to calculate fluxes in Cores 108-664D-15H through -19H were: Core 108-664D-15H = 1.07, Core 108-664D-16H = 1.03, Core 108-664D-17H = 1.09, Core 108-664D-18H = 1.00, and Core 108-664D-19H = 1.04.